A Preliminary Study into Non Invasive Breast Cancer Diagnosis using Magnetic Resonance Elastography

A thesis submitted in partial fulfilment of the requirements for the Degree

of Doctor of Philosophy

in Bio-Mechanical Engineering

at the University of Canterbury

by David Viviers

University of Canterbury

2013

Abstract

Attenuation and damping in elastography are naturally of great interest as the presence of these effects in biological tissue goes without question and therefore must be addressed if quantitative assessment of tissue elastic properties is to be achieved. Additionally, given the change in the tissue structure present in the diseases that elastographic imaging seeks to detect and diagnose, there is every reason to expect that the resulting lesions will also exhibit a change in their attenuation behaviour, indicating diagnostic value to any description of the damping property distribution elastographic methods are able to provide.

This thesis will present the unique contribution of the development of several Elastographic models for MR based reconstructions of soft tissue. A method for the reconstruction of both Viscoelastic and Rayleigh damping based damped elastic properties has been developed for use with MR detected time-harmonic motion data and has been shown to lead to reasonable results in both homogeneous and heterogeneous phantoms of varying material types.

A poro-elastic modelling is thought to provide a more accurate description of tissue structure by accounting for, in part, the complex interactions between the solid and fluid phases present in vivo. The foundation for a poro-elastic material behaviour will be explored and presented to support the premise. A meaningful mapping of the orthotropic shear moduli distributions in three directions has demonstrated enough evidence that the orthotropic MRE can be a feasible technique to determine orthotropic elasticity parameters of a biological tissue, noninvasively. The orthotropic achievements throughout this project can be useful for future clinical cancer diagnostics by augmenting the information obtained from the orthotropic MRE reconstructions between normal tissue and tumours.

Table of Contents

List of Figures

4. Scattering and Dispersion

5.   **Anisotropic Reconstruction**

List of Tables

Nomenclature

μ - shear modulus

u - displacement vector

ρ - density

λ - Lame's constant

t - time

ν - poisson's ratio

α - proportionality constant

β - proportionality constant

γ - shear strains

ε - elastic strain

ξ - damping ratio

M - Mass matrix

C - Damping matrix

K - Stiffness matrix

A - FEM material property matix

ω - angular frequency

RC - Rayleigh Composition

ϕ – Error function

τ - shear stresses

E - Young's modulus

K- Bulk Modulus

σ - elastic stress

θ - Material property distribution

R - Right Hand Side vector

J - Jacobian matrix

H - Hessian matrix

p - Property search direction

Ω - Global property domian

Γ - Sub-zone domian

κ - Bulk modulus

S - Compliance matrix

V - Volume

g - Gradient

y - Measured property

f - Calculated property

Chapter 1

Introduction

1.1 Breast Cancer

Breast cancer occurs due to the development and interactions of a defective gene. Healthy cells divide as many times as the body requires and then stop at sufficient levels. These healthy cells attach to other cells forming specific structures within the tissue. Cells become cancerous when mutations destroy their ability to stop dividing, or to attach to other cells and form normal structures and to remain integrated into the tissue structure, (American Cancer Society, 2005 [1] & Jemal et al, 2008 [2]).

Normal cells will die when they are no longer needed, and be replaced with healthy cells. While cells are required by the body, they are protected by several protein clusters and pathways, cancer cells may also be protected by these protein clusters and pathways preventing these corrupted cells from dying and being replaced, (American Cancer Society, 2005 [1] & Jemal et al, 2008 [2]).

As one of the leading causes of death, cancer is obviously a major health concern. Worldwide, in 2008, breast cancer comprised 22.9% of all cancers (excluding non-melanoma skin cancers) found in women and breast cancer caused 458,503 deaths (13.7% of cancer deaths in women), (IARC, 2008 [5]). Figure 1.1 displays a vector map of international breast cancer deaths, per 100 000 people, in 2004, (WHO, 2009 [6]).
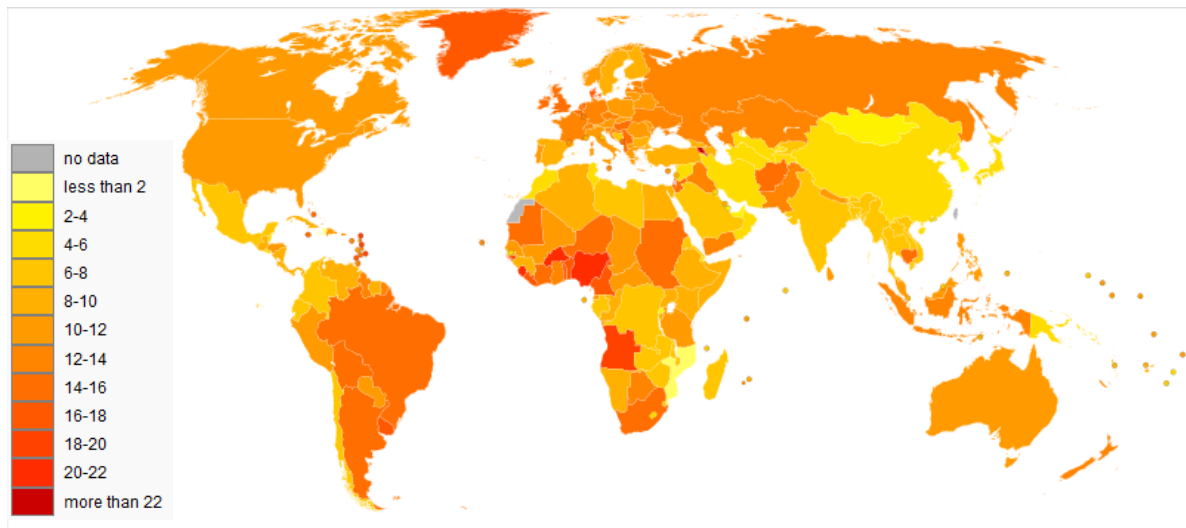
Figure 1.1: Vector map of Breast Cancer Deaths per 100 000 in 2004 [6]

Figure 1.2 and 1.3 show cancer statics for women in the USA, for the year 2008. These pie charts indicate that 26% of all cancers found in women are breast cancers and that, 15% of cancer related mortality is a direct result of breast cancer. Early detection and diagnosis has the potential to significantly impact mortality rates and possibly even cure breast cancer by identifying and treating at risk patients before severe tissue damage has been done, (American Cancer Society, 2007 [7]).
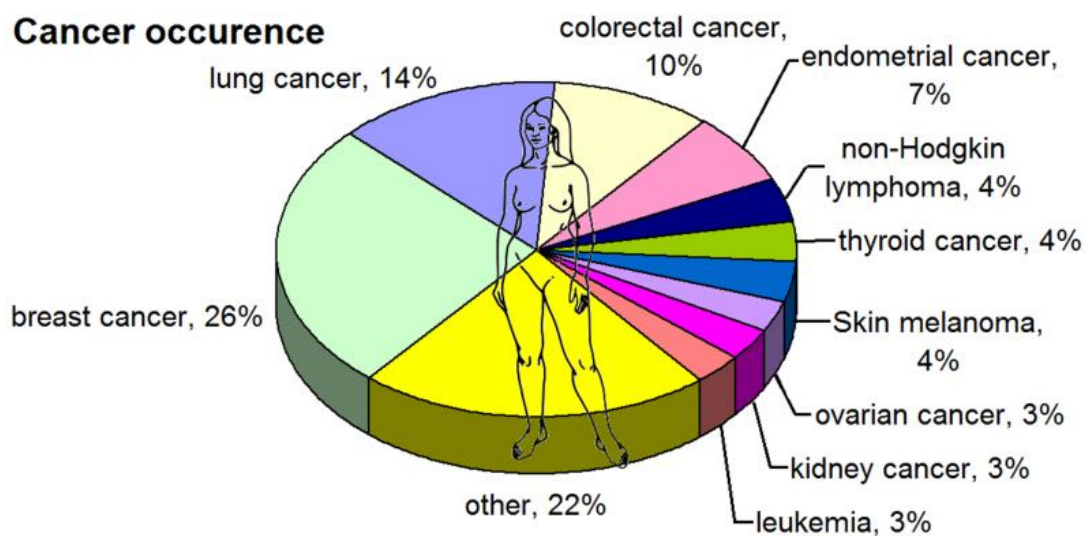
Figure 1.2: Pie Chart of Cancer Occurrence in Females in 2008 [2]

Cancer mortality

- breast cancer, 15%
- colorectal cancer, 9%
- pancreatic cancer, 6%
- ovarian cancer, 6%
- non-Hodgkin lymphoma, 3%
- leukemia, 3%
- uterine cancer, 3%
- liver & intrahepatic bile duct, 2%
- brain and other nervous system, 2%
- other, 25%
- lung cancer, 26%
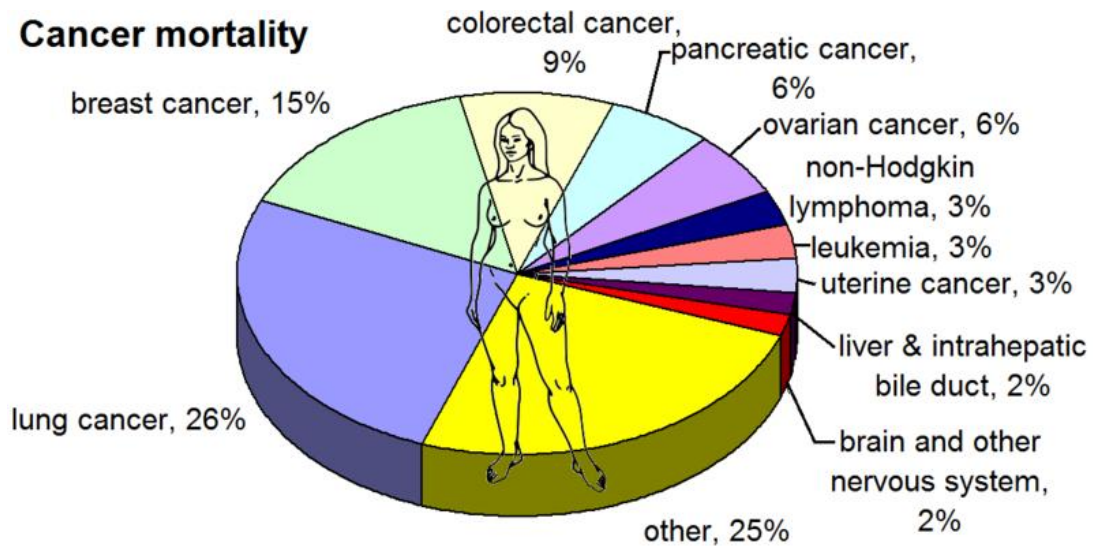
Figure 1.3: Pie Chart of Cancer Mortality in Females in 2008 [2]

1.2 Breast Tissue

The internal structures within the breast include the milk glands (lactiferous ducts), connective tissue (collagen, elastin), adipose tissue (white fat), and the suspensory Cooper's ligaments (Tortora et al, 2001 [10]). Figure 1.4 displays an anotomical cross section of the human breast. The primary regions are identified in the Key, labelled 1 through 10. The Figure clearly depicts the complex internal tissue structure, and organs.

3

1	Chest wall
2	Pectoralis muscles
3	Lobules
4	Nipple surface
5	Areola
6	Lactiferous duct
7	Fatty tissue
8	Skin
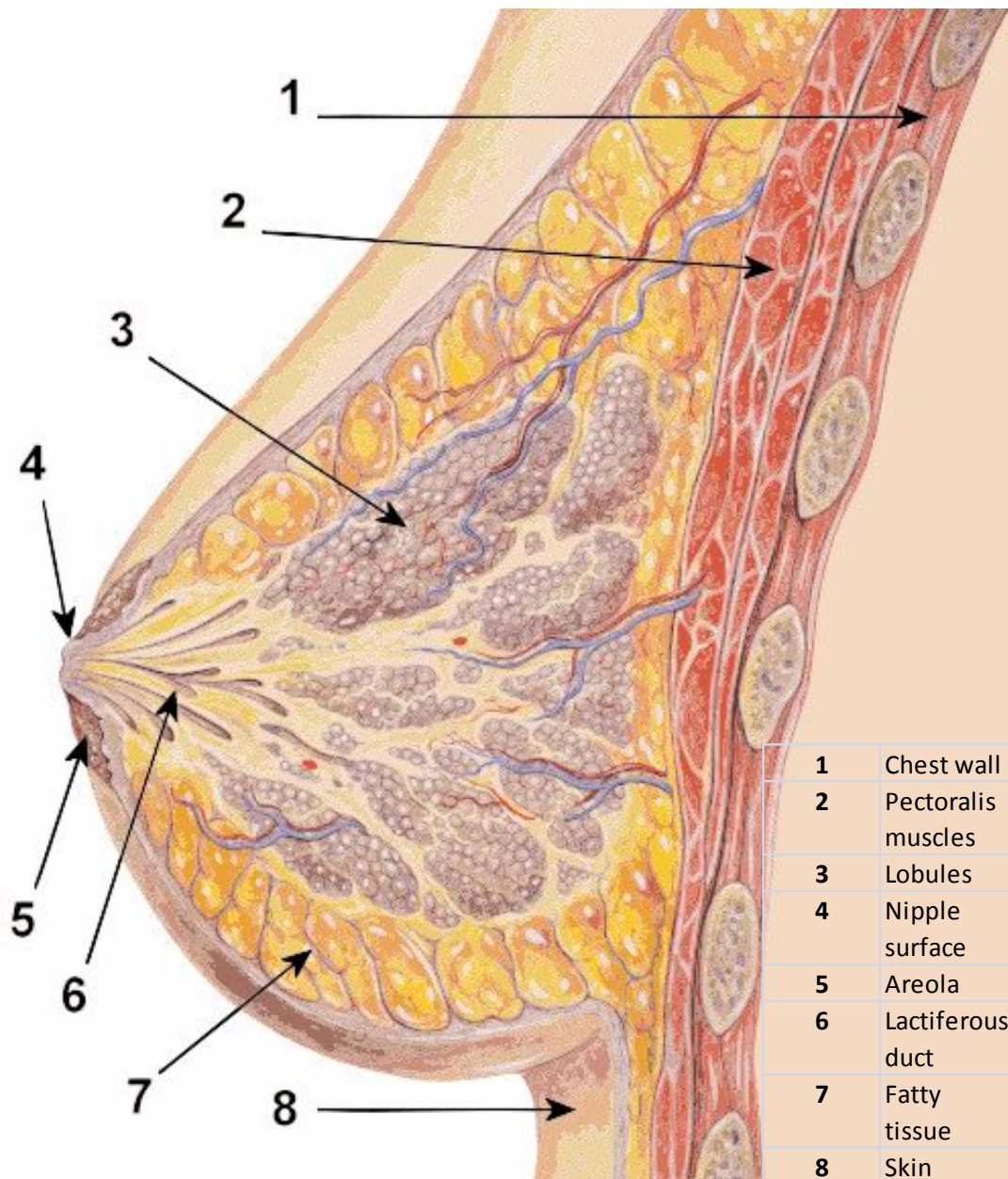
Figure 1.4: Cross section of female breast anatomy [183]

1.3 Medical Imaging

Mammography is a common screening method and is currently the medical standard for screening breast cancer. Figure 1.5 illustrates the clinical procedure as well as a smple mammogram screening image. The most aggressive breast cancers are found in dense breast tissue, which mammograms can not image (Gøtzsche et al, 2009 [11]). Computer-aided detection and digital mammography are methods used to reduce the human error in

interpretation of mammographic images. Computers digitally analyze the the images from the mammogram and identify regions of interest automatically. Alternatively computers are able to calculate a thickkness correction to enhance the periphery of the mammographic image (Snoeren et al, 2004 [43]).

Figure 1.5: A) Example of patient positioning for a craniocaudal mammogram. B) A healthy breast, left, and a breast tumour, right, as seen on a image from a mammogram.

1.4 Magnetic Resonance Elastography (MRE)

Elasticity imaging comprises three basic steps: applying a known static or cyclic mechanical load through an object, measuring the deformation of the medium as the displacement pattern, and then calculating the elasticity modulus. MRE as an imaging technique has been developed to measure the elastic properties of soft tissue (Van Houten et al, 2003 [90], 2003 [91] & 2001 [92] and Samani et al, 2004 [93]). There are two dominant MRE methods currently prevalent in research, namely quasi-static and dynamic. The dynamic method uses shear wave propagation to produce the desired motion within the tissue. This method was developed as a phase-contrast technique by using harmonic shear vibrations and synchronized cyclic motion gradients to map the motion as a displacement field. The recorded data is utilized to reconstruct the image. The quasi-static technique uses a phase-contrast technique as well, however the data acquisition in this method is often slow (Perrinez, 2005 [94]).

The MRI applies a sequence of radiofrequency excitation pulses and a series of magnetic field gradients to produce an image by locating and encoding the spatial position of hydrogen nuclei (spins) in volume elements (voxels) within a tissue (Hornak, 1996 [95] and Morrow, 2000 [96] and Thomas et al, 1988 [97]). Furthermore, the MRE method integrates a motion encoding gradient (MEG) to other magnetic field gradients at the same frequency and direction as the actuator (Perrinez, 2005 [94]).

In dynamic MRE, a piezoelectric actuator is used to actuate the tissue sample being imaged with a sinusoidal driving signal. The MRI can scan the resulting harmonic motions within the volume of the tissue using the phase contrast motion encoding gradients (Hornak, 1996 [95]) which record the accumulated phase shift of the spins at different points along the sinusoidal signal (Kruse, 2000 [98]). These motions can be mapped in a 3D space to describe the motion at every point in the measured volume within the tissue. This method generates a complex displacement value at each point on a grid within the sample volume (Muthupillai et al, 1995 [99]). The wavelength of shear waves produced by an actuator can be defined as:

$$\lambda = \frac{1}{f}\sqrt{\frac{\mu}{\rho}}$$

eq. 2.1

where λ is the shear wavelength, f is the actuation frequency in Hz, μ is the shear modulus of the material, ρ is the density (Engan et al, 1988 [100]).

Chapter 2

Theory

2.1 The Inverse Problem

In elastography the material properties of an object can be determined given the mechanical response. The forward problem can be defined as, determine the mechanical response, u, given the material property distribution, θ, and boundary condition data. While the inverse problem is defined as, determine the material property distribution, η, given the mechanical response, u, and boundary condition data. The inverse problem can be solved by a direct inversion of the elasticity equation, as long as there are at least as many measurements as unknown parameters. Inverse problem systems, arising from image reconstruction methods, are usually large and ill-conditioned. The inverse problem formula is given as:

$$Z(u).\{\eta\} = \{R_{inv}\}$$

<div align="right">eq. 2.13</div>

where Z(u) is the inverse matrix containing terms related to known MR-detected displacements obtained from the MRE imaging procedure, unknown material properties η and R_{inv} the direct inversion of the RHS vector (Samarskii et al, 2007 [140] and Aster et al, 2005 [141] and Vogel, 2002 [142]). This can be a conversion of the displacement solution obtained from equation (2.12) as a set of measurements into an estimate of elasticity parameters throughout the domain. The inverse problem in MRE mostly involves finding a shear modulus, μ(x) which can satisfy the equation (2.12) given measurements of the displacement field amplitude obtained from an MRI at discrete locations and boundary condition data (Weaver et al, 2001 [105] and Glaser et al, 2003 [106] and Wall et al, 2006 [107] and Paulsen et al 2005 [108]).

A typical issue that arises in the solution of an inverse problem is that a very small amount of noise in the data can cause large errors in the estimates. This instability phenomenon defines the problem as ill-posed. By definition a problem is well posed when a solution exists and it is unique. For a real data set, the image reconstruction by a computed solution suffers, as, in a physical sense the solution is not exact but an approximation of the real data. The noise in the experimental data increases the error preventing the computation from reproducing the original data completely. This problem is ill posed even for a small perturbation, which produces a large oscillation for a small change in the data (Bertaja et al, 2000 [109]). Another concern regarding the inverse problem is the condition number K(A) of a matrix A which is defined as:

$$K(A) = \|A\|_\infty \|A^{-1}\|_\infty$$

eq. 2.14

where $\|A\|$ is the size of matrix A given by absolute maximum row summation as:

$$\|A\|_\infty = \max_{i=1,\dots,n} \left\{ \sum_j^n |a_{ij}| \right\}$$

eq. 2.15

Suppose, Ax = b, where x is the exact solution to the linear system defined by A and b and similarly $Ax_c = b_c$, where x_c is the calculated solution and b_c is the corresponding RHS. By definition, the relationship between relative error $\frac{\|x-x_c\|}{\|x\|}$ and relative residual $\frac{\|b-b_c\|}{\|b\|}$ can be shown as:

$$\frac{\|x - x_c\|}{\|x\|} \le K(A) \frac{\|b - b_c\|}{\|b\|}$$

eq. 2.16

The condition number determines the value of error. If K(A) $\approx$ 1, the system is well conditioned and it means the small inaccuracies in the residual give small errors, but if K(A) $\geq$ 1, the system is ill-conditioned and with a small perturbation in the residual causes a large error (Long-ji et al, 1991 [110]).

2.2 Conjugate Gradient (CG) Method

The conjugate gradient (CG) method (Shewchuk, 1994 [17]) is a more efficient formulation of the steepest descent method. In the minimization problem the gradient of the error function $-\nabla\Psi_k$ can take the general form as:

$$-\nabla\Psi_k = r_k = b - Ax_k$$

eq. 2.23

where A is an n×n matrix that is symmetric and a positive definite. By introducing error vector $e_k = \eta_{k+1} - \eta_k$, which shows the distance from the actual solution, and residual r_k in equation (2.23) that represents the distance from the correct value of b , the equation (2.23) is transformed to:

$$r_k = -Ae_k$$

eq. 2.24

This shows the residual is the error transformed by A into the same space as b . As the error is unknown, it can be transformed to the known residual space. An interesting property of the CG method is its ability to produce a set of linearly independent conjugate vectors {p_0, p_1, ...p_l} with respect to the symmetric positive definite matrix A. The conjugacy property is shown as:

$$p_i^T Ap_j = 0$$

eq. 2.25

9

As will be shown, linear CG is an iterative method for solving linear systems with positive definite matrices and the conjugacy property guarantees successively minimization of the function along the individual directions after n steps by setting the iterative sequence as $\eta_{k+1} = \eta_k + \alpha_k p_k$, where α_k is the step length along the search direction p_k . The value of α_k can be obtained using the fact that the error $e_{(k+1)}$ should be orthogonal to the previous search direction p_k because this not only avoids the skipping in the direction of p_k again, but also corresponds to the minimum point along p_k . This leads to:

$$p_k^T e_{k+1} = 0$$

<div align="right">eq. 2.26</div>

$$p_k^T(e_k + \alpha_k p_k) = 0$$

<div align="right">eq. 2.27</div>

$$\alpha_k = \frac{p_k^T e_k}{p_k^T p_k}$$

<div align="right">eq. 2.28</div>

As the e_k is unknown so by using (2.24) the e_k can be transformed to the r_k, space which is known as:

$$\alpha_k = \frac{p_k^T r_k}{p_k^T A p_k}$$

<div align="right">eq. 2.29</div>

If the search direction p_k will be set up in the direction of gradient or r_k the value of α_k can take the form of the same value in the steepest descent, given by:

$$\alpha_k = \frac{r_k^T r_k}{p_k^T A p_k}$$

This iterative minimization is updated along both error and residual space. This leads to:

$$r_{k+1} = -Ae_{k+1} = -A(e_k + \alpha_k p_k)$$

$$r_{k+1} = r_k - \alpha_k A p_k$$

$$e_{k+1} = e_k + \alpha_k p_k$$

CG is based on conjugate direction but with a very special property that means it is able to generate the next search direction p_{k+1} using a linear combination of the current gradient, $-\nabla \Psi_k$ known as residual, r_k and the previous search direction, p_k . This advantage of the CG method is remarkable because it does not need to know all the previous elements, thus it requires little storage and computation. This concept is expressed as:

$$p_{k+1} = r_{k+1} + \beta_{k+1} p_k$$

The constant β_k is being chosen so that p_k and p_{k+1} will form as they must be, and be conjugate with respect to A. By pre-multiplying (2.34) by $p_k^T A$ and applying the condition of conjugacy $p_k^T A p_{k+1} = 0$, it is found that:

$$\beta_k = \frac{r_{k+1}^T A p_k}{p_k^T A p_k}$$

<div align="right">eq. 2.35</div>

As the matrix A is difficult to calculate, to remove it from the equation (2.35) the term Ap_k is replaced by $r_{k+1} - r_k/\alpha_k$ from equation (2.32). Now by using (2.34) and substituting the equation (2.35) and applying the two facts that each residual is orthogonal to the previous search direction, and also orthogonal to the previous residuals as they are shown in (2.36) and (2.37), leads to β_k as a ratio of a new and previous gradient norm as it is shown in (2.38).

$$r_k^T r_{k+1} = 0$$

<div align="right">eq. 2.36</div>

$$p_k^T r_{k+1} = 0$$

<div align="right">eq. 2.37</div>

$$\beta_{k+1} = \frac{r_{k+1}^T r_{k+1}}{r_k^T r_k}$$

<div align="right">eq. 2.38</div>

The algorithm proceeds by producing vector sequences iteratively to approximate and update the solution, residuals, and search directions, successively. (Wolfe, 1969 [134] and Fu et al, 1997 [135] and Gill et al, 1979 [136] and Shapira, 2008 [137]).

2.3 The Adjoint Gradient Calculation

Although the CG technique requires calculating the gradient to obtain the search direction in each iteration, calculating the Jacobian to build the residual is computationally intensive. The adjoint gradient method has been recently developed to provide a very efficient method to compute the gradient. In gradient based optimization, the adjoint technique is widely utilized for the gradient computation when there is a problem dealing with a large number of

parameters. While other methods, such the Jacobian matrix or a finite difference approximation use as many forward solutions as there are parameters, the adjoint approach requires only two forward solutions to obtain the gradient for any number of reconstructed parameters. Here the discrete adjoint gradient calculation for MRE is expressed. By definition the variation of a function F(x) in the direction δx is denoted by δF and it is given by,

$$\delta F = \frac{\partial F}{\partial x}.\,\delta x = \frac{d}{d\varepsilon}\lim_{\varepsilon \to 0} F(x + \varepsilon\delta x)$$

<div align="right">eq. 2.58</div>

where $\frac{\partial F}{\partial x}$ which also is shown by this notation $D_x F$ is a directional derivative of the function F(x) and represents the perturbation rate of the function by the presence of small changes in the variable. The general weak form of the forward problem can be defined as

$$A\left(w_{ap}, u_{ap}^c; \eta_{ap}\right) = \oint w_{ap}.\,\Phi\, ds$$

<div align="right">eq. 2.59</div>

where $A(:,:;\eta_{ap})$ is a bilinear operator which represents an equivalent weak form of the elasticity equation which represents the inner product between two tensors w and u respectively and depends on the elasticity parameter vector η. The discretized weighting function w is expressed as $w_{ap}(x,y,z) = \sum_{i=1}^{N} w_i \phi_i(x,y,z)$ and the approximation of the calculated displacement field can be shown as $u_{ap}^c[x,y,z,\eta(x,y,z)] = \sum_{i=1}^{N} u_i \phi_i(x,y,z)$. The RHS shows the traction on the boundaries obtained from Green's theorem. The inverse adjoint elasticity formulation for the TK discretized function is introduced as follows:

$$\phi_{TK} = \frac{1}{2}\left\|u_{ap}^c - u^m\right\|^2 + \frac{\alpha_{TK}}{2}\|\eta - \eta_0\|^2 + A\left(w_{ap}, u_{ap}^c; \eta_{ap}\right) - \oint w_{ap}.\,\sigma\, ds$$

<div align="right">eq. 2.60</div>

The variation of the equation (2.60) is computed by using the functional derivative defined in equation (2.58) and can be written as:

$$\delta\phi_{TK} = \frac{\partial\phi}{\partial u^c}\delta u^c + \frac{\partial\phi}{\partial w_{ap}}\delta w_{ap} + \frac{\partial\phi}{\partial\eta_{ap}}\delta\eta_{ap} = 0$$

<div align="right">eq. 2.61</div>

Assuming the presence of TK regularization, the variation of the equation (2.61) due to w is:

$$\frac{\partial\phi}{\partial w_{ap}}\delta w_{ap} = A\left(w_{ap}, u_{ap}^c; \eta_{ap}\right) - \oint w_{ap}.\sigma\, ds$$

<div align="right">eq. 2.62</div>

Setting this variation to be equal to zero (i.e. $= \frac{\partial\phi}{\partial w_{ap}}\delta w_{ap} = 0$) leads to u_{ap}^c satisfying the weak form of the elasticity equation. On the constraint boundaries of the equation (2.62), the equation (2.60) reduces to the original objective function (2.52). Equation (2.61) can be further simplified if the weighting function is chosen so that $\frac{\partial\phi}{\partial u^c}\delta u^c = 0$. This leads to:

$$A\left(w_{ap}, \delta u_{ap}^c; \eta_{ap}\right) = -\left(u_{ap}^c - u^m\right)$$

<div align="right">eq. 2.63</div>

As the elasticity operator A is self-adjoint and symmetric, thus it is equal to its transposed A^T. Therefore, the equation (2.63) can be rewritten as,

$$A^T\left(\delta u_{ap}^c, w_{ap}; \eta_{ap}\right) = -\left(u_{ap}^c - u^m\right)$$

<div align="right">eq. 2.64</div>

From (2.61) and (2.52) it can be shown that:

$$\delta\phi = \frac{\partial\phi}{\partial\eta_{ap}}\delta\eta_{ap} = \frac{\partial}{\partial\eta_{ap}}\left[A\big(w_{ap}, u_{ap}^c; \eta_{ap}\big) + \frac{\alpha_{TK}}{2}\|\eta - \eta_0\|^2\right]\delta\eta_{ap}$$

<div align="right">eq. 2.65</div>

$$\delta\phi = \frac{\partial\phi}{\partial\eta_{ap}}\delta\eta_{ap} = A\big(w_{ap}, u_{ap}^c; \eta_{ap}\big) + \alpha_{TK}\|\eta - \eta_0\|$$

<div align="right">eq. 2.66</div>

Now this gradient will be minimized by setting $\frac{\partial\phi}{\partial\eta_{ap}}\delta\eta_{ap} = 0$ this follows as:

$$A\big(w_{ap}, u_{ap}^c; \eta_{ap}\big) = \alpha_{TK}\|\eta - \eta_0\|$$

<div align="right">q. 2.67</div>

2.4 Finite Element (FE) Approximation

One of the most efficient numerical approaches for computing the displacements in a forward solution, or the material properties in an inverse problem, is the finite element method. In the forward problem approach, this method approximates the governing equations (2.12) over a continuous medium as a mesh of elements.

Ultimately, for an N-node mesh system, the problem will reach the solution of a matrix equation of the form $[A(\eta)]\{u\} = \{R_{fwd}\}$, where $[A]$ is an n×n matrix, sparse as it is involved with basis functions which are strictly non zero at each node, over the domain. Usually a basis function, or a shape function, $\Phi_i(x, y, z)$ if is centered on each node and the magnitude of the

parameter of interest is measured at every point in the meshed area as a weighted sum of these basis functions given as:

$$u_{ap}(x, y, z) = \sum_{i=1}^{n} u_i \phi_i(x, y, z)$$

where the index "ap" here represents the approximate functions in the finite dimensional space and u_{ap}(x, y, z) is the approximate displacement value at a point (x, y, z), Φ_i(x, y, z) are known FE basis functions corresponding with i^{th} node and u_i is the displacement value at node i.

In the inverse problem approach, the FE approximation of the matrix equation [Z(u)]{η} = {R_{inv}}, takes the form as implementation of nodal material property distribution using basis functions for the element as:

$$\eta_{ap}(x, y, z) = \sum_{i=1}^{n} \eta_i \phi_i(x, y, z)$$

where $\eta_{ap}(x, y, z)$ is the approximate material property value at a point (x, y, z) that can be calculated as the sum of N basis functions that are valued by N constants, $\eta_i \phi_i(x, y, z)$ is FE basis function corresponding with i^{th} node. η_i is material parameter at node i which is unknown. The expansion of this equation for the approximation of elasticity parameters μ_{ap}(x, y, z), λ_{ap}(x, y, z), and ρ_{ap}(x, y, z) on the nodes will take the form

$$\mu_{ap}(x, y, z) = \sum_{i=1}^{n} \mu_i \phi_i(x, y, z)$$

$$\lambda_{ap}(x,y,z) = \sum_{i=1}^{n} \lambda_i \phi_i(x,y,z)$$

$$\rho_{ap}(x,y,z) = \sum_{i=1}^{n} \rho_i \phi_i(x,y,z)$$

eq. 2.78

where the index "ap" again represents the approximate functions in the finite dimensional space and μ_i, λ_i, ρ_i, u_i are the discrete parameter values at node i of the N total nodes within the FE mesh, known as shear modulus, bulk modulus, and density respectively. The weighted residual method is a useful approach, which is widely applied in MRE finite element approximation. This method takes the weak form of the general forward problem, multiplies the error, 'r' due to substituting the approximate solution, $\eta_{ap}(x,y,z)$, in a weighted function $\omega_j(x, y, z)$, then the product is integrated over the domain, Ω, and ultimately the result is set to equal zero which can be written as $\int_{\Omega} \omega_j(x,y,z) r \, dV = 0$.

One simple way to solve a FE weak form is using Galerkin method which chooses a linear basis function, $\Phi_i(x, y, z)$ as the weighting function, Φ_{ap} which leads to $\phi_{ap}(x,y,z) = \omega_{ap}(x,y,z) = \sum_{i=1}^{n} \omega_i \phi_i(x,y,z)$.

In the MRE time harmonic case, the solution is naturally oscillatory, and applying fine and suitable meshes regarding the physical geometry of the problem plays an important role in accurately capturing the convergence of the solution with respect to the mesh size. (Maniatty et al, 2005 [150] and Grandin, 1991 [151] and Cuvelier et al, 1986 [152] and Zienkiewicz et al, 1994 [153])

2.5 The Sub-Zone Method

A subzone based reconstruction method is used to in order to reconstruct the material property distribution for very large MRI datasets.

This technique works efficiently to solve an iterative inverse reconstruction across a large parameter set with reasonable computational load. The 3D subzone procedure for the sub-domain inverse problem uses the known internal displacements to solve an iterative inversion process on small partitions of the total problem domain. This approach generates a high degree of spatial discretization and, utilizes the data rich environment obtained from MRI. The image reconstructions show that the zoned inversion strategy is capable of producing accurate elasticity modulus distribution images from displacement data obtained from MR even in the presence of high noise.

This method has proven successful in reconstructing stiffness distributions using MR-detected motion datasets from both gelatine phantoms and real patients. (Van Houten et al, 1999 [22], 2000 [23] & 2001 [24]).
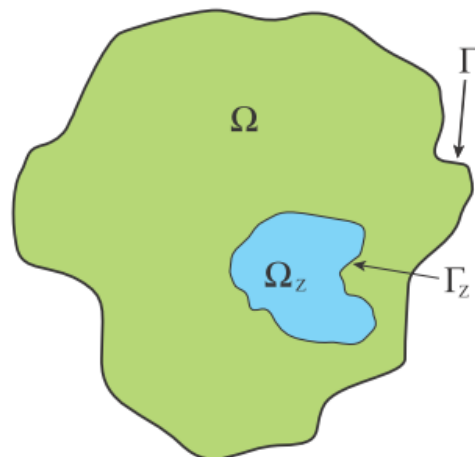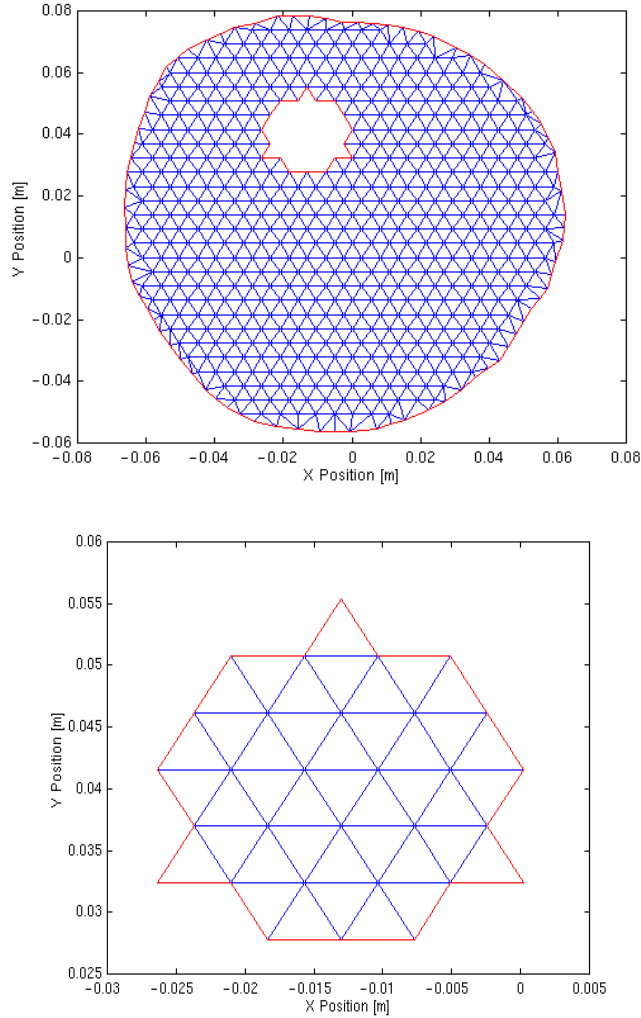
Figure 2.1: Schematic & FE Mesh representation of subzone concept

In Figure 2.1 the global problem domain is represented by Ω with boundary Γ, and the domain of the subzone is represented by Ω_z with boundary Γ_z

$$F(\theta) = \sum_{z=1}^{Q} F_z(\theta_z)$$

eq. 2.79

Equation (2.79) defines the global minimisation problem, where θ_z is the nodal parameter distribution for all nodes within the region of subzone z.

19

$$\min_{\theta}(F) = \min_{\theta_z} \left(\sum_{z=1}^{Q} F_z \right) \Rightarrow \sum_{z=1}^{Q} \min_{\theta_z} (F_z)$$

<div align="right">eq. 2.80</div>

The global minimisation process is then performed under the assumption presented in that equation (2.80). There are many advantages to this distributed approach, such as reducing the enormous size of the inversion problem which must be solved.

Each subzone inversion works independently, so the total procedure involves so many different minimizations that a failure on one of the subzones due to local error minima in the error minimization process does not mean the entire reconstruction will fail. This advantage of the subzone technique increases the reliability of the reconstructions, because if a solution from a subzone fails, another set of subzones can be made to cover the region of the failed subzone and this subzone solution can simply be ignored.

At each global iterate, the centre point (the seed location) for the grid of overlapping subzones is determined randomly. In each round of dividing the geometry into the subzone grid, a different set of subzones will be implemented. This will reduce the boundary related artefacts in the final material property image. When the master processor receives the solution obtained from each zone it will be located into the correct place in the global solution arrays. There are several subzone geometry parameters which may affect the improvement of the subzone reconstruction such as zone size (subzone edge length factor), zone shape and the subzone grid overlapping. Figure 2.2 is a flowchart representing the processes employed by the algorithm.
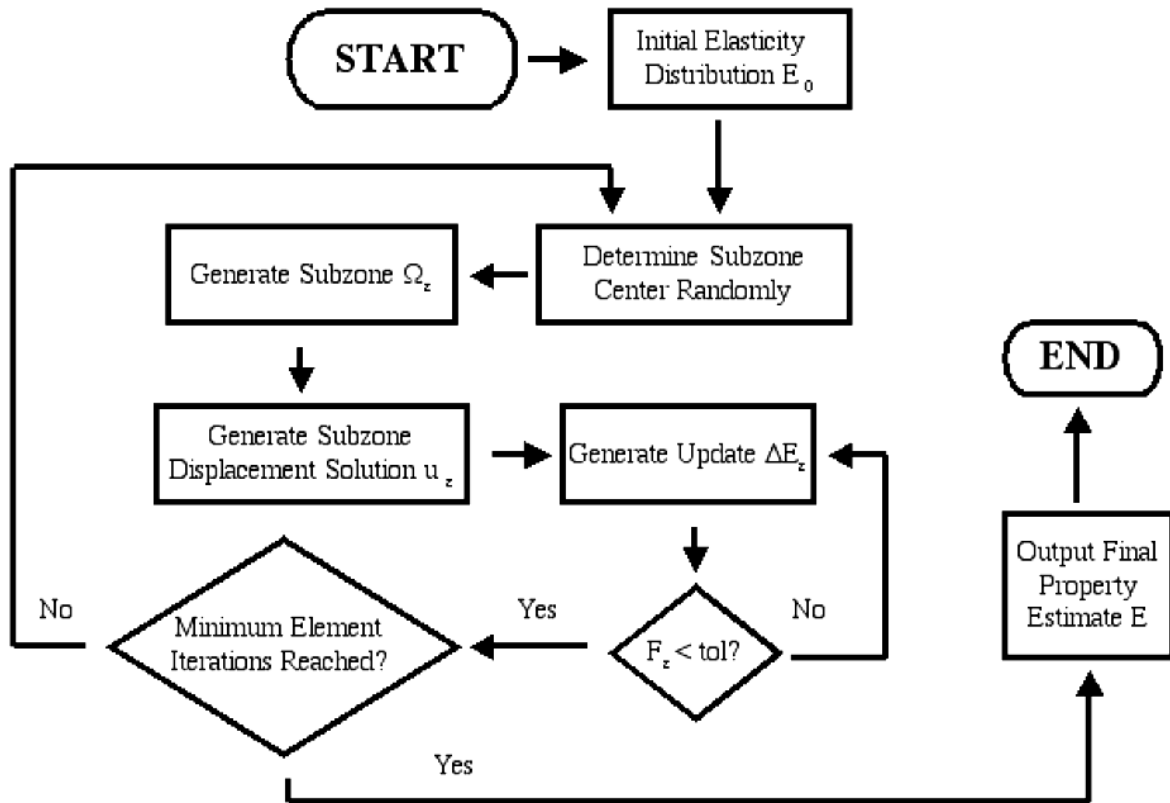
Figure 2.2: Flowchart of Subzone Inversion Algorithm

Experience has shown there is an optimum size for building the subzone grid for better reconstruction results. For example, by increasing the number of subzones in one domain and reducing the size of the each subzone, the time to run a reconstruction in one subzone will be decreased as the problem is being solved in a smaller area. However, this may cause loss of accuracy of the results as most of the internal nodes inside each subzone have sufficient data to accurately determine the underlying parameter distribution. Technically, the nodes on the boundaries are less useful in the minimization process. Thus, raising the number of subzones in one grid will lead to a higher overall ratio of boundary nodes, and this means the information from internal nodes possibly lead to reduced accuracy. In fact, the sensitivity of the boundary nodes is lower than internal nodes as they receive relatively less information. The internal nodes are surrounded on all sides by motion data while the boundary nodes only have motion data on one side. This may be shown by calculating the ratio between the internal and external nodes in one grid. Another factor is the geometry of the grid, especially in a 3-D case, which should be compatible with the physical geometry of the problem. The geometric size should be defined so that each subzone comprises at least a half wave length of the mechanical shear wave.

Chapter 3

Rayleigh Damped MRE

Both the Rayleigh Damped and Viscoelastic forms of the elastic equilibrium conditions can be investigated by considering the basic elastic shear-wave equation

$$\nabla(\mu\nabla u) = -\rho\omega^2 u$$

[Eq. 3.14]

Where μ represents the shear modulus, u represents the displacement vector, ω represents the angular frequency and ρ represents the density. A Rayleigh Damped system contains both complex valued shear modulus and density, such that

$$\rho = \rho_R + \rho_I \; \& \; \mu = \mu_R + \mu_I$$

[Eq. 3.15]

To consider the equivalent viscoelastic material (i.e. when density is purely real), we can substitute Eq. 3.14 into Eq. 3.15 and multiply both sides by $\frac{\rho_R}{\rho}$, which results in

$$-\rho_R\omega^2 = \left(\frac{\rho_R}{\rho}\right)\nabla(\mu\nabla u)$$

[Eq.3.16]

Expanding the divergence of the product $\mu\nabla u$ leads to the following

$$-\rho_R\omega^2 = \frac{\rho_R}{\rho}(\nabla\mu)\nabla u + \left(\frac{\rho_R}{\rho}\mu\right)(\nabla^2 u)$$

<div align="right">[Eq. 3.17]</div>

Given the product rule $\partial(\alpha\beta) = (\partial\alpha)\beta + \alpha(\partial\beta) \Rightarrow \alpha(\partial\beta) = \partial(\alpha\beta) - (\partial\alpha)\beta$ we can expand the first derivative term in Eq. 3.17 to

$$-\rho_R\omega^2 = \left[\nabla\left(\frac{\rho_R}{\rho}\mu\right) - \left(\nabla\left(\frac{\rho_R}{\rho}\right)\right)u\right]\nabla u + \left(\frac{\rho_R}{\rho}\mu\right)(\nabla^2 u)$$

<div align="right">[Eq. 3.18]</div>

Defining a new, *effective viscoelastic* complex shear modulus, $\bar{\mu} = \frac{\rho_R}{\rho}\mu$ and substituting into Eq. 3.18, leads to

$$-\rho_R\omega^2 = [(\nabla\bar{\mu})\nabla u + \bar{\mu}(\nabla^2 u)] - \left(\nabla\left(\frac{\rho_R}{\rho}\right)\right)u\nabla u$$

<div align="right">[Eq. 3.19]</div>

where it can be seen that only the final term, with the spatial derivative $\nabla(\frac{\rho_R}{\rho})$, is all that differentiates Eq. 3.19 from an equivalent viscoelastic system,

$$-\rho_R\omega^2 = [(\nabla\bar{\mu})\nabla u + \bar{\mu}(\nabla^2 u)] = \nabla(\bar{\mu}\nabla u)$$

<div align="right">[Eq. 3.20]</div>

Eq. 3.19 shows that, without spatial variation in density (either in the real or complex components), there is no way of distinguishing the Rayleigh Damped system described in Eq. 3.14 from the equivalent viscoelastic system described in Eq. 3.20. Therefore, the significance of the Rayleigh Damping attenuation model will only be seen at material boundaries, along the edges of material heterogeneities.

Hence Rayleigh Composition is defined as,

$$RC = \frac{\frac{\mu_I}{\mu_R}}{-\frac{\rho_I}{\rho_R} + \frac{\mu_I}{\mu_R}}$$

<div align="right">[Eq. 3.13]</div>

Where RC = 0 is a system with 0% viscoelastic behavior or RC = 1 for a 100% viscoelastic behavior.

The presence of damping forces proportional to the inertial terms in an elastic system will lead to artefacts in a viscoelastic property reconstruction of the real shear modulus. These forces in non-homogeneous regions of a material mean that the viscoelastic equilibrium equations cannot fully characterize the system dynamics. While a Rayleigh Damped approach is still a simplified model of complex materials, such as soft tissue, it will account for an additional component of the damping effect.

3.1 Gel Phantom Studies

3.1.1 Viscoelastic Reconstruction

A phantom study was conducted on a silicon phantom with two inclusions. The background material was designed to have viscoelastic behaviour manufactured with 7.8% gelatine and 10% glycerol, while the inclusions are purely elastic with 10% gelatine and $CuSO_4$ content, in the larger inclusion, and 20% gelatine and $CuSO_4$ in the smaller inclusion. This composition is designed to craft a phantom with a soft background and two stiff inclusions with the smaller inclusion being highly damped, while the latter is undamped.

Figure 3.1 shows the MR image of the phantom, with 11 coronal slices, and a 128x128 Field of View (FOV). This phantom was imaged at an actuation frequency of 125Hz in a Phillips 1.5T MRI scanner using a spin echo based phase-contrast sequence with 2mm isotropic voxels.
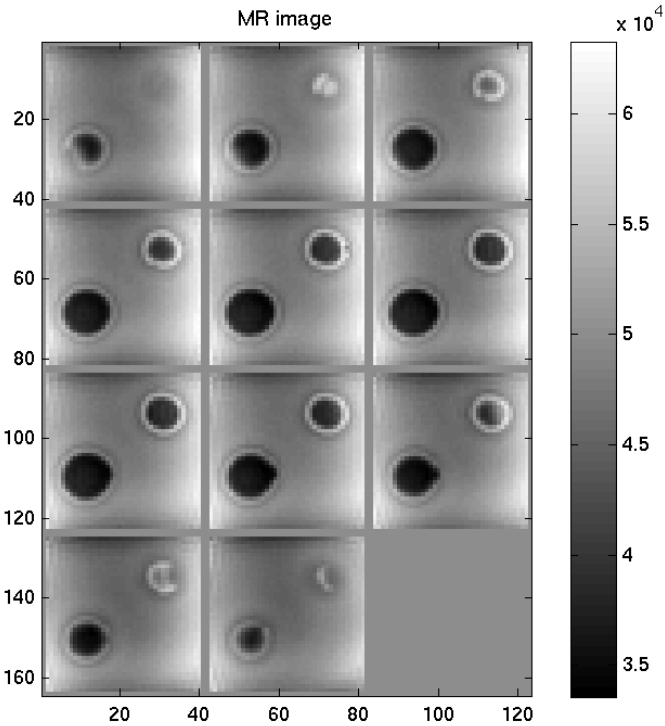
Figure 3.1: MRI of Gelatine 2 Inclusion Phantom

Figures 3.2 and 3.3 show the results from a Viscoelastic reconstruction. Figure 3.2 shows the reconstructed real shear modulus, which identifies the 2 stiffer inclusions accordingly. Figure 3.3 shows the reconstructed damping ratio which identifies the highly damped "smaller" inclusion in the top left of the phantom.
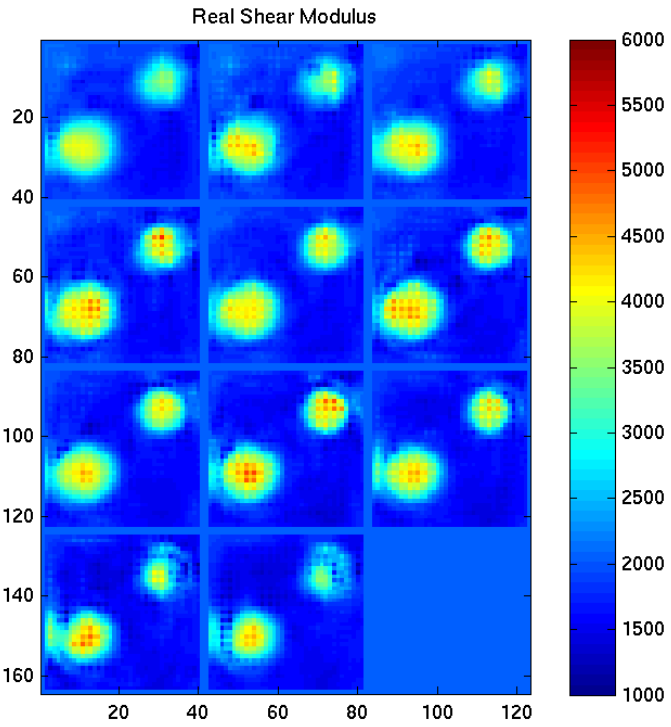
Figure 3.2: Real Shear Modulus, Viscoelastic Reconstruction on 2 Inclusion Phantom
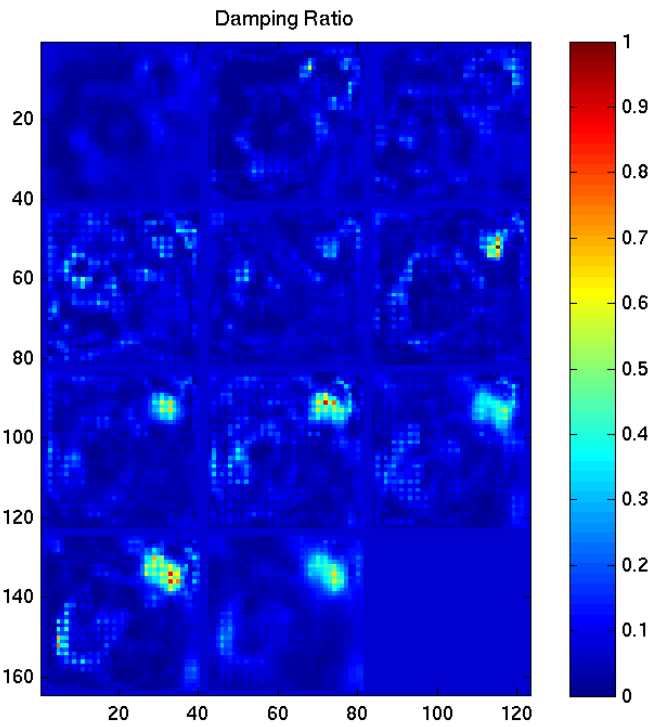
Figure 3.3: Damping Ratio, Viscoelastic Reconstruction on 2 Inclusion Phantom

3.1.2 A Simulated Rayleigh Damped Reconstruction

As a Viscoelastic reconstruction does not account for any Rayleigh damping effects, a simulation study was done for the purpose of comparison. A mesh was created to imitate the phantom under consideration. Figure 3.4 shows the simulated real shear modulus which identifies the stiff regions located in the same locations as the phantom's inclusions.

Figure 3.5 shows the simulated damping ratio, which identifies higher damping in both of the stiffer regions. This is due to the simplistic nature of the simulation. Once again the result is indicative of the actual phantom structure. Figure 3.6 is the simulated Rayleigh composition, which as expected identifies both of the stiffer regions.
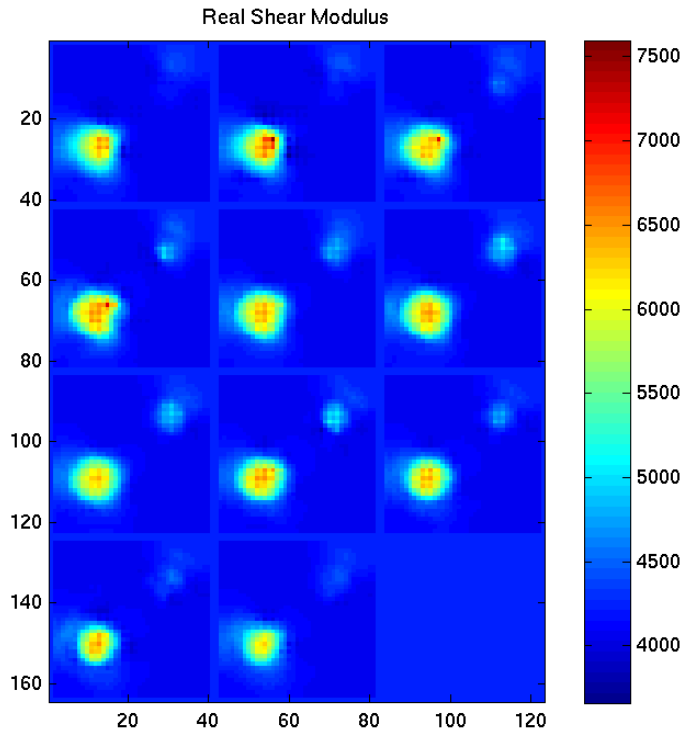
Figure 3.4: Real Shear Modulus, Simulated RD reconstruction on 2 Inclusion Phantom
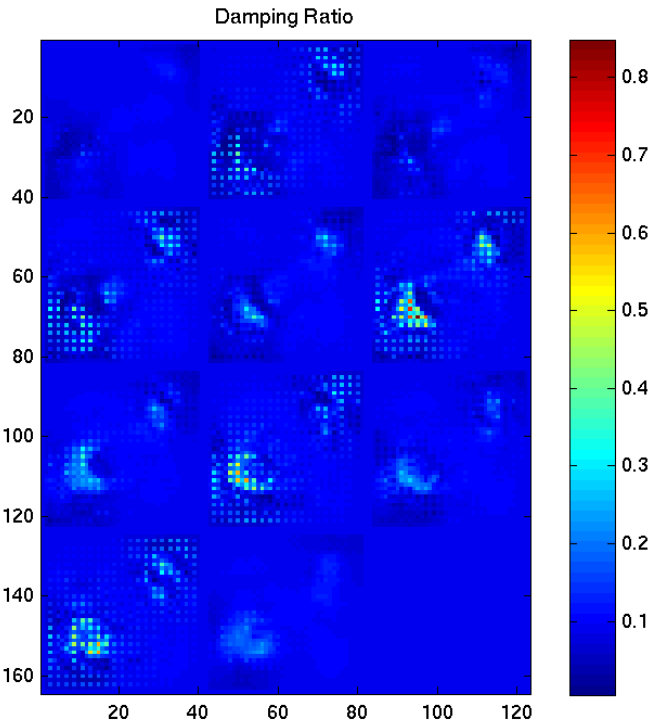
Figure 3.5: Damping Ratio, Simulated RD reconstruction on 2 Inclusion Phantom
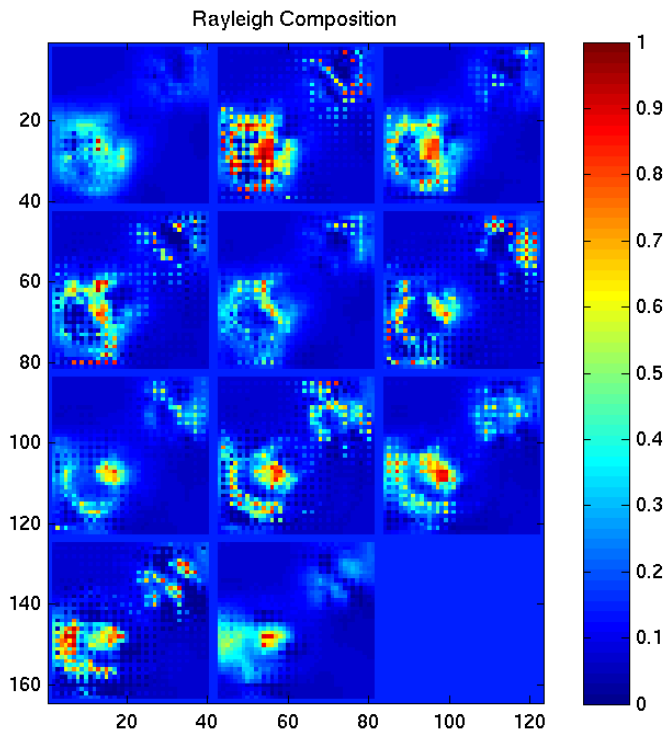
Figure 3.6: Rayleigh Composition, Simulated RD reconstruction on 2 Inclusion Phantom

28

3.1.3 Rayleigh Damped Reconstruction

Figure 3.7 shows the reconstructed real shear modulus which identifies both of the stiffer inclusions. Figure 3.8 shows the reconstructed damping ratio, which identifies high damping in the smaller inclusion, similarly to the Viscoelastic reconstruction. Figure 3.9 is the reconstructed Rayleigh composition, which shows a distribution of artefacts in the homogenous background material. According to the original proof and the inherent nature of a Rayleigh Damped approximation this result is appropriate. However despite the presence of artefacts the phantoms actual structure and the presence of two inclusions is still clear.

Enforcing a Total Variation Minimization (TV) should improve the condition of solutions for the Rayleigh Composition within the homogeneous regions by penalizing movement away from well defined values ascertained at material boundaries. The current reconstruction was done with a TV threshold of 1e-9.
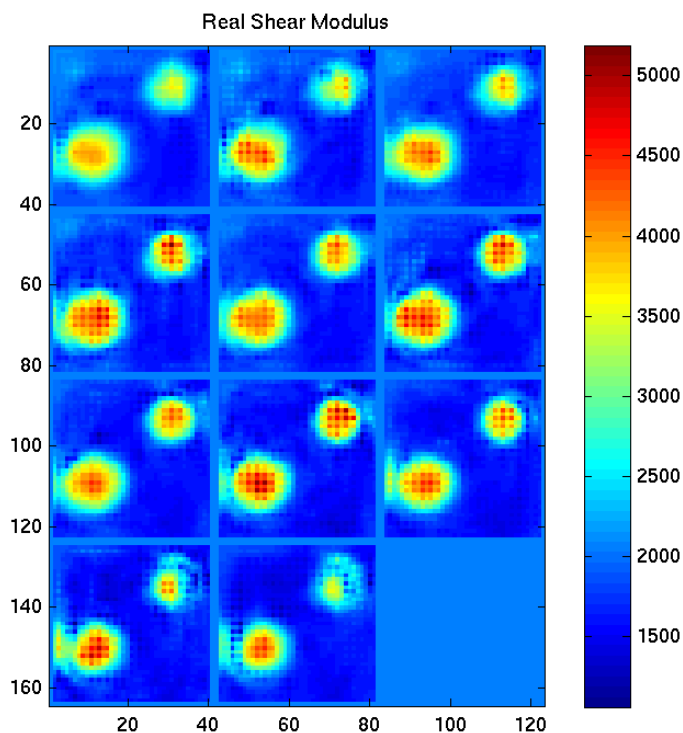
Figure 3.7: Real Shear Modulus, Rayleigh Damped reconstruction on 2 Inclusion Phantom

29
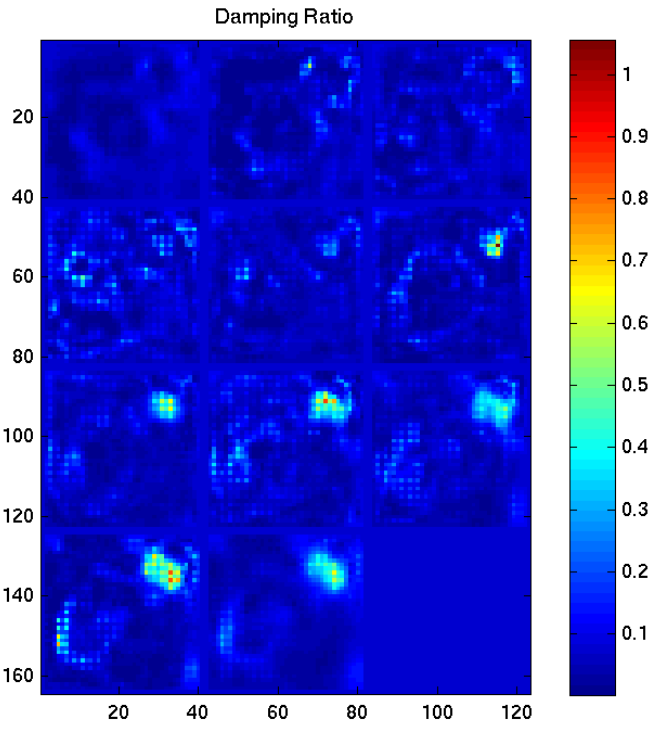
Figure 3.8: Damping Ratio, Rayleigh Damped reconstruction on 2 Inclusion Phantom
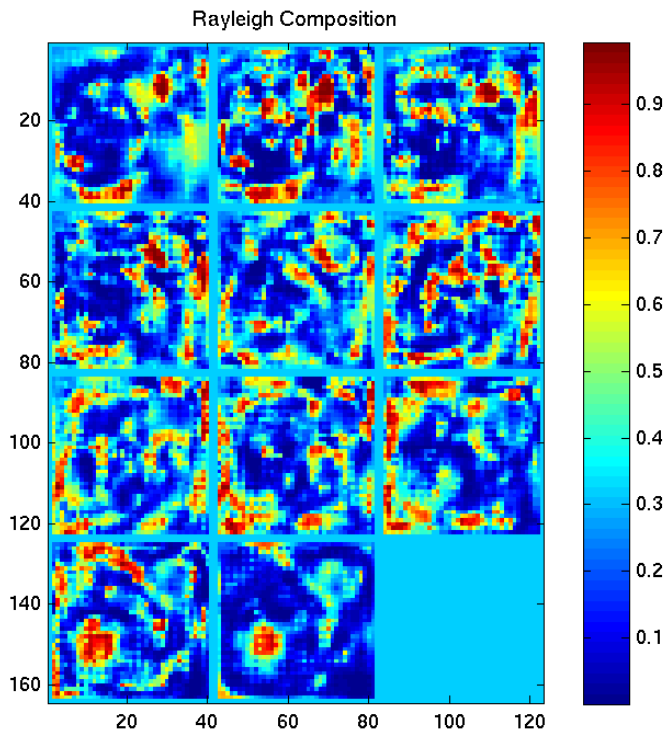
Figure 3.9: Rayleigh Composition, Rayleigh Damped reconstruction on 2 Inclusion Phantom

3.1.4 Rayleigh Damped Reconstruction with High TV

A TV threshold of 1e-6 was established to be the highest TV at which the reconstruction converged on a suitable solution. Figure 3.10 shows the reconstructed real shear modulus which identifies both of the stiffer inclusions. However the smoothing effects of the TV are apparent, though the overall structure of the phantom is not compromised.

Figure 3.11 shows the reconstructed damping ratio, which once again identifies high damping in the smaller inclusion. However the result is less clearly defined due to the applied TV minimisation. Figure 3.12 is the reconstructed Rayleigh composition, which shows a distribution of artefacts in the homogenous background material. With the higher TV applied the resulting reconstruction is more clearly defined, with a noticeable correlation to the phantom structure.
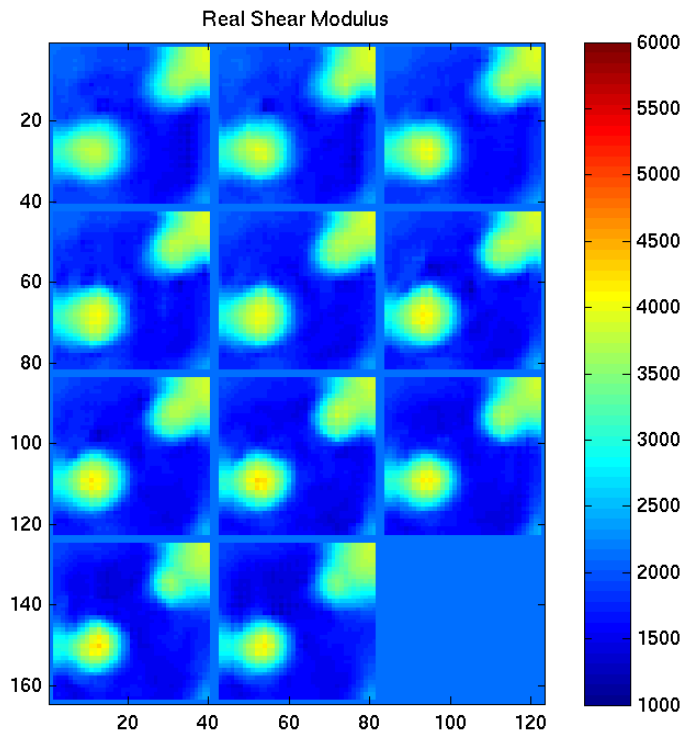
Figure 3.10: Rayleigh Composition, Rayleigh Damped reconstruction (high TV) on 2 Inclusion Phantom
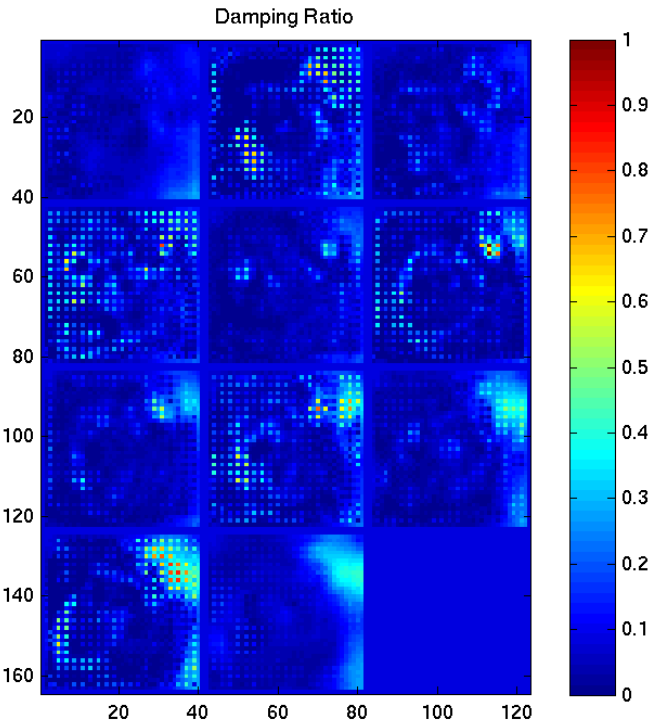
Figure 3.11: Rayleigh Composition, Rayleigh Damped reconstruction (high TV) on 2 Inclusion Phantom
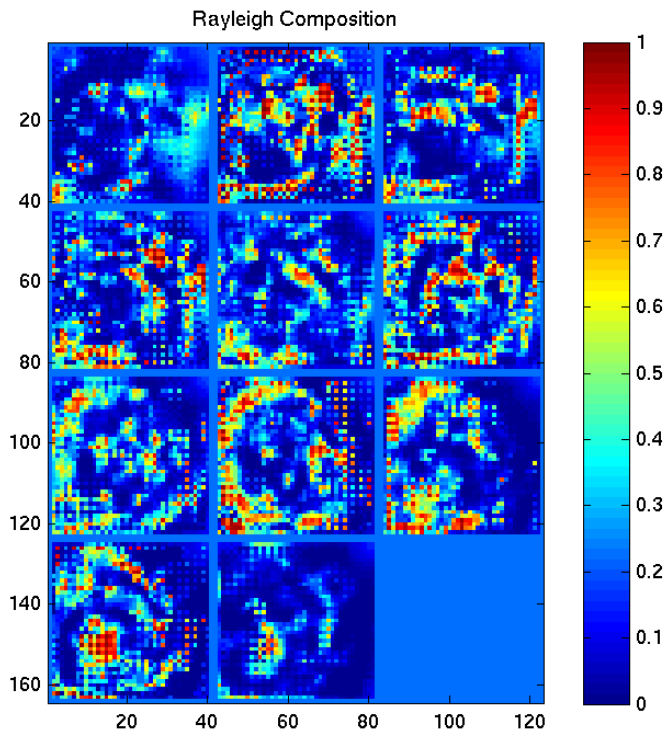
Figure 3.12: Rayleigh Composition, Rayleigh Damped reconstruction (high TV) on 2 Inclusion Phantom

Figure 3.13: Superimposed MRI of sample regions, background, large inclusion and small inclusion respectively

	Real Shear Modulus (Pa)				Damping Ratio (%/100)				Rayleigh Composition (%/100)			
	mean	std dev	max	min	mean	std dev	max	min	mean	std dev	max	min
Phantom Properties												
Background	1500											
Small Inclusion	3500											
Large Inclusion	4000											
Viscoelastic												
Background	2113	37.49	2177	3727	0.111	0.0101	0.193	0.057				
Small Inclusion	4065	381.22	5381	2874	0.382	0.227	0.827	0.143				
Large Inclusion	4256	477.13	5582	1852	0.167	0.104	0.4	0.0899				
Simulated RD												
Background	4112	27.23	4196	4004	0.1004	0.0649	0.1927	0.0305	0.1151	0.0713	0.15667	0.000131
Small Inclusion	4919	210.34	5676	4021	0.2444	0.1712	0.3512	0.181826	0.309409	0.214521	0.808158	0.103056
Large Inclusion	5997	379.11	7112	5226	0.39821	0.2272	0.44301	0.24298	0.639107	0.346034	0.902233	0.210732
Rayleigh Damped (TV = 1e-9)												
Background	1835	56.75	2579	1337	0.054191	0.0337	0.44513	0.00209	0.2843	0.21842	0.97724	0.001752
Small Inclusion	3873	406.57	4911	1902	0.27831	0.21581	1.4331	0.01153	0.3206	0.20909	0.95787	0.096606
Large Inclusion	4171	245.58	4759	3443	0.06319	0.04539	0.43966	0.005017	0.330375	0.29553	0.91141	0.010115
Rayleigh Damped (TV = 1e-6)												
Background	1647	126.6667	2130	1290	0.0658	0.0413	0.4896	0.003	0.23516	0.22099	0.98165	0.00102
Small Inclusion	3216	216.07	3583	2679	0.22885	0.12781	0.7445	0.03692	0.13268	0.11323	0.75764	0.00241
Large Inclusion	3633	267.43	4382	2829	0.059188	0.0913	0.6574	0.00202	0.33759	0.31059	0.99382	0.001579

Table 3.1: Table of gel phantom reconstruction results analysed from sample regions

Figure 3.13 show select regions used to conduct a numerical analysis of all the aforementioned reconstructions. These results are displayed in Table 3.1. The numerical results indicate that the separate inclusions are poorly distinguished by the Viscoelastic reconstruction as well as the Rayleigh Damped reconstruction with the low TV threshold (1e-9).

The Rayleigh Damped reconstruction with a higher TV threshold (1e-6) had very promising results. The reconstructed real shear modulus values were lower than actual phantom values, most likely due to the applied smoothing such as the TV minimisation, mixing of the inclusion and background material during construction and the continuity requirements of the finite element based elastic modulus description.

If we consider the numerical result for each parameter, the real shear modulus values from the reconstruction are within 10% of the estimated phantom values. The three regions within the phantom have only two clear damping ratios, i.e. the larger undamped inclusion melds with the softer background. The Rayleigh Composition values, however, have the inclusions varying by approximately 50% increase or decrease with respect to the background for the undamped and highly damped inclusions respectively. Hence the three material regions in the phantom are individually defined by shear stiffness, a high or low damped response and a percentage measure of Viscoelastic behaviour.

3.2 Tofu Phantom Studies

A tofu phantom study was conducted to investigate the different attenuation behaviour in phantoms with separate material compositions. The two tofu phantoms considered were crafted from *Mori-Nu Silken Soft* tofu, to form the soft background material. Tofu is a commonly used material in elastography as it has a poro-elastic structure with high water content, similar in nature to soft tissue. The phantoms were all imaged at a frequency of 100 Hz, in a Phillips 1.5T MRI scanner using a spin echo based phase-contrast sequence with 2mm isotropic voxels, and 128x128 FOV. The stiff gelatine inclusions were mixed from 10% Sigma Aldrich porcine skin gelatine. A complete homogenous gelatine phantom was also made to determine the various material properties of this mixture for better numerical analysis. The results from a Rayleigh Damped and Viscoelastic reconstructions and DMA analysis are presented in Table 3.2.

	Real Shear Modulus (Pa)			Damping Ratio (%)			Rayleigh Composition (%)	
	mean	std dev		mean	std dev		mean	std dev
RD Recon	8056	623		7.52	5.07		64.18	25.08
VE Recon	8952	1634		9.56	10.43			
DMA	8800	900		6.09	0.13			

Table 3.2: Homogeneous 10% gelatine phantom properties

3.2.1 Single Inclusion Tofu Phantom (T-16)

The single inclusion tofu phantom was created as rectangular tofu volume with a cylindrical gelatine inclusion located in the centre. Figure 3.14 shows the MR image of the phantom, with 17 coronal slices.
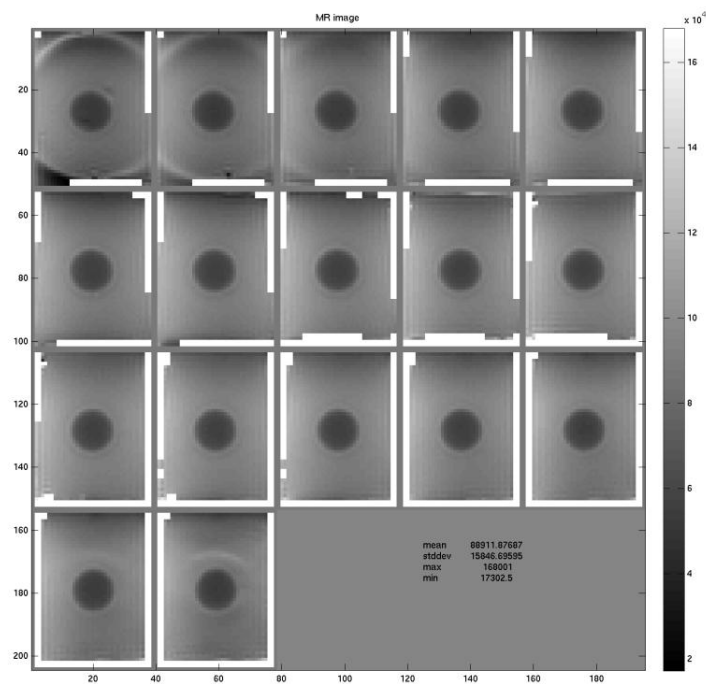
Figure 3.14: MRI of Tofu T-16 Single Inclusion phantom

The Rayleigh Damped reconstruction results are presented in Figures 3.15 through 3.17, with real shear modulus, damping ratio and Rayleigh composition respectively. The reconstruction clearly identifies the stiffer inclusion in the real shear modulus image, however only minor damping effects are observed near the boundaries. The Rayleigh composition image identifies the phantom structure with the expected presence of some artefacts.

Figure 3.15: Rayleigh Damped reconstruction of Real Shear Modulus

Figure 3.16: Rayleigh Damper reconstruction of the Damping Ratio

Figure 3.17: Rayleigh Damped reconstruction of the Rayleigh Composition

The Viscoelastic reconstruction results are presented in Figures 3.18 and 3.19, with real shear modulus and damping ratio respectively. The results are similar to the Rayleigh Damped reconstruction. The stiffer inclusion is clearly represented in the real shear modulus image. Again the damping ratio only exhibits minor effects near the material boundaries. This most likely caused by the adhesion between the tofu and the gel inclusions.
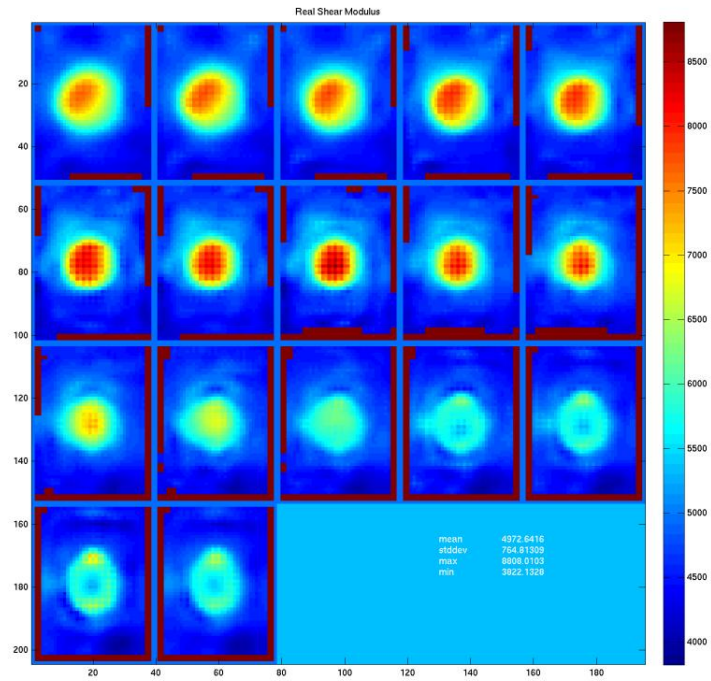
Figure 3.18: Viscoelastic reconstruction of Real Shear Modulus

Figure 3.19: Viscoelastic reconstruction of the Damping Ratio

38
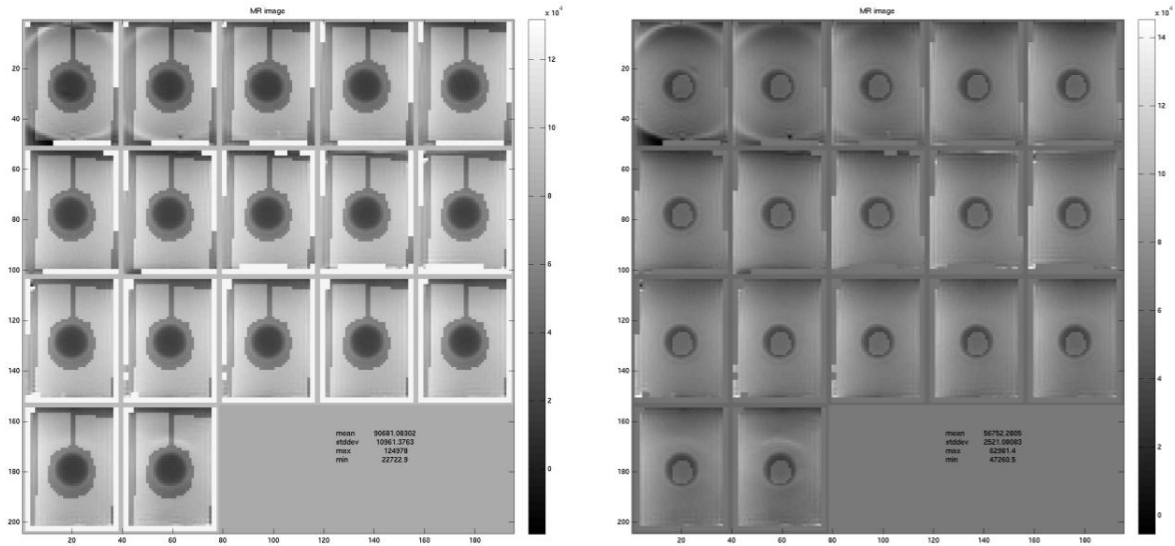
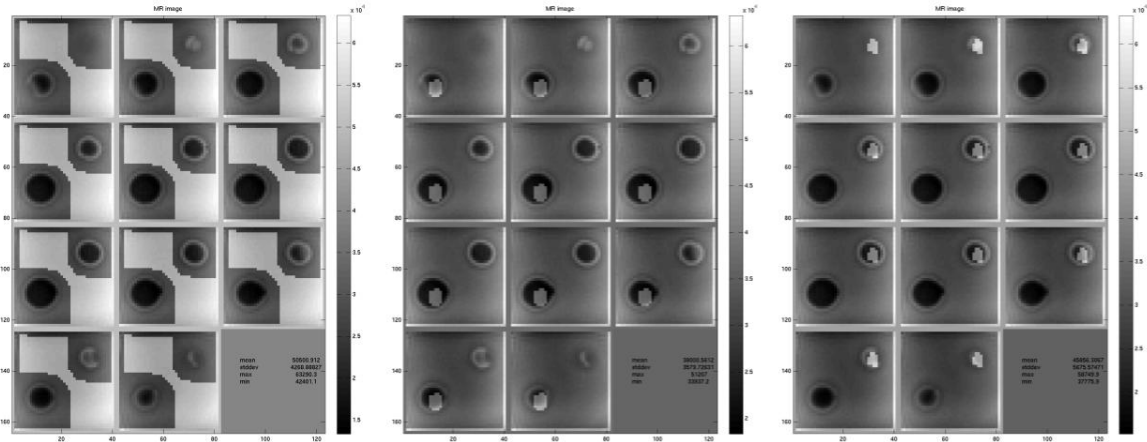**Figure 3.20**: Superimposed MRI of sample regions, background and inclusion respectively

		Real Shear Modulus (Pa)			Damping Ratio (%)			Rayleigh Composition (%)	
		mean	std dev		mean	std dev		mean	std dev
RD Recon									
	Tofu	4863	556		4.75	2.45		14	12.3
	Gel Incl.	9021	1039		1.06	0.95		33.86	22.39
VE Recon									
	Tofu	4810	667		2.35	1.17			
	Gel Incl.	9470	1176		0.81	0.8			
DMA									
	Tofu	7203	989		11.2	4.45			
	Gel Incl.	10236	3860		10.94	14.9			

Table 3.3: Table of single inclusion tofu phantom reconstruction results analysed from sample regions

Figure 3.20 show select regions used to conduct a numerical analysis of all the aforementioned reconstructions. These results are displayed in Table 3.3. The Rayleigh Damped and Viscoelastic reconstructions had similar results for real shear modulus and damping ratio, though both reconstructions were numerically lower than the measured phantom properties, this is likely a result of mixing between the stiff gelatine material and the surrounding soft tofu as well as the continuity requirements of the finite element based elastic modulus description. The Rayleigh composition however showed approximately a 242% increase within the inclusion providing a strong contrast between the materials.

3.2.2 Two Inclusion Tofu Phantom (T-21)

The second tofu phantom was created as a rectangular tofu volume with two cylindrical gelatine inclusion located. Figure 3.14 shows the MR image of the phantom, with 15 coronal slices. The top inclusion is highly damped for this phantom while the lower inclusion remains similar to the tofu, as in the T-16 phantom case above.
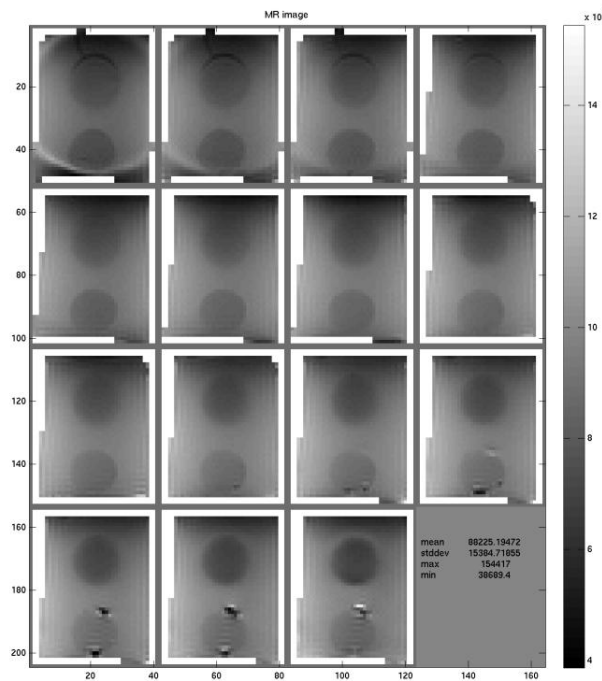
Figure 3.21: MRI of Tofu T-21 Two Inclusion Phantom

The Rayleigh Damped reconstruction results are presented in Figures 3.22 through 3.24, with real shear modulus, damping ratio and Rayleigh composition respectively. The reconstruction identifies the two stiffer inclusions in the real shear modulus image, with TV set to 1e-6 the image displays some melding effects. The damping effects observed show nearly no contrast between the tofu and either inclusion except near the base of the top cylinder, shown in the later slices. This is most likely due to a "settling" effect from mixing a highly damped gelatine cylinder. The Rayleigh composition image identifies both inclusions with noticeable response to the change in damping in the top cylinder.
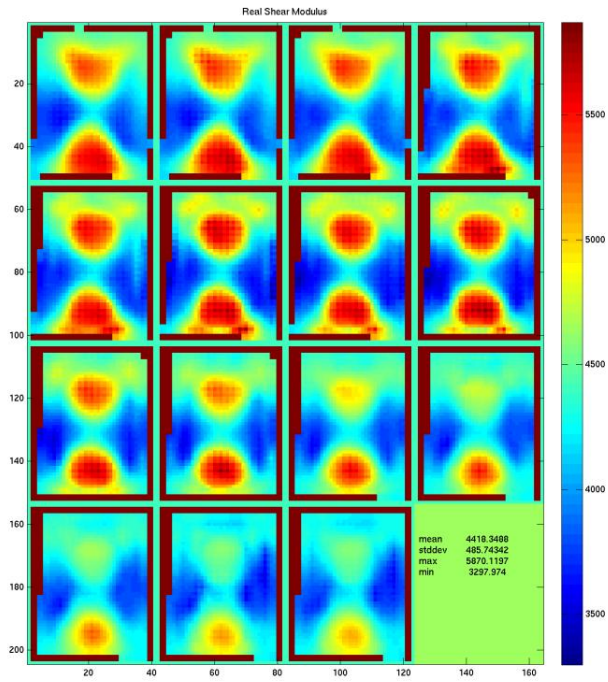
Figure 3.22: Rayleigh Damped reconstruction of Real Shear Modulus
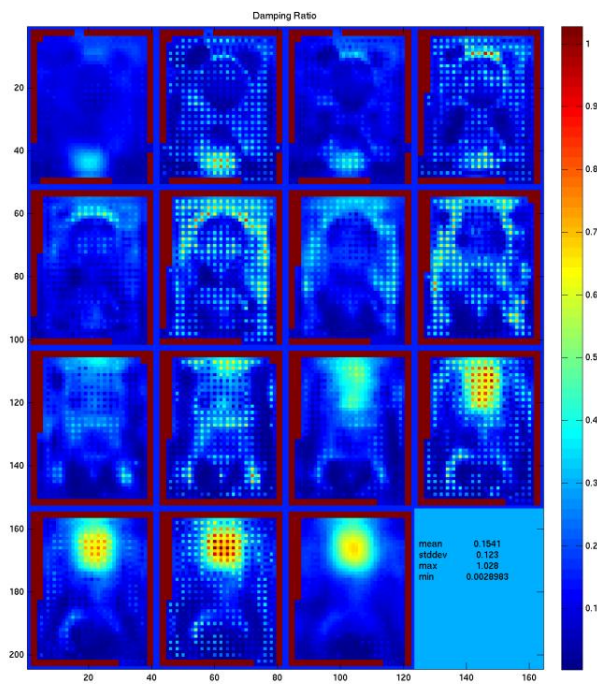
Figure 3.23: Rayleigh Damped reconstruction of the Damping Ratio
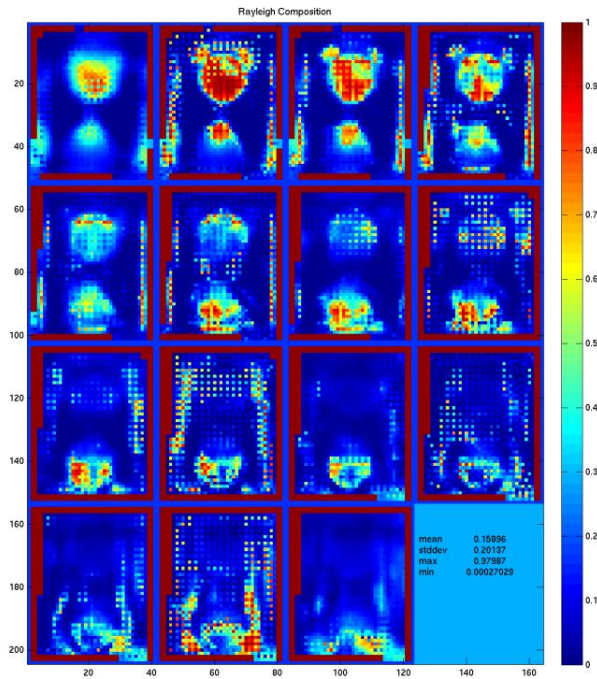
Figure 3.24: Rayleigh Damped reconstruction of the Rayleigh Composition

The Viscoelastic reconstruction results are presented in Figures 3.25 and 3.26, with real shear modulus and damping ratio respectively. The results are similar to the Rayleigh Damped reconstruction. The stiffer inclusions are more clearly represented in this reconstruction of the real shear modulus image, (TV here is set to 1e-9). The damping ratio again, only exhibits minor effects throughout except near the base of the top cylinder which is highly damped.
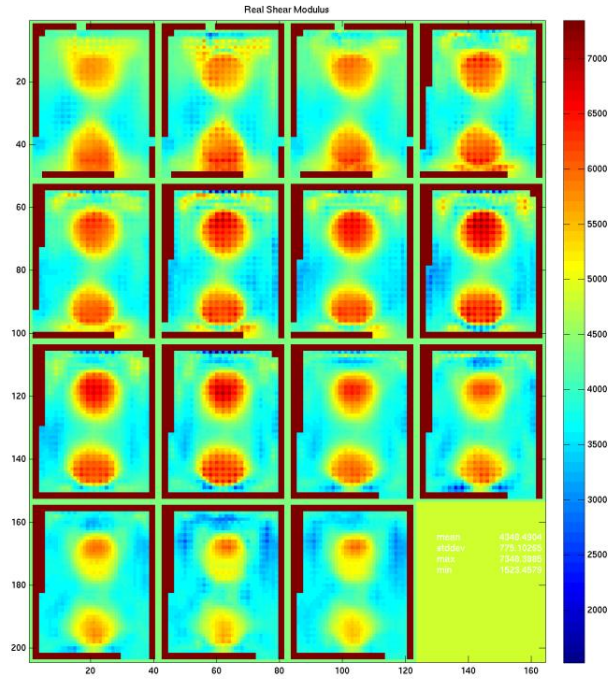
Figure 3.25: Viscoelastic reconstruction of the Real shear Modulus
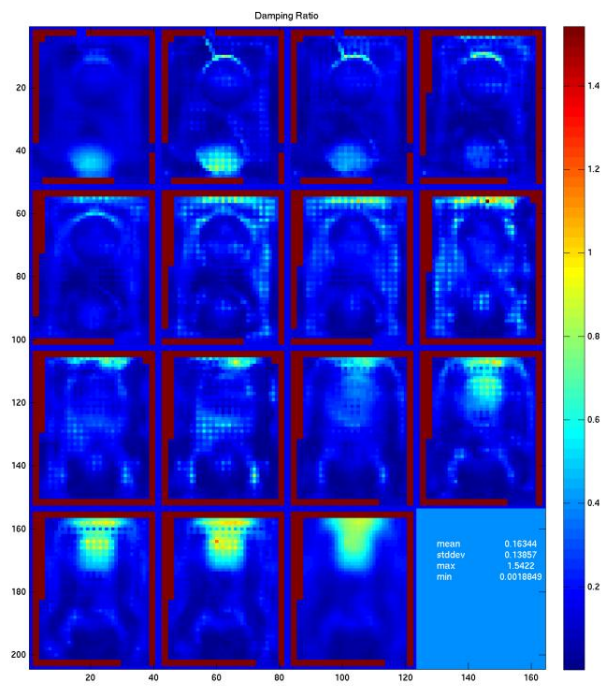
Figure 3.26: Viscoelastic reconstruction of the Damping Ratio
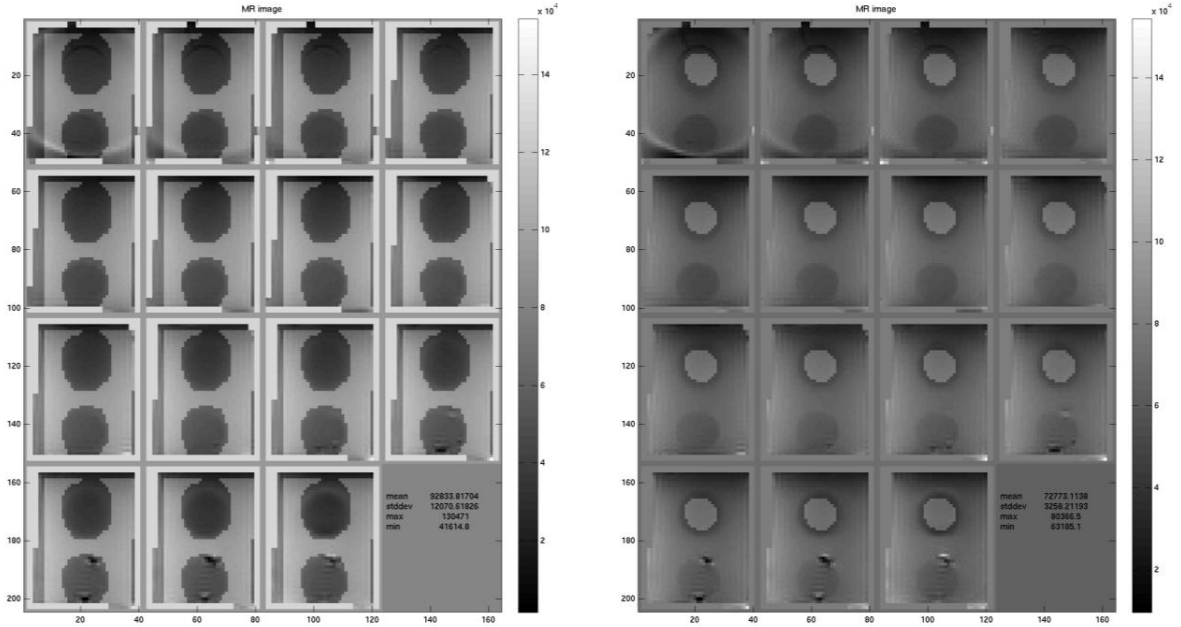
Figure 3.27: Superimposed MRI of sample regions, background and inclusion respectively

		Real Shear Modulus (Pa)		Damping Ratio (%)			Rayleigh Composition (%)	
		mean	std dev		mean	std dev		mean	std dev
RD Recon									
	Tofu	4195	351		13.64	9.45		10.7	16.3
	Gel Incl.	5015	348		24.98	18.65		29.95	18.37
VE Recon									
	Tofu	3986	390		13.16	9.06			
	Gel Incl.	5646	451		25.2	16.19			
DMA									
	Tofu	7203	989		11.2	4.45			
	Gel Incl.	10236	3860		10.94	14.9			

Table 3.4: Table of two inclusion tofu phantom reconstruction results analysed from sample regions

Figure 3.27 show select regions used to conduct a numerical analysis of all the aforementioned reconstructions. These results are displayed in Table 3.4. The Rayleigh Damped and Viscoelastic reconstructions had similar results for real shear modulus and damping ratio, as before the reconstructions are numerically lower than the measured phantom properties. The damping ratios in both reconstructions identify the highly damped inclusion, with approximately double the damping of the tofu background. The Rayleigh composition has a 280% contrast between the inclusion and the background. This is approximately 40% higher than T-16 phantom result, which could be attributed the higher damping value.

3.3. In Vivo Results

A Rayleigh damped reconstruction was performed on motion data obtained from a cancer patient undergoing neoadjuvant chemotherapy. This data was captured at 85 Hz with similar MRI setting to the previous studies outlined above. The reconstruction result were compared to the mechanical properties of breast tissue determined by Viscoelastic based MRE result from (Sinkus et al, 2005 [25]). Taken at 65 Hz. Figure 3.28 shows the MR image for the patient, with 7 coronal slices.
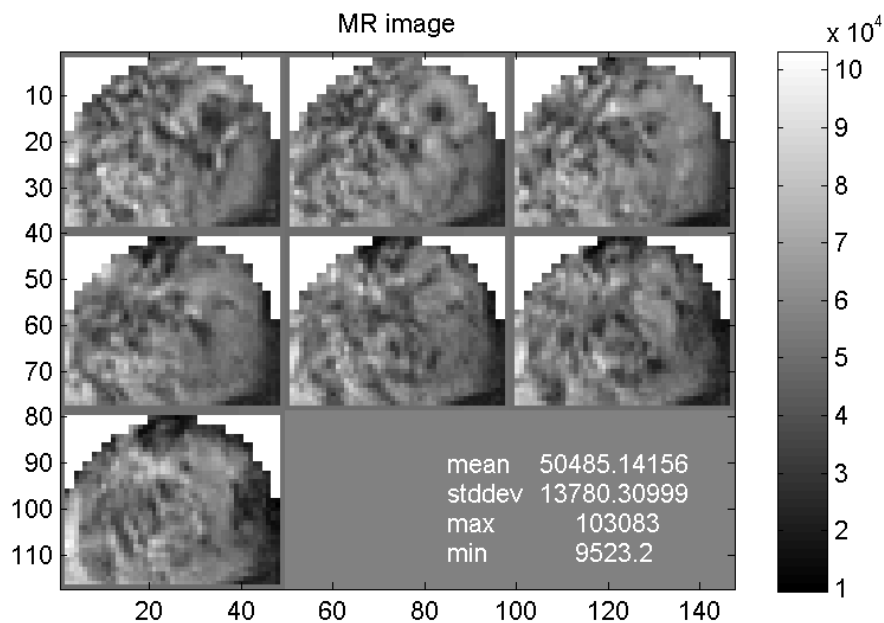
Figure 3.28: T2* MRI of Patient 3004-S2

Figures 3.29, 3.30 and 3.31 present the reconstruction results for real shear modulus, damping ratio and Rayleigh composition respectively. The tumour is clearly visible, in the real shear modulus image, as the bright stiff region on the left hand side. The damping ratio is almost uniformly low throughput the breast with no noticeable damping effects in the region of the tumour. The Rayleigh composition appears to respond to the presence of a tumour, however as previously determined there are some artefacts in the image as well.
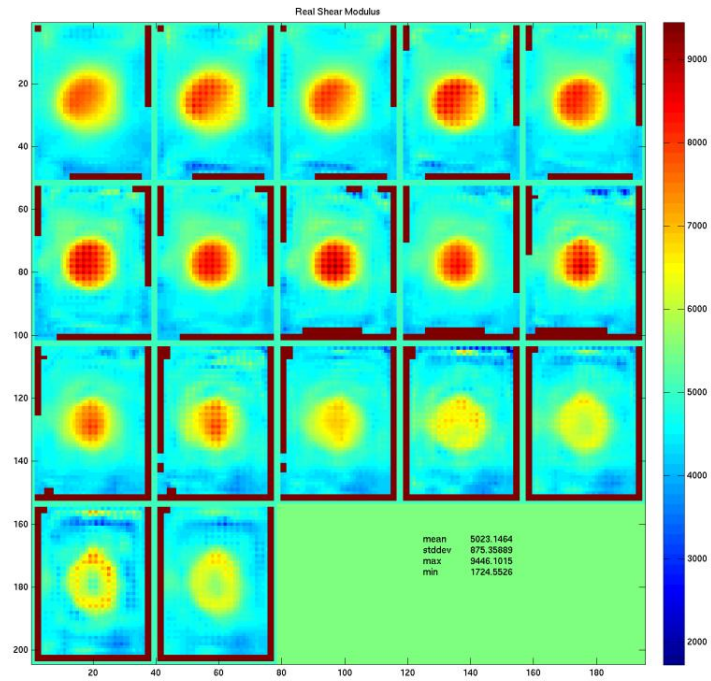
45
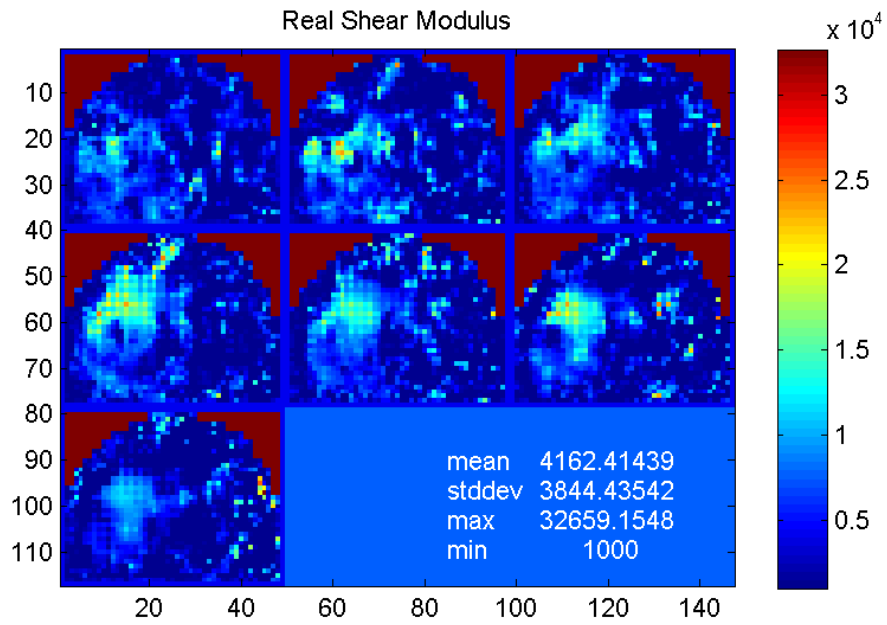
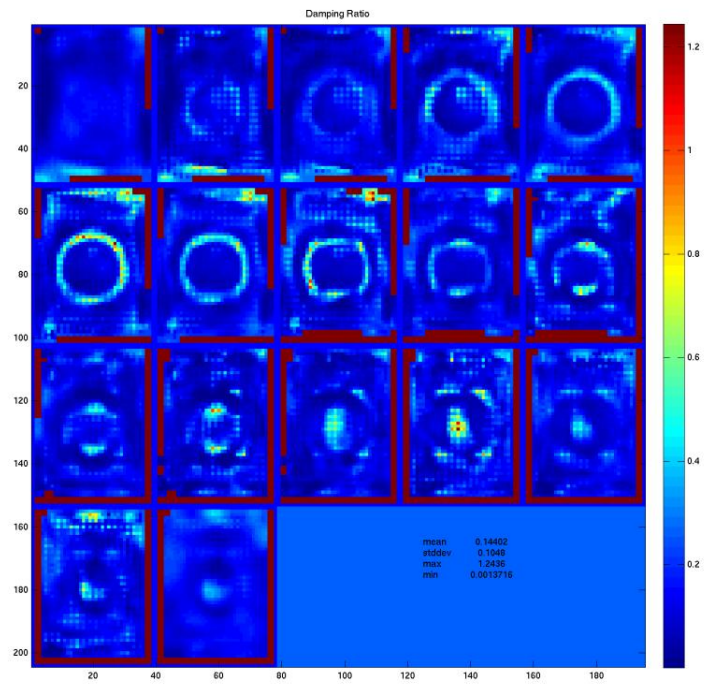**Figure 3.29**: Rayleigh Damped Reconstruction of the Real Shear Modulus
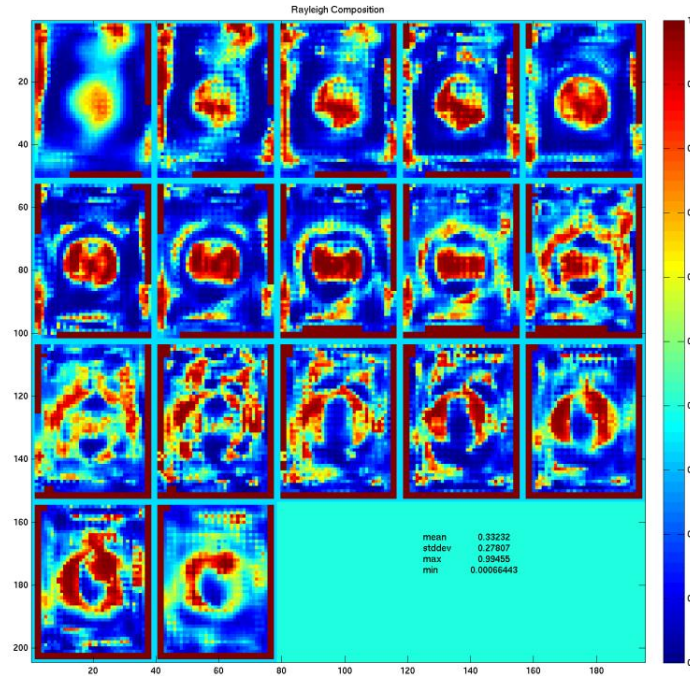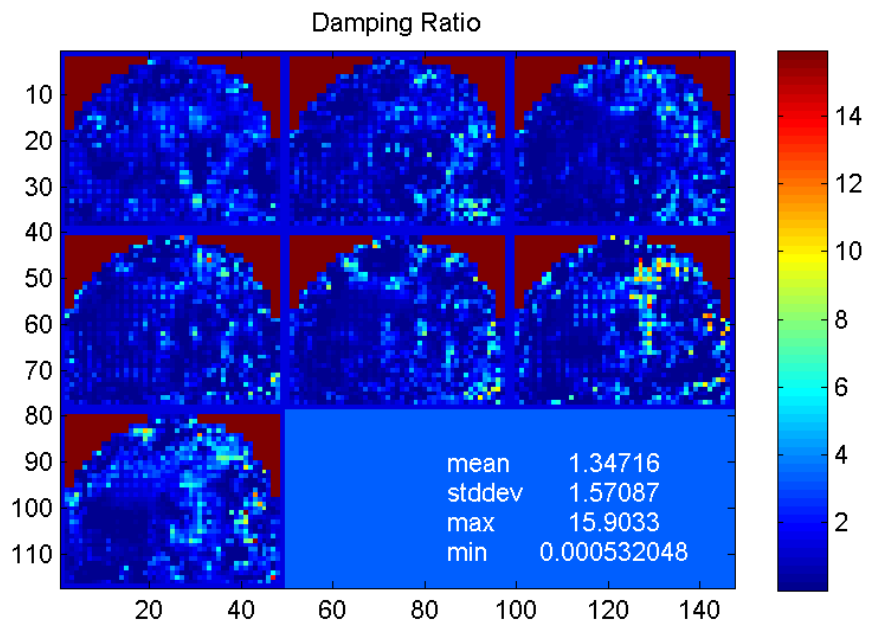

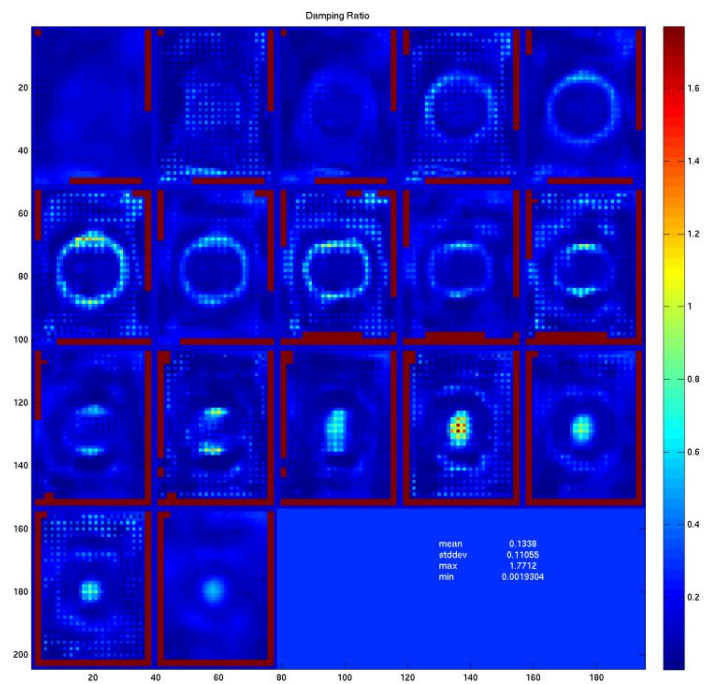
Figure 3.30: Rayleigh Damped Reconstruction of the Damping Ratio

46
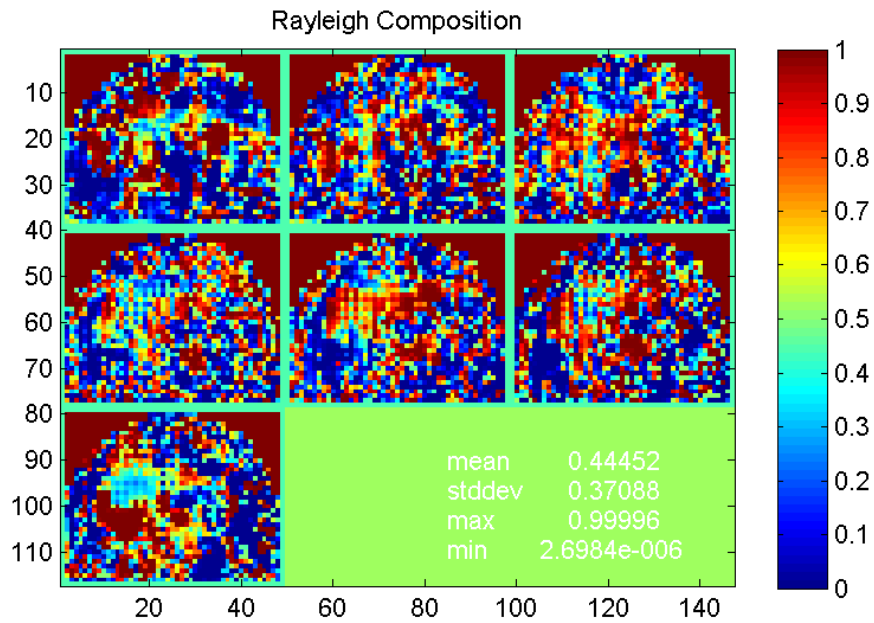
Figure 3.31: Rayleigh Damped Reconstruction of the Rayleigh Composition

Figures 3.32 and 3.33 show the regions selected to represent healthy and cancerous tissue respectively. These results are compared in Table 3.5 to the tissue properties presented (Sinkus et al, 2005 [25]).
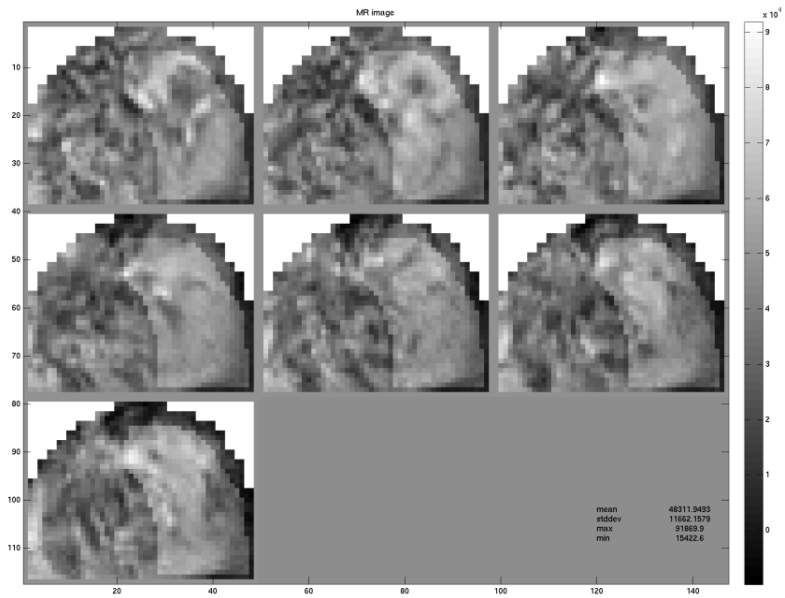
Figure 3.32: Superimposed MRI of sample region of healthy tissue
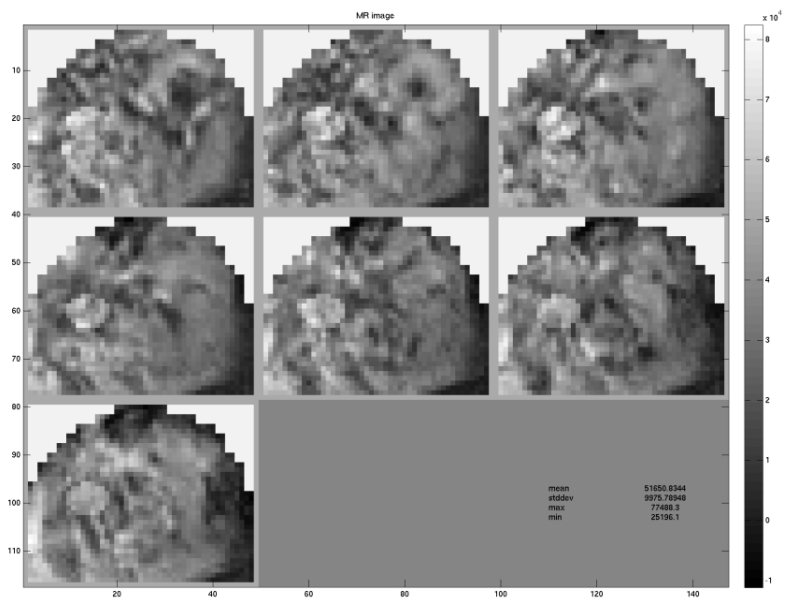
Figure 3.33: Superimposed MRI of sample region of cancerous tissue

		Real Shear Modulus (Pa)			Damping Ratio (%)			Rayleigh Composition (%)	
		mean	std dev		mean	std dev		mean	std dev
RD Recon									
	Healthy	2964	3100		173.45	186.13		43.57	37.58
	Cancer	10681	4247		73.36	62.99		63.81	28.61
VE Recon									
	Healthy	870	150		12.8	0.61			
	Cancer	2900	300		158.31	103.33			

Table 3.5: Patient data reconstruction results analysed from sample regions, tissue properties from [25].

The numerical results from the Rayleigh Damped reconstruction are much higher than the tissue values determined by (Sinkus et al, 2005 [25]). This could be due to several factors, namely the actuation frequency 65 Hz as opposed to 85 Hz, the actuation methods including the pre-compression of the tissue, excitation source and mode (Xydeas et al, 2005 [26]).

The reconstructed real shear modulus shows cancer to be three times stiffer than healthy breast tissue. While not numerically similar, there is a consistent ratio in both cases. The Rayleigh damped model however has much lower damping in the cancer and much higher damping in the healthy tissue, this is most likely due to the differences in measurement methods, however could also be attributed to the regions under consideration. The selected "healthy" tissue region is comprised of fatty tissue, which is highly saturated. Hence it is reasonable to expect higher levels of damping as opposed to the fibrous tissue located immediately adjacent to the tumour. The Rayleigh composition result is very promising showing approximately 150% contrast between health and cancerous tissue.

The reconstructions presented clearly show that the Rayleigh damped method produced comparable results to the Viscoelastic method. The additional parameter, Rayleigh composition, had a distinct contrast in different material regions and identified the pathology in the patient. This would suggest that there is great potential for Rayleigh composition to contribute to a diagnostic model, which uniquely characterizes malignant breast cancer from at least three reconstructed parameters.

Chapter 4

Scattering and Dispersion

4.1 Rayleigh Scattering Simulation

A simulation study was designed to analyse scattering and dispersive effects from an elastic shear wave in soft tissue, where the complex internal structure of fibrous tissue could potentially produce scattering behaviour. A highly one dimensional mesh was generated (i.e. a mesh with a distinct principle length), with a single boundary surface. The mesh used standard 4-node tetrahedral elements. The mesh length was selected to be approximately ten wavelengths. Two separate cases were considered, firstly a mesh with scatterers present in the initial half of the mesh, and secondly a mesh with scatterers present throughout a lateral half of the mesh.

These mesh characteristics can be seen in Figures 4.1 through 4.3. The boundary surface was actuated at 100 Hz to propagate an elastic shear wave. The mesh material had a Young's modulus of 15 KPa and poison's ratio of 0.48 with approximately 5% damping, similar to soft tissue.
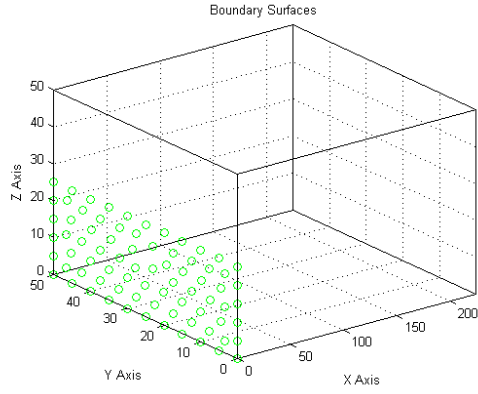
Figure 4.1: Simulation Boundary Surface
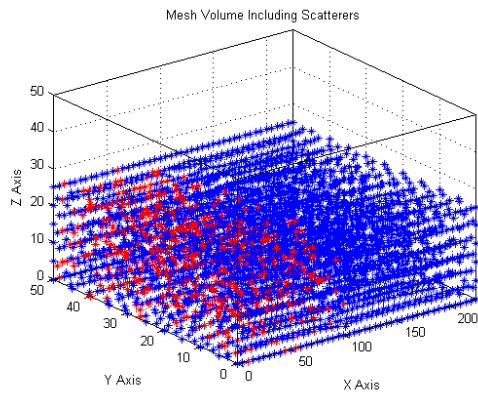
Figure 4.2: Simulation Node Mesh with Scatterers in the initial half
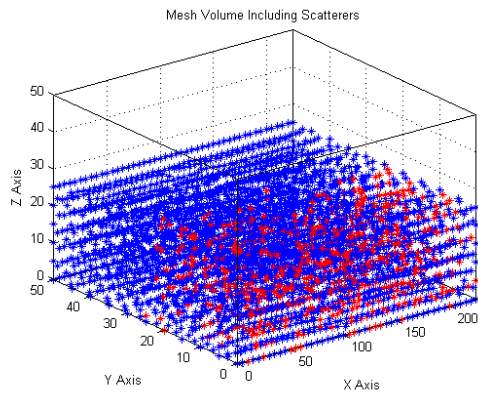
Figure 4.3: Simulation Node Mesh with Scatterers in the lateral half

Four possible scattering conditions were simulated, namely 10% or 20% scatterer density and scatterers that 10 or 100 times stiffer than the background.

51

$$x = \frac{2\pi r}{\lambda}$$

[Eq. 4.1]

Scatterer size was equivalent to a single element, which ensured the scatterer size was much less than 1 according to the Rayleigh scattering formulation in Eq. 4.1, where x is the scatterer size, r the characteristic dimension and λ the wavelength.

The simulation results were converted into an MRI voxel format and transposed onto hex27 mesh to be reconstructed using the Rayleigh damped algorithm. This follows the standard reconstruction methods used for phantom and in vivo analysis.

4.1.1 Initial Half Scattering Reconstruction

This simulation placed scatterers in the initial half of the phantom so that the shear wave would travel through sections of scattering and no scattering in series. Figure 4.4 shows the artificial MR image for the reconstruction. There are 9 coronal slices with the actuated boundary located at the top of the slice as displayed in the image.
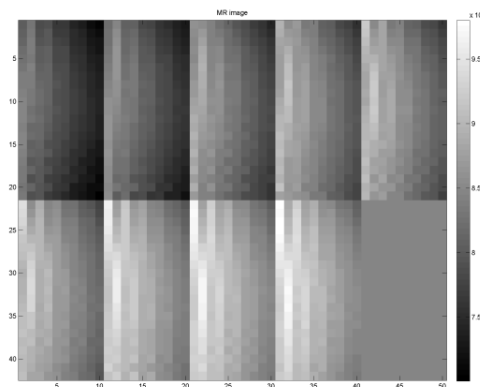
Figure 4.4: Artificial MRI image for reconstructed mesh

The first set of scattering conditions is a scattering density of 10% with all scatterers approximately 10 times stiffer than the background. Figure 4.5 displays the damping ratio, which is almost entirely unaffected by the presence of scatterers, with low damping throughout the mesh. Figure 4.6 displays the Rayleigh composition which appears to respond to the scatterers, suggesting higher viscoelastic behaviour in the scattering region. Figure 4.7 displays the reconstructed real shear modulus which is mostly homogeneous with a slight increase in stiffness in the scattering region.
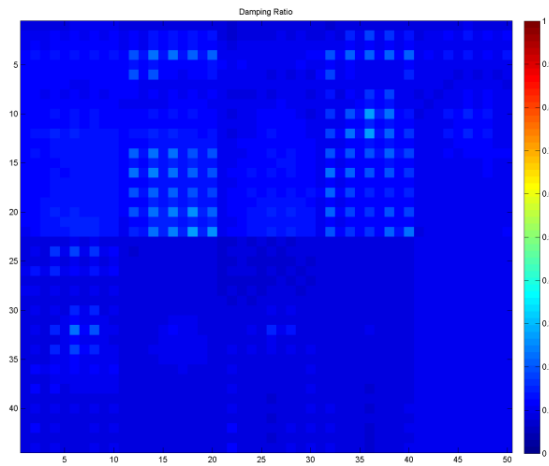
Figure 4.5: Damping Ratio 10% scattering 10x stiffer
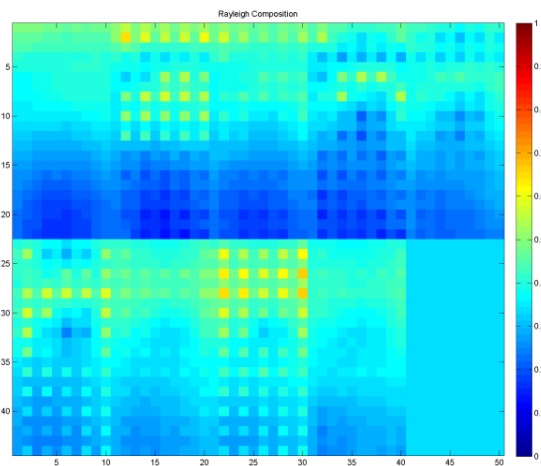
Figure 4.6: Rayleigh Composition 10% scattering 10x stiffer

Figure 4.7: Real Shear Modulus 10% scattering 10x stiffer

The second set of scattering conditions is a scattering density of 20% with all scatterers approximately 10 times stiffer than the background. Figure 4.8 displays the damping ratio, which displays very little affect from the presence of scatterers, with low damping throughout the mesh. Figure 4.9 displays the Rayleigh composition which appears to respond to the scatterers. The Rayleigh composition here has slightly higher values than the 10% simulation. Figure 4.10 displays the reconstructed real shear modulus which, as before, is mostly homogeneous with a slight increase in stiffness in the scattering region, due to a distributed increased stiffness from the scatterers.

Figure 4.8: Damping Ratio 20% scattering 10x stiffer

Figure 4.9: Rayleigh Composition 20% scattering 10x stiffer

Figure 4.10: Real Shear Modulus 20% scattering 10x stiffer

The third set of scattering conditions is a scattering density of 10% with all scatterers approximately 100 times stiffer than the background. Figure 4.11 displays the damping ratio, which remains consistently unaffected by the presence of scatterers, with low damping uniformly throughout the mesh. Figure 4.12 displays the Rayleigh composition which shows a significant increase in the region compared to the softer scatterers presented previously. Figure 4.13 displays the reconstructed real shear modulus which displays an almost two tone mesh with the scattered region appearing much stiffer. The distribution of the stiff scatterers and

smoothing effects in the reconstruction, such as total variation, cause the region to appear more homogenous.

Figure 4.11: Damping Ratio 10% scattering 100x stiffer

Figure 4.12: Rayleigh Composition 10% scattering 100x stiffer
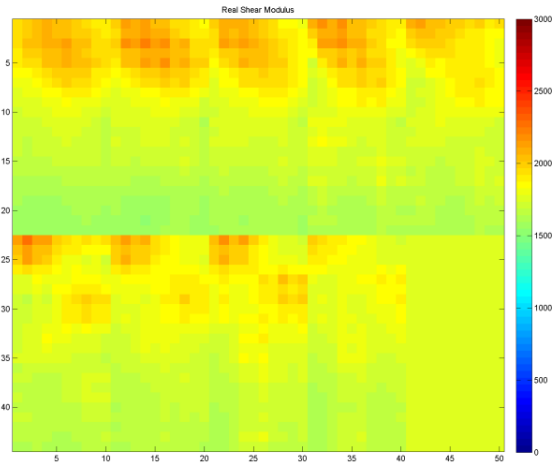
Figure 4.13: Real Shear Modulus 10% scattering 100x stiffer

The fourth and final set of scattering conditions is a scattering density of 20% with all scatterers approximately 100 times stiffer than the background. Figure 4.14 displays the damping ratio, which, similarly to the previous simulations, is seemingly unaffected by the presence of scatterers, with low damping throughout the mesh. Figure 4.15 displays the Rayleigh composition which shows a significant increase in the scattered region compared with only a minor increase to the previous condition. Figure 4.16 displays the reconstructed real shear modulus which displays a similar two tone result with only minor increases to the previous condition.
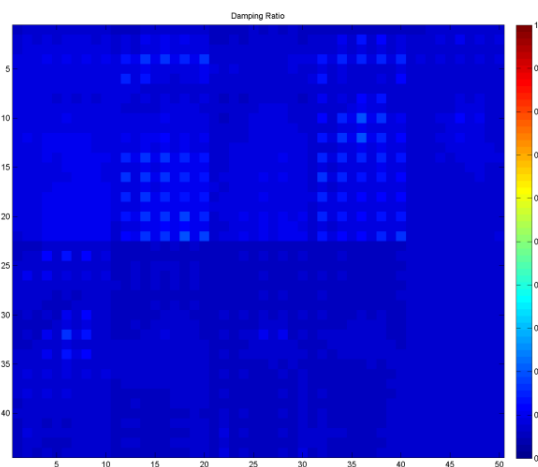
Figure 4.14: Damping Ratio 20% scattering 100x stiffer
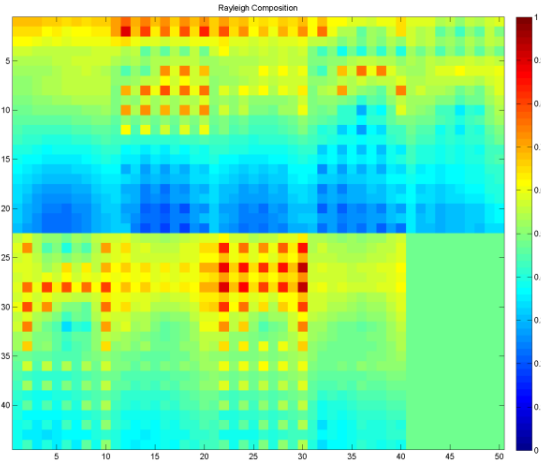
Figure 4.15: Rayleigh Composition 20% scattering 100x stiffer
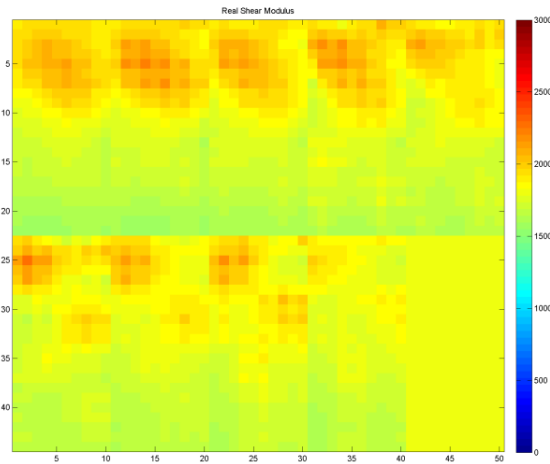
Figure 4.16: Real Shear Modulus 20% scattering 100x stiffer

	Damping Ratio				**Rayleigh Composition**				**Real Shear Modulus**			
	mean	stddev	max	min	mean	stddev	max	min	mean	stddev	max	min
10%10x												
Scatter	0.1021	0.002	0.3002	0.017	0.5171	0.0622	0.6773	0.4918	1691	18.38	1703	1613
Back Ground	0.10174	0.0017	0.3011	0.024	0.35828	0.0257	0.4101	0.1634	1507	11.111	1542	1488
20%10x												
Scatter	0.1036	0.0018	0.30303	0.016	0.5521	0.0478	0.7415	0.4469	1804	23.3333	1837	1751
Back Ground	0.10201	0.0022	0.3107	0.019	0.29272	0.02212	0.4457	0.1337	1492	10.5758	1515	1473
10%100x												
Scatter	0.1026	0.0014	0.2706	0.013	0.7216	0.1023	0.89796	0.5547	2034	42.306	2217	1768
Back Ground	0.1028	0.0011	0.02575	0.011	0.35303	0.0333	0.4041	0.2282	1587	31.0127	1811	1521
20%100x												
Scatter	0.1005	0.003	0.2023	0.014	0.707	0.1412	1	0.4973	2203	57.26	2259	1784
Back Ground	0.1011	0.0025	0.2169	0.009	0.3478	0.04001	0.6606	0.1513	1605	24.81	1824	1556

Table 4.1: Table of reconstruction results, for initial half simulation

A quantitative analysis is presented in table 4.1. The damping ratio is steady throughout the reconstructions, with approximately 10% damping. The simulation used 5% damping for the background material, hence the increased damping is likely due to the inclusion of stiff scatterers.

The Rayleigh composition shows approximately 150% increase for the softer scatterers (10x) in both the 10% and 20% scattering densities, and approximately 200% increase in both cases for the 100 times stiffer scatterers. This would suggest the Rayleigh composition is more sensitive to scattering stiffness than density and is directly affected by the presence of scatterers. This result is supported by the formulations in chapter 3 that showed mathematically RC is clearly defined on boundaries and ill-defined in homogenous regions

The real shear modulus showed an 11-14 % increase in stiffness across the reconstructions, corresponding to findings by (Papazoglou et al, 2009 [27], Sinkus et al, 2007 [28], Muki et al, 2003 [29]). That the presence of stiff scatterers can lead to stiffer behaviour within the medium.

4.1.2 Lateral Half Scattering Reconstruction

This simulation placed scatterers in the lateral half of the phantom such that the shear wave would travel through two parallel regions, one with and one without scatterers present. Figure 4.17 shows the artificial MR image for the reconstruction. There are 8 coronal slices with the actuated boundary located at the top of the slice as displayed in the image.

The first set of scattering conditions, are a scattering density of 10% with all scatterers approximately 10 times stiffer than the background. Figure 4.18 displays the damping ratio, which, similarly, is unaffected by the presence of scatterers, with low a damping ratio throughout the mesh. Figure 4.19 displays the Rayleigh composition which has a noticeable increase in the scattering region. Figure 4.20 displays the reconstructed real shear modulus which is mostly homogeneous with a slight increase in stiffness in the scattering region.
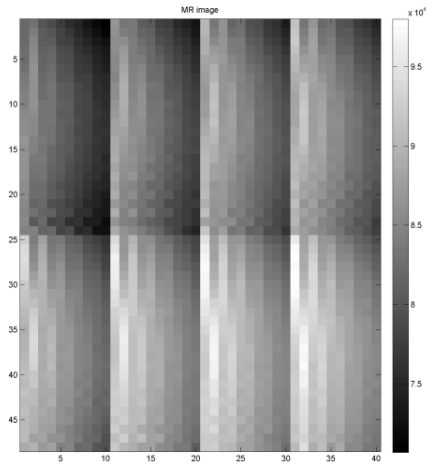
Figure 4.17: Artificial MRI image for reconstructed mesh
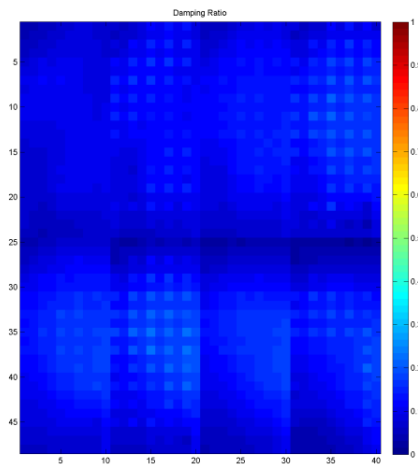
Figure 4.18: Damping Ratio 10% scattering 10x stiffer
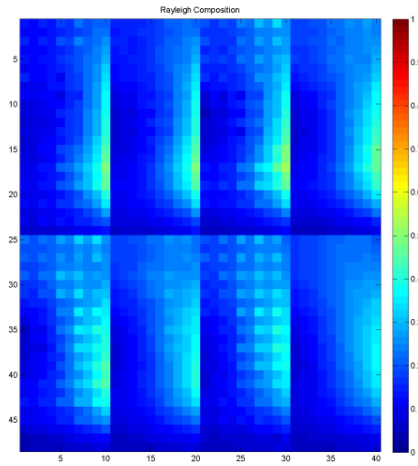
Figure 4.19: Rayleigh Composition 10% scattering 10x stiffer
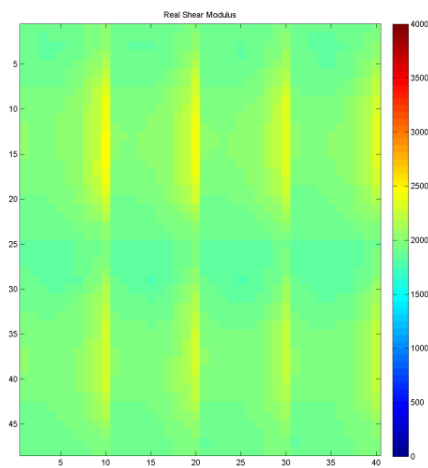
Figure 4.20: Real Shear Modulus 10% scattering 10x stiffer

The next set of scattering conditions are a scattering density of 20% with all scatterers approximately 10 times stiffer than the background. Figure 4.21 displays the damping ratio, consistently unaffected by the presence of scatterers, with low damping throughout. Figure 4.22 displays the Rayleigh composition which, has slightly higher values in the region than the previous 10% condition. Figure 4.23 displays the reconstructed real shear modulus which has a slight increase in stiffness in the scattering region, which is also a numerically stiffer region then the previous simulation.
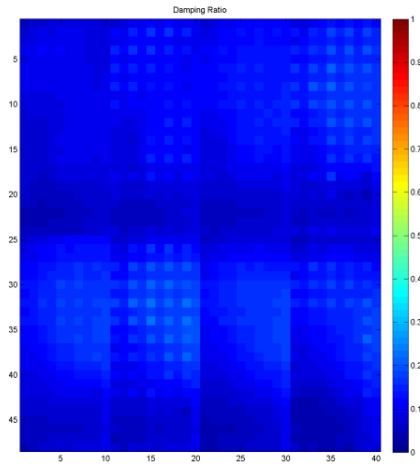
Figure 4.21: Damping Ratio 20% scattering 10x stiffer
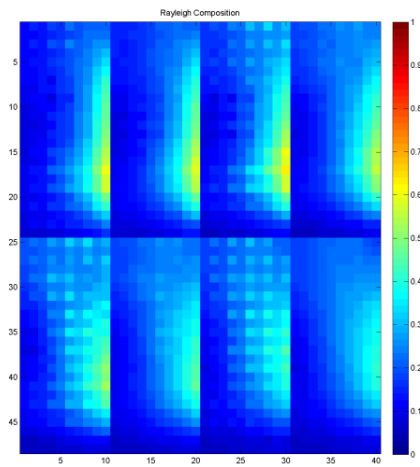
Figure 4.22: Rayleigh Composition 20% scattering 10x stiffer
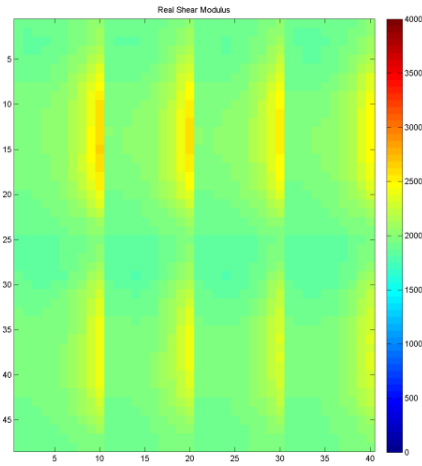
Figure 4.23: Real Shear Modulus 20% scattering 10x stiffer

The third set of scattering conditions is a scattering density of 10% with all scatterers approximately 100 times stiffer than the background. Figure 4.24 displays the damping ratio, which is displays a small increase in damping on the scattering side, with low damping throughout the mesh. Figure 4.25 displays the Rayleigh composition which shows an increase in the region compared to the softer scatterers presented previously, however it seems to be a smaller difference than the initial scattering mesh. Figure 4.26 displays the reconstructed real shear modulus which again tends towards a two tone mesh with the scattered region appearing much stiffer.
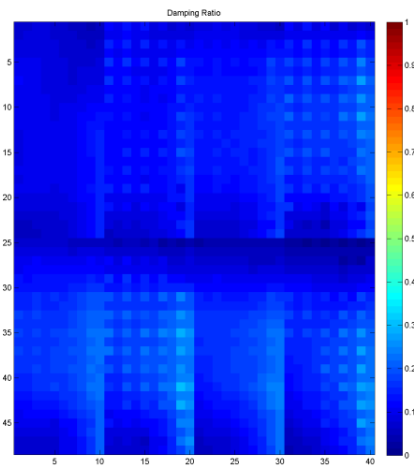
Figure 4.24: Damping Ratio 10% scattering 100x stiffer
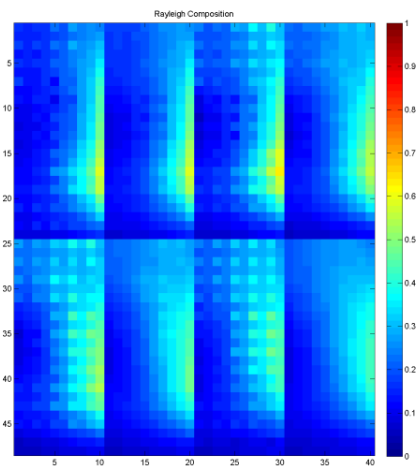
Figure 4.25: Rayleigh Composition 10% scattering 100x stiffer
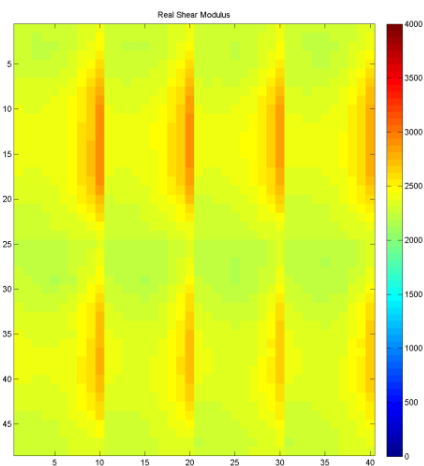
Figure 4.26: Real Shear Modulus 10% scattering 100x stiffer
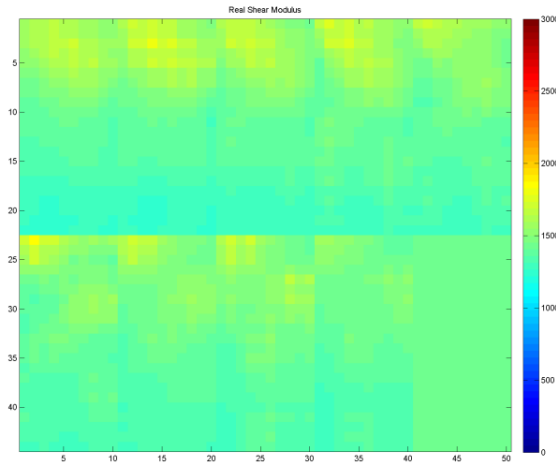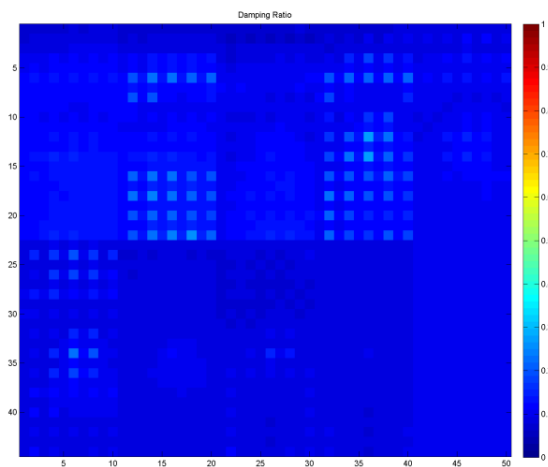
The final set of scattering conditions is a scattering density of 20% with all scatterers approximately 100 times stiffer than the background. Figure 4.27 displays the damping ratio, which displays a slight increase on the scattering side, with low damping throughout the mesh. Figure 4.28 displays the Rayleigh composition which shows a significant increase in the scattered region compared with any previous condition. Figure 4.29 displays the reconstructed real shear modulus which displays a similar two tone result with a noticeable increase to the previous condition.

64
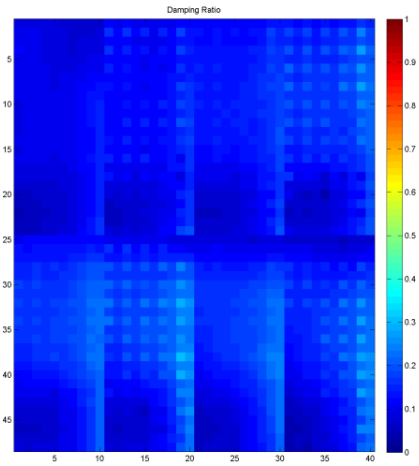
Figure 4.27: Damping Ratio 20% scattering 100x stiffer
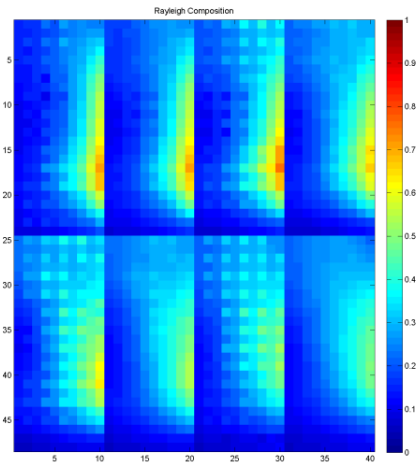
Figure 4.28: Rayleigh Composition 20% scattering 100x stiffer

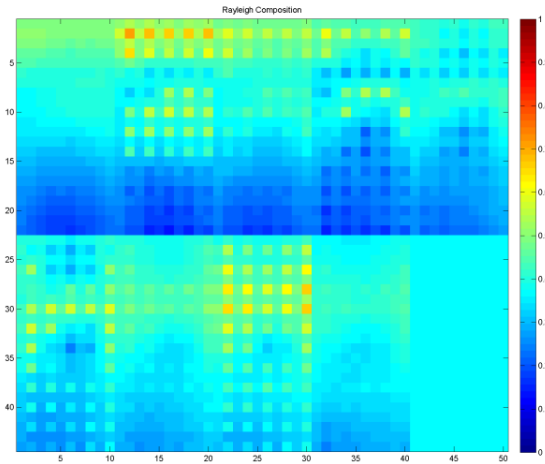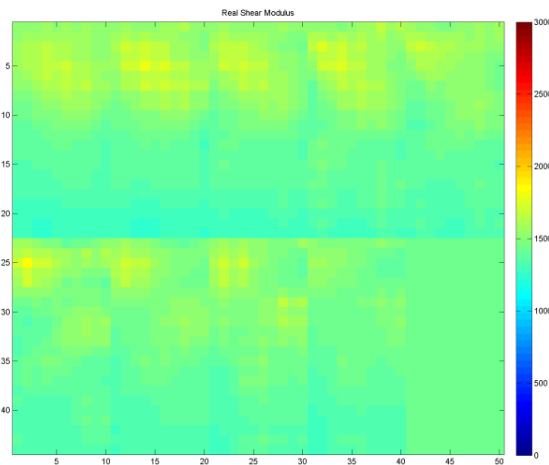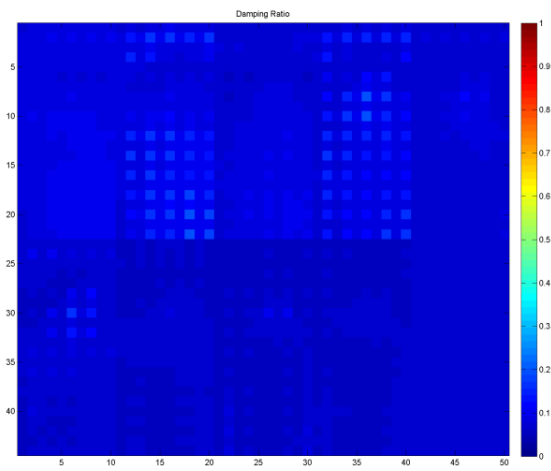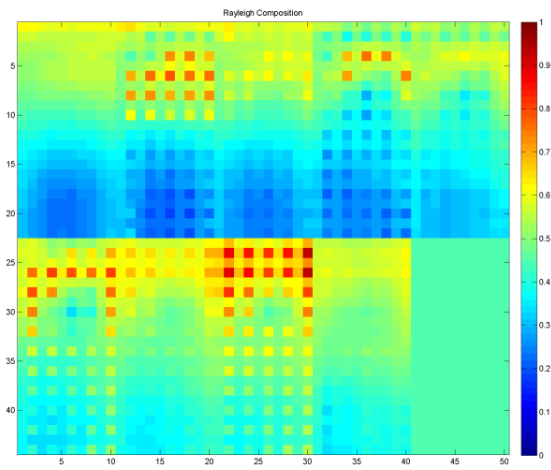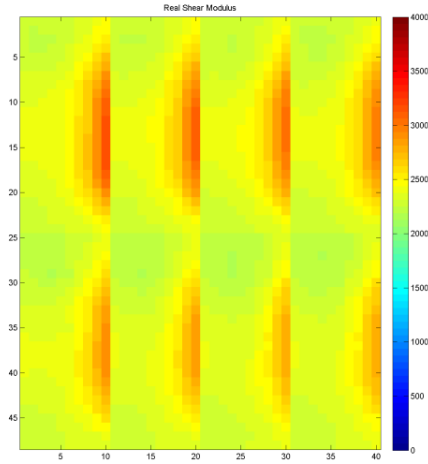**Figure 4.29**: Real Shear Modulus 20% scattering 100x stiffer

	Damping Ratio				Rayleigh Composition				Real Shear Modulus			
	mean	stddev	max	min	mean	stddev	max	min	mean	stddev	max	min
10%10x												
Scatter	0.1707	0.0101	0.299	0.055	0.3733	0.0348	0.476	0.3574	2417	33.336	2481	2027
Back Ground	0.1352	0.01121	0.268	0.042	0.2124	0.01915	0.3003	0.09389	2003	24.87	2111	1984
20%10x												
Scatter	0.1818	0.002	0.2582	0.047	0.447	0.0478	0.624	0.383	2486	45.667	2715	2080
Back Ground	0.1574	0.0171	0.2642	0.053	0.2517	0.02212	0.4457	0.3614	2037	31.049	2134	2013
10%100x												
Scatter	0.2215	0.1022	0.3463	0.1009	0.5347	0.06065	0.666	0.5547	2754	51.017	2984	2111
Back Ground	0.1974	0.0109	0.2726	0.0601	0.3445	0.10422	0.5317	0.2751	2130	39.994	2273	2041
20%100x												
Scatter	0.2138	0.1147	0.402	0.1897	0.5861	0.1793	0.726	0.4199	3040	63.9	3495	2528
Back Ground	0.1896	0.0202	0.2805	0.0877	0.3316	0.0616	0.4391	0.1948	2257	37.18	2403	2087

Table 4.2: Table of reconstruction results, for lateral half simulation

A quantitative analysis for the second mesh conditions is presented in table 4.2. The damping ratio is more or less steady throughout the reconstructions, with approximately 20% damping. The two regions, scatters and no scatterers, have about a 3% difference in damping. The simulation used 5% damping for the background material, the increased damping is likely due to the inclusion of stiff scatterers, however the effects of scattering along the entire mesh seems to have increased the damping further.

The Rayleigh composition shows approximately 175% increase for all four cases considered. This is an interesting result, indicating a consistent scattering effect along the shear wave. As opposed the previous mesh condition of only initially scattering the wave. The real shear modulus showed a 21-34 % increase in stiffness across the reconstructions, corresponding to

work done by (Papazoglou et al, 2009 [27], Sinkus et al, 2007 [28], Muki et al, 2003 [29]). That the presence of stiff scatterers can lead to stiffer behaviour within the medium. This seems to indicate that scatterers present along the shear wave have a larger effect than a region of scatterers which the wave passes through. This would imply that regions with high inertial damping may cause a significant loss in energy within the shear wave.

4.2 Dispersion

Frequency dispersion in geophysics can be approximated to a ratio of the elastic moduli, defined under different attenuations (Adelinet et al, 2010 [30], Zimmerman et al, 1986 [32]). Eq. 4.1 shows this ratio, where M is either the bulk or shear modulus.

$$Dispersion = \frac{M_{HF}^{sat} - M_{LF}^{sat}}{M_{LF}^{sat}}$$

[Eq. 4.1]

In the case of equant pores, where the cavities are of a uniform shape, such as spherical or whole elements as in our scattering mesh, then the low frequency saturated modulus is approximately equal to the high frequency unsaturated modulus. Note a non equant pore condition, such as cracking, is the propagation of a low volume pore which is highly directional and uniquely shaped. This is an unlikely condition in soft tissue.

Eq. 4.2 is the ratio between the background material and the effective bulk moduli, where κ_0 is the background modulus, κ_{HF}^{sat} is the effective modulus. The pore porosity is defined by ϕ_p, and v_0 is the poisons ratio.

$$\frac{\kappa_0}{\kappa_{HF}^{sat}} = 1 + \phi_p \frac{3(1 - v_0)}{2(1 - 2v_0)} \left(\frac{\delta_p}{1 + \delta_p} \right)$$

[Eq. 4.2]

Eq. 4.3 defines δ_p which describes the coupling between matrix compliance, fluid compressibility and equant pore geometry, where E_0 is the background material's Young's modulus and κ_f is the pore bulk modulus. (Shaffiro et al, 1996 [31],)

$$\delta_p = \frac{2E_0}{9(1 - \upsilon_0)}\left(\frac{1}{\kappa_f} - \frac{1}{\kappa_0}\right)$$

[Eq. 4.3]

Figure 4.30 displays the frequency dispersion relationships with a varying κ_f the pore modulus (blue shear and red bulk), with a fixed number of pores, and with a fixed bulk modulus while the number of pores vary (blue soft and red hard pores). These trends show that small variations in the bulk modulus have a much larger effect than small variations in pore saturation.

The scattering result indicated the same trends in both cases considered. The impact of increased shear modulus was clearly more significant than the increased scattering density. While mechanical characteristics of tissue such as viscoelasticity are most likely to influence tissue deformation it seems apparent that mechanical property distributions representative of cellular structure in fluid-saturated tissue are likely to augment the deformation behaviour.

Studies into the attenuation behaviour of poro-elastic materials, (Perriñez et al, 2009 [35] & 2010 [36]) found a high sensitivity with respect to material properties such as bulk modulus as opposed to pore size or frequency. This would appear to correlate with the dispersion and scattering formulations, indicating observed elastic behavior is more representative of material property distribution than material structure. This is a promising result as biological structures are unique to every case, or patient, where as a material property distribution is more adaptable and hence a more valuable metric.
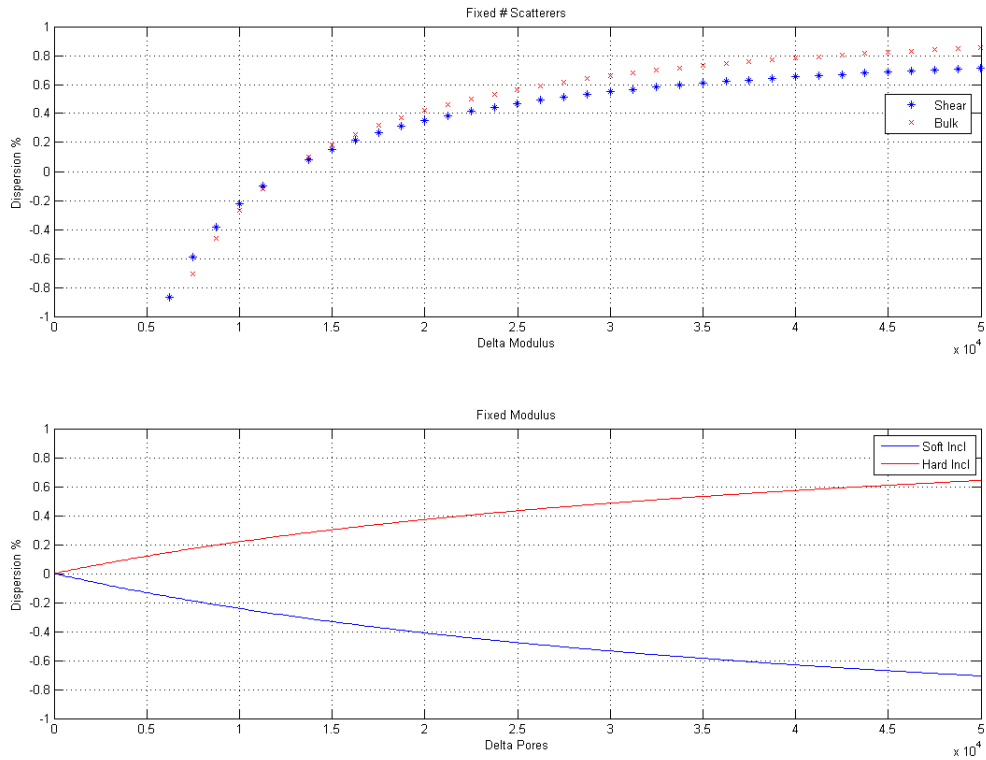
Figure 4.30: Elastic Dispersion Trends, % dispersion vs. delta modulus and delta pores respectively

The simulations suggest that dense cellular structure, as found with pathology in soft tissue, would cause both scattering of the shear wave and frequency dispersion, due to the complex interlaced structure and the variant material properties. It may be possible to incorporate for these influences in a diagnostic model as cancer is known to alter both the micro-structure and the fluid content or pressure.

Chapter 5

Anisotropic Reconstruction

Breast tissue, due to its natural development, has a complex orthotropic structure. An imaging algorithm which utilises an anisotropic reconstruction may more accurately describe the material condition of the tissue. However, an anisotropic reconstruction is very computationally intensive, this is further exaggerated in MR Elastography which is has a data rich environment from the high resolution measurement system. In spite of these obstacles, a reconstruction algorithm with an orthotropic material condition could potentially be instrumental in the development of a diagnostic tool (Sinkus et al, 2005 [34]). This chapter will discuss the methods implemented to make orthotropic reconstructions more feasible.

5.1 Anisotropic Materials

Although elastography imaging techniques have been introduced as powerful medical imaging modalities, most approaches consider isotropic material properties (Zhu et al, 2003, [161], Khang et al, 2003 [162] and Liu et al, 20030 [163]). There is little quantitative information available in the MRE literature regarding the behavior of orthotropic materials and most anisotropic MRE reconstructions are in 2-D (Cox et al, 1997 [164]). To study a more realistic behavior of tissue and cancerous tumors it is necessary to develop a 3-D model with actual geometry which includes sufficient details about orthotropic elasticity parameters. This chapter introduces the existing formulations for anisotropic and orthotropic material models. In solid mechanics, there are some conditions related to equations of equilibrium which must be satisfied to solve a problem. These conditions are strain-displacement relations and material constitutive laws. The first condition does not require the material property parameters while the second one, which relates the stress to strain components at any point in the solid, is a function of elasticity modulus.

Since the behavior of the real material is complex and difficult to comprehend, it is necessary to make assumptions and perform simplifications to make a mathematical model of the material's behavior by applying suitable theories and adequate experimental tests. This mathematical model can calculate a particular property to express the material behavior in a certain condition (Weaver et al, 2002 [167] and Barber et al, 1992 [168]).

In the most generalized anisotropic model, material symmetry does not exist and mechanical properties are different in all directions (Francois et al, 1998 [169] and Ting et al, 1996 [170]). In the condition that there are different degrees of material symmetries, the material can be categorized as, for example, orthotropic or isotropic and so on. In this chapter, certain elastic models based on the existence of elastic symmetry axes are considered. In these axes, known as elastic principal axes, the constitutive relations remain invariant.

Anisotropy means the mechanical property of a material is directionally dependent. This can be expressed as a difference in a physical or mechanical property such as elasticity modulus, density, etc. In the chemical aspect, anisotropy is defined as phenomena of chemical bond strengths which are directionally dependent (Lekhnitskii et al, 1981 [171]). Elastic properties will be anisotropic when deformation depends on the direction of a particular stress (Ambartsumyan et al, 1991 [172]). Many biological materials, such as tissue, are anisotropic materials that display directionally variations in material properties. Inhomogeneous material property distributions can also be a pathological sign, as in the case of breast carcinomas. The discussion on tissue structures provides many micro-scale examples of mechanical behavior (Fung, 1993 [165] and Sinkus et al, 2000 [166]).

To study anisotropy it is essential to know the constitutive equation that describes the elastic behavior of the material and also determines the elasticity tensor, C_{ijkl} and its components. In the linear elasticity, the relationship between current stress and current strain remains linear. The constitutive equation which is the generalized form of Hooke's law can be written as:

$$\sigma_{ij} = C_{ijkl}\varepsilon_{kl}$$

[Eq. 5.1]

where σ_{ij} and ε_{kl} are second order stress and strain tensors respectively, and C_{ijkl} is the fourth order elasticity or stiffness tensor. The symmetric stress and strain tensors can be written as six-dimensional vectors in an ortho-normal coordinate system (Eq. 5.2). The anisotropic form of Hooke's law in matrix expression is shown in (Eq. 5.3).

$$\{\sigma\} = \begin{Bmatrix} \sigma_{11} \\ \sigma_{22} \\ \sigma_{33} \\ \sigma_{23} \\ \sigma_{31} \\ \sigma_{12} \end{Bmatrix} = \begin{Bmatrix} \sigma_1 \\ \sigma_2 \\ \sigma_3 \\ \sigma_4 \\ \sigma_5 \\ \sigma_6 \end{Bmatrix} \quad \& \{\varepsilon\} = \begin{Bmatrix} \varepsilon_{11} \\ \varepsilon_{22} \\ \varepsilon_{33} \\ 2\varepsilon_{23} \\ 2\varepsilon_{31} \\ 2\varepsilon_{12} \end{Bmatrix} = \begin{Bmatrix} \varepsilon_1 \\ \varepsilon_2 \\ \varepsilon_3 \\ \varepsilon_4 \\ \varepsilon_5 \\ \varepsilon_6 \end{Bmatrix}$$

[Eq. 5.2]

$$\begin{Bmatrix} \sigma_1 \\ \sigma_2 \\ \sigma_3 \\ \sigma_4 \\ \sigma_5 \\ \sigma_6 \end{Bmatrix} = \begin{bmatrix} C_{11} & C_{12} & C_{13} & C_{14} & C_{15} & C_{16} \\ C_{21} & C_{22} & C_{23} & C_{24} & C_{25} & C_{26} \\ C_{31} & C_{32} & C_{33} & C_{34} & C_{35} & C_{36} \\ C_{41} & C_{42} & C_{43} & C_{44} & C_{45} & C_{46} \\ C_{51} & C_{52} & C_{53} & C_{54} & C_{55} & C_{56} \\ C_{61} & C_{62} & C_{63} & C_{64} & C_{65} & C_{66} \end{bmatrix} \begin{Bmatrix} \varepsilon_1 \\ \varepsilon_2 \\ \varepsilon_3 \\ \varepsilon_4 \\ \varepsilon_5 \\ \varepsilon_6 \end{Bmatrix}$$

[Eq. 5.3]

A material has symmetry if its elastic properties are the same in certain directions. If symmetry exists in all directions, the material is called isotropic otherwise, it is anisotropic. In general, C_{ijkl} contains 81 constants, but since both stress and strain tensors are symmetrical ($\sigma_{ij} = \sigma_{ji}$ and $\varepsilon_{kl} = \varepsilon_{lk}$), and with the assumption that there exists a strain energy function U given by:

$$U = \frac{1}{2} C_{ijkl} \varepsilon_{ij} \varepsilon_{kl}$$

[Eq. 5.4]

where,

$$\sigma_{ij} = C_{ijkl}\varepsilon_{kl} = \frac{\partial U}{\partial \varepsilon_{ij}} => C_{ijkl} = \frac{\partial^2 U}{\partial \varepsilon_{ij}\partial \varepsilon_{kl}}$$

[Eq. 5.5]

It is seen that the stiffness tensor must be symmetrical so that $C_{ijkl} = C_{klij}$ because of the arbitrary order of differentiation ε_{ij} and ε_{kl} . As a result, the number of elastic constants can be reduced to 21 coefficients (Lai et al, [173] and Haupt et al, 2002 [174]).

According to (Love, 1944 [175]) and (Chen et al, 1982 [176]), the equations that govern engineering problems are related to the stored energy in a solid. Therefore, the energy developed by the external work is stored in an elastic solid and may be developed as potential elastic energy that is known as strain energy.

During this process the body is deformed, but may recover its original shape and size. An interesting point is that the presence of certain types of symmetry in an elastic body, simplify the constitutive relations. These simplifications are represented in different ways, for example those applied by Love, where the strain energy function remains unchangeable by all symmetrical coordinate system substitutions (Desai et al, 1984 [177]).

5.2 A Direct Analytical Formulation

The conjugate gradient method (CG) is a commonly used method for computational problems. As a gradient descent method, CG performs an optimization or reconstruction of a parameter θ based on the minimization of an error function F.

$$\theta = \min_{\theta}\{F(\theta)\}$$

[Eq. 5.6]

The residual, as required in the CG method, is the derivative of Eq. 5.6 with respect to θ and given as follows

$$\frac{\partial F}{\partial \theta} = -2 \left(\frac{\partial f}{\partial \theta} \right)^T \| \bar{u} - f(\theta) \|$$

[Eq. 5.7]

Where the Jacobian ($J = \frac{\partial f}{\partial \theta}$) is either obtained by a finite deference expression or a direct analytical approach. A finite difference expression, while accurate, will require the algorithm to calculate a complete forward solve for each individual iteration. Conversely a direct analytical approach could approximate the Jacobian matrix after a single forward solve. Given the high computational cost, a direct approach would be optimal.

A direct analytical solution requires a defined material model for incompressible orthotropic elastic property distribution. The stress (σ_i), strain (ε_i) and compliance (S_{ij}) tensors are defined as follows,

$$\sigma_i = (\sigma_1, \sigma_2, \sigma_3, \tau_{12}, \tau_{23}, \tau_{31})$$

$$\varepsilon_i = (\varepsilon_1, \varepsilon_2, \varepsilon_3, \gamma_{12}, \gamma_{23}, \gamma_{31})$$

$$S_{ij} = \begin{bmatrix} S_{11} & S_{12} & S_{13} & 0 & 0 & 0 \\ S_{21} & S_{22} & S_{23} & 0 & 0 & 0 \\ S_{31} & S_{32} & S_{33} & 0 & 0 & 0 \\ 0 & 0 & 0 & S_{44} & 0 & 0 \\ 0 & 0 & 0 & 0 & S_{55} & 0 \\ 0 & 0 & 0 & 0 & 0 & S_{66} \end{bmatrix}$$

[Eq. 5.8]

The compliance matrix is symmetrical, therefore $S_{12} = S_{21}$, $S_{13} = S_{31}$ and $S_{23} = S_{32}$. The constitutive elastic relationship can be written in the following form,

$$\varepsilon_i = S_{ij} \sigma_j$$

[Eq. 5.9]

74

With these basic relationships defined, a set of constitutive equations for an incompressible orthotropic solid can be derived. Eq. 5.10 and Eq. 5.11 where obtained by following the methods presented in (Taylor et al, 1968 [33]).

$$\sigma_j = B_{ji}^{-1}(\varepsilon_i - \beta_{ik}F_kH) \qquad i,j,k = 1,2,...,6$$

[Eq. 5.10]

$$\left(F_i\beta_{ij}F_j + F_i\beta_{ik}B_{kl}^{-1}\beta_{lj}F_j\right)H - F_i\beta_{ik}B_{kj}^{-1}\varepsilon_j = 0 \qquad i,j,k = 1,2,...,6$$

[Eq. 5.11]

β is the auxiliary matrix, B is the modified compliance matrix and F is the dilation coefficient vector. H represents the pressure term for the system. F, β and B are presented in Eq. 5.12, Eq. 5.13 and Eq. 5.14 respectively,

$$F = [1,1,1,0,0,0]$$

[Eq. 5.12]

$$\beta = \begin{bmatrix} \dfrac{S_{32}S_{11} - S_{12}S_{31}}{S_{23}} & 0 & 0 & 0 & 0 & 0 \\ 0 & -\dfrac{S_{21}S_{32} - S_{22}S_{31}}{S_{13}} & 0 & 0 & 0 & 0 \\ 0 & 0 & \dfrac{S_{21}S_{33} - S_{23}S_{31}}{S_{12}} & 0 & 0 & 0 \\ 0 & 0 & 0 & S_{44} & 0 & 0 \\ 0 & 0 & 0 & 0 & S_{55} & 0 \\ 0 & 0 & 0 & 0 & 0 & S_{66} \end{bmatrix}$$

[Eq. 5.13]

$$B = \begin{bmatrix} S_{11} - \dfrac{S_{32}S_{11} - S_{12}S_{31}}{S_{23}} & S_{12} & S_{13} & 0 & 0 & 0 \\ S_{21} & S_{22} + \dfrac{S_{21}S_{32} - S_{22}S_{31}}{S_{13}} & S_{23} & 0 & 0 & 0 \\ S_{31} & S_{32} & S_{33} - \dfrac{S_{21}S_{33} - S_{23}S_{31}}{S_{12}} & 0 & 0 & 0 \\ 0 & 0 & 0 & 0 & 0 & 0 \\ 0 & 0 & 0 & 0 & 0 & 0 \\ 0 & 0 & 0 & 0 & 0 & 0 \end{bmatrix}$$

[Eq. 5.14]

With the expanded terms above, the constitutive equations (Eq. 5.10 and Eq. 5.11) may be simplified through substitution and tensor multiplication. The resulting form for these equations is presented below. (Eq. 5.11 is presented in Appendix D)

$$\sigma_j = [\frac{\left(\varepsilon_1 - \left(S_{11} - \dfrac{S_{32}S_{11} - S_{12}S_{31}}{S_{23}} + S_{21} + S_{31}\right)H\right)S_{23}}{S_{32}S_{11} - S_{12}S_{31}};$$

$$-\frac{\left(\varepsilon_2 - \left(S_{21} + S_{22} + \dfrac{S_{21}S_{32} - S_{22}S_{31}}{S_{13}} + S_{32}\right)H\right)S_{13}}{S_{21}S_{32} - S_{22}S_{31}};$$

$$\frac{\left(\varepsilon_3 - \left(S_{31} + S_{32} + S_{33} - \dfrac{S_{21}S_{33} - S_{23}S_{31}}{S_{12}}\right)H\right)S_{12}}{S_{21}S_{33} - S_{23}S_{31}};$$

$$\frac{\varepsilon_4}{S_{44}}; \frac{\varepsilon_5}{S_{55}}; \frac{\varepsilon_6}{S_{66}}]$$

[Eq. 5.15]

Eq. 5.16 is a vector of the weighting functions, which, if multiplied to our stress vector (σ in Eq. 5.15), determines the distributed stress vector (K) for the system, shown in Eq. 5.17.

$$DD = \left[\frac{\partial}{\partial x}\varphi_{ix}(x,y,z), \frac{\partial}{\partial y}\varphi_{iy}(x,y,z), \frac{\partial}{\partial z}\varphi_{iz}(x,y,z), \frac{\partial}{\partial y}\varphi_{ix}(x,y,z)\right.$$

$$+ \frac{\partial}{\partial x}\varphi_{iy}(x,y,z), \frac{\partial}{\partial z}\varphi_{iy}(x,y,z) + \frac{\partial}{\partial y}\varphi_{iz}(x,y,z), \frac{\partial}{\partial z}\varphi_{ix}(x,y,z)$$

$$\left. + \frac{\partial}{\partial x}\varphi_{iz}(x,y,z)\right]$$

[Eq. 5.16]

$$K = \frac{\left(\varepsilon_1 - \left(S_{11} - \dfrac{S_{32}S_{11} - S_{12}S_{31}}{S_{23}} + S_{21} + S_{31}\right)H\right)S_{23}}{S_{32}S_{11} - S_{12}S_{31}}\left(\frac{\partial}{\partial x}\varphi_{ix}(x,y,z)\right)$$

$$-\frac{\left(\varepsilon_2 - \left(S_{21} + S_{22} + \dfrac{S_{21}S_{32} - S_{22}S_{31}}{S_{13}} + S_{32}\right)H\right)S_{13}}{S_{21}S_{32} - S_{22}S_{31}}\left(\frac{\partial}{\partial y}\varphi_{iy}(x,y,z)\right)$$

$$+\frac{\left(\varepsilon_3 - \left(S_{31} + S_{32} + S_{33} - \dfrac{S_{21}S_{33} - S_{23}S_{31}}{S_{12}}\right)H\right)S_{12}}{S_{21}S_{33} - S_{23}S_{31}}\left(\frac{\partial}{\partial y}\varphi_{ix}(x,y,z)\right)$$

$$+\frac{\varepsilon_4}{S_{44}}\left(\frac{\partial}{\partial y}\varphi_{ix}(x,y,z) + \frac{\partial}{\partial x}\varphi_{iy}(x,y,z)\right)$$

$$+\frac{\varepsilon_5}{S_{55}}\left(\frac{\partial}{\partial z}\varphi_{iy}(x,y,z) + \frac{\partial}{\partial y}\varphi_{iz}(x,y,z)\right)$$

$$+\frac{\varepsilon_6}{S_{66}}\left(\frac{\partial}{\partial z}\varphi_{ix}(x,y,z) + \frac{\partial}{\partial x}\varphi_{iz}(x,y,z)\right)$$

[Eq. 5.17]

The elastic strains, ε, can be expanded into the divergence of the displacements shown in Eq. 5.18.

$$\varepsilon_1 = \frac{\partial}{\partial x}u(x,y,z)$$

$$\varepsilon_2 = \frac{\partial}{\partial y}v(x,y,z)$$

$$\varepsilon_3 = \frac{\partial}{\partial z}w(x,y,z)$$

$$\varepsilon_4 = \frac{\partial}{\partial y}u(x,y,z) + \frac{\partial}{\partial x}v(x,y,z)$$

$$\varepsilon_5 = \frac{\partial}{\partial z}v(x,y,z) + \frac{\partial}{\partial y}w(x,y,z)$$

$$\varepsilon_6 = \frac{\partial}{\partial z}u(x,y,z) + \frac{\partial}{\partial x}w(x,y,z)$$

[Eq. 5.18]

With the newly derived constitutive equations, and the weighted stress formulation, and by substituting the strain formulation, it is possible to build a stiffness matrix for the forward problem. This stiffness matrix, A, is shown in Appendix D.

In order to build the Jacobian matrix directly, it is necessary to determine the derivative terms for the stiffness matrix with respect to the compliance terms analytically. The 16 non-zero derivate terms have been expanded in Appendix D.

With the above equations it is possible to program a solver to calculate the necessary matrix terms directly (Taylor et al, 1968 [33]), implementing only two forward solutions with a CG approach, as opposed to a finite difference approach which requires a forward solution for every parameter reconstructed.

5.3 Programming the Analytical Approach

The orthotropic reconstruction algorithm employs a weighted residual FEM formulation. Algorithm 5.1 presents the pseudo-code of the FEM orthotropic adjoint gradient formulation. It an overview of the looping structured employed to build the FE matrix-vector system of equations. A sample of the FORTRAN code is presented in Appendix E.

Algorithm 5.1

% Loop over all the elements

do el = 1, # elms   (element looping)

- *Build Gauss integration values*
  - *Weights*
  - *Co-ordinate transforms*
- *Build material properties at each GP*
- *Build Compliance Matrix at each GP = S_g*
- *Calculate Compliance derivatives $dS_g/d\vartheta$*

% Loop over every node in each element

do ii = 1,NPE   *(interpolating functions)*
do jj = 1,NPE   *(weighting functions)*
do kk = 1,NPE   *(Basis functions for material properties)*

Assemble A matrix terms (Eq. 5.15)

$$\begin{pmatrix} \ddots & & \Big| & \\ & \mathbf{A}_{dd} & \Big| & \mathbf{A}_{dp} \\ & & \ddots \Big| & \\ \hline & \mathbf{A}_{pd} & \Big| & \mathbf{A}_{pp} \end{pmatrix} \begin{Bmatrix} \vdots \\ \mathbf{u}_t \\ \vdots \\ \hline \mathbf{P}_t \end{Bmatrix}$$

With Add = < $\Phi_i\Phi_i$ >, Apd = < $\Phi_i\Psi_i$ >, App = < $\Psi_i\Psi_i$ >
and $u_t = \Sigma\, u_i\Phi_i$ and $P_t = \Sigma\, P_i\Psi_i$

% Loop over all the Gauss integration points

do = ig = 1,NGP   *(Gauss point looping)*
do = jg = 1,NGP
do = kg = 1,NGP

- *Calculate the stiffness matrix derivatives dA/dS_g (Eq. 5.16 through Eq. 5.31)*

- *Calculate the Jacobian matrix $dA/d\vartheta = dA/dS_g * dS_g/d\vartheta$*

- *Calculate the volume integral terms $< > = \Sigma\, |J|\,w_g f(g)$*

     end kg
     end jg
     end ig   *(end of GP looping)*

- *Build RHS terms*

     End kk
     end jj
     end ii   *(end of nodal looping*
end elm   *(end of element loop)*

Anisotropic MRE reconstructions are not only computationally intensive, with the finite difference algorithm requiring hundreds of hours to converge, they also require complex actuation methods in order to generate shear wave displacements in three unique directions. As a result a sample test mesh was used to conduct simulation to compare the adjoint residual code, described above, to the original finite difference code.

The test mesh created was a simple square 125 (5x5x5) elements in volume. Twenty seven node hexahedral elements were used, which is standard for the MRE reconstructions, the entire mesh had 1331 nodes. The simulation study compared performance in solving the forward problem only, as this is the where either method is relevant in the reconstruction process. Figure 5.1 displays the resulting residual magnitude for each method. The first plot is the real part and the second is the imaginary part. The finite difference result, plotted in red, was multiplied by "- 1" for a better visual comparison. As the figure displays the adjoint method and the finite difference had almost identical results confirming at least the accuracy of the adjoint formulation.
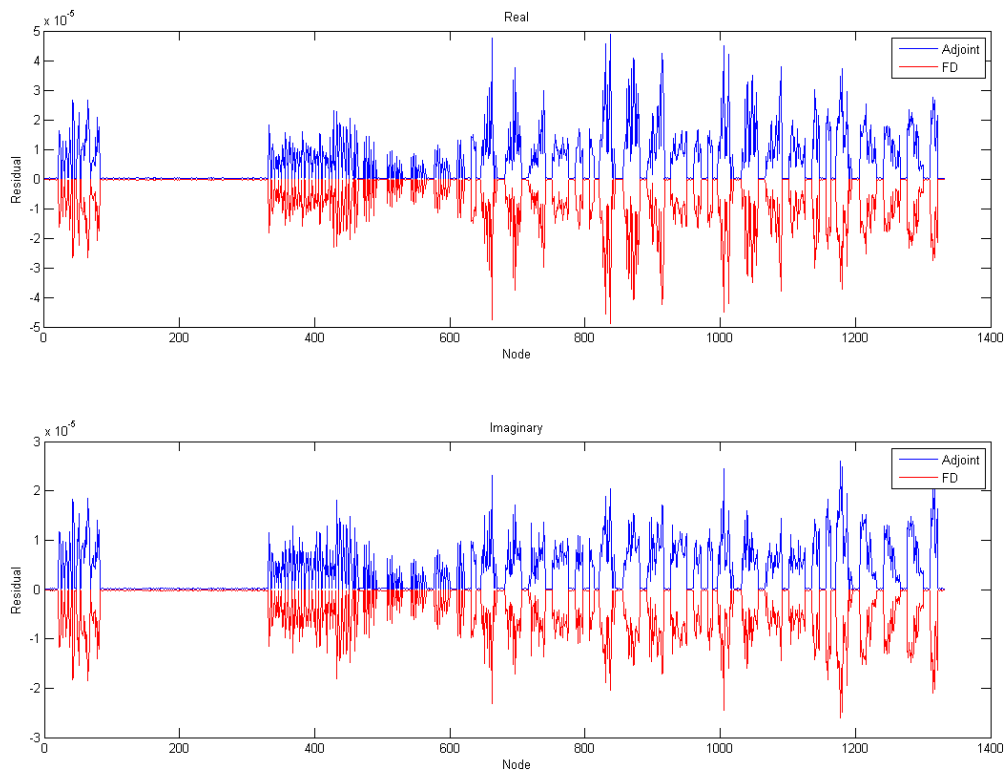
Figure 5.1: Finite Difference and Adjoint Residual comparison

80

The simulations that were conducted ran for 30 global iterations, utilising 32 processors on the HPC (see appendix). Each global iteration consisted of between 12 and 15 zone iterations, with an average subzone size of 300 nodes ranging from 214 to 391.

	Finite Difference	Adjoint Residual
sub zone	0.73589	0.50579
global	9.56667	6.57531

Table 5.1: Table of simulation run times in hours

Table 5.1 compares the runtimes of each algorithm. The adjoint method performed optimally with approximately 30% faster reconstruction times. Due to the small mesh size it is likely that the direct adjoint calculation will save even more time for larger more complex meshes. Ideally this will make anisotropic MRE reconstructions more feasible, leading to more accurate physiological reconstructions, which could potentially improve cancer detection and diagnosis.

5.4 Orthotropic Incompressible Phantoms

To evaluate a realistic orthotropic incompressible model, two biological phantoms were reconstructed. Constructing a phantom that mimics an orthotropic material can be very challenging, as there is little quantitative information available in MRE experiments regarding orthotropic phantom fabrication. This thesis is based on the orthotropic incompressible phantom image reconstruction, to describe the orthotropic behaviour. Several orthotropic image reconstructions where carried out to map orthotropic elasticity properties in 3D using a few MRI datasets which are presented in this chapter.

Recently, ex vivo phantom elastography such as muscle phantoms, have been developed for non-invasively measuring the stiffness of biological tissues (Flewellen, 2008 [179]). As real cancerous tissue is not always available for MRE testing, a series of muscle phantoms, that could mimic the tissue and tumours with orthotropic properties, was used.

Due to the structural properties and myofibril protein orientations within the muscle, this material can be a good example of orthotropic incompressible behaviour. As muscle is known to be highly orthotropic (Blemker et al, 2005 [180]), to develop clinically realistic orthotropic phantoms, bovine muscle was chosen and tested. Two different kinds of phantoms were designed, and then tested with using a pneumatic actuator.

The phantom was scanned in three dimensions by rotating the phantom box 90° in 3-D. To obtain enough motion data from an orthotropic material, multiple measurements in 3-D are required. The phantom was scanned in three stages with one specific excitation frequency of 100 Hz. In each stage, this load condition was assigned to the side of the phantom box which was coupled to the pneumatic actuator in the excitation direction (Z).
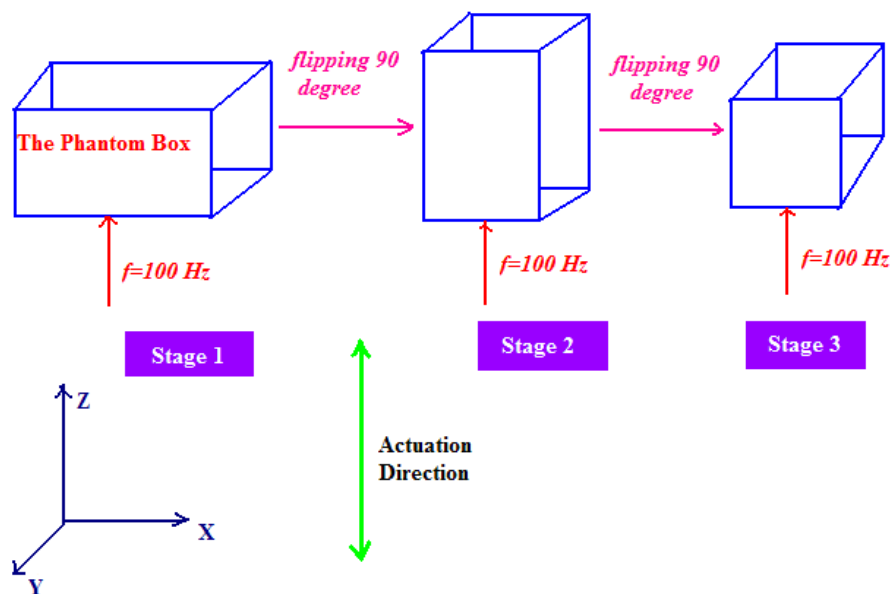
Figure 5.2: Phantom Orientation for excitation

Figure 5.2 depicts three stages of the boundary conditions applied to the muscle gelatine phantom. The figure illustrates that only one specific frequency of 100Hz was assigned to the phantom in 3D while the phantom is being excited in the Z direction. The phantom has been flipped 90° in each 3 stages.

Physical material properties of the tissue (i.e. the stiffness) can be changed by applying heat. This method was applied to create an inclusion inside a muscle phantom to simulate an orthotropic tumour within the tissue. Following this approach, several methods were developed to create an inclusion within the muscle phantom using either heating or chemical processes. These techniques took advantage of a laser system to produce heat in a small area inside the muscle phantom or using a chemical material such as formalin to change the elastic property of the tissue.

Multi-mode fibre was inserted into the bovine tissue as multi-mode fibre has a large light carrying core and as a result a large area can be heated by the laser (Fig. 5.13). The laser transmission along the fibre was then carried out for twenty minutes to heat an area within the muscle phantom and create a stiff inclusion (Fig. 5.11).

Figure 5.3: Multi-mode fibre undergoing laser heating
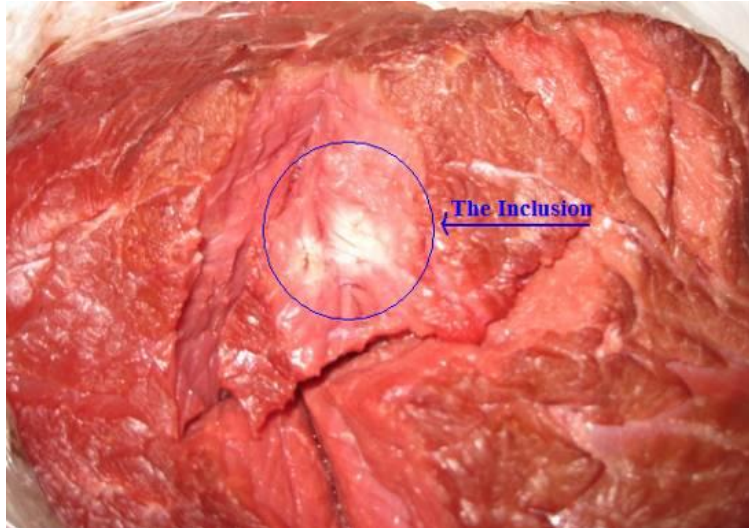
Figure 5.4: Dissection of bovine phantom to inspect inclusion

Figure 5.3 depicts multi-mode fibre with 1 mm diameter located inside the muscle phantom for twenty minutes in order to heat and create an inclusion using the laser transmission. Figure 5.4 shows a view of the bovine muscle phantom which has been cut to observe the heated area. The circled spot exhibits the material property changing within the tissue. The changed colour area represents the generated inclusion of about 20 mm diameter.

As the previous phantom was cut for the observation, another muscle phantom was fabricated in the same manner using the multi-mode fibre for the MRI scan. A coordinate system was defined for the phantom using three fiducial markers (MR-SPOTS, Beekley Corporation, USA) as shown in Figure 5.5.

Figure 5.5: Co-ordinate tabs fixed to new bovine phantom

The performance of the final muscle phantom which was used for the MRI scan. A coordinate system was defined for the phantom using three fiducial markers as shown in this picture. The muscle phantom was scanned with an excitation frequency of 100 Hz in three directions by rotating the phantom to measure sufficient MRI motion data. Boundary conditions applied to the muscle phantom show that only one face of the phantom which is located on the contact plate is restricted and the phantom is free on the remaining five sides.

Figures 5.6 to 5.8 display the three directional reconstructions for the heat modified bovine phantom. The ortho-code recon managed to converge on a solution and the resulting calculation clearly depicts the presence of a stiff inclusion in the phantom.
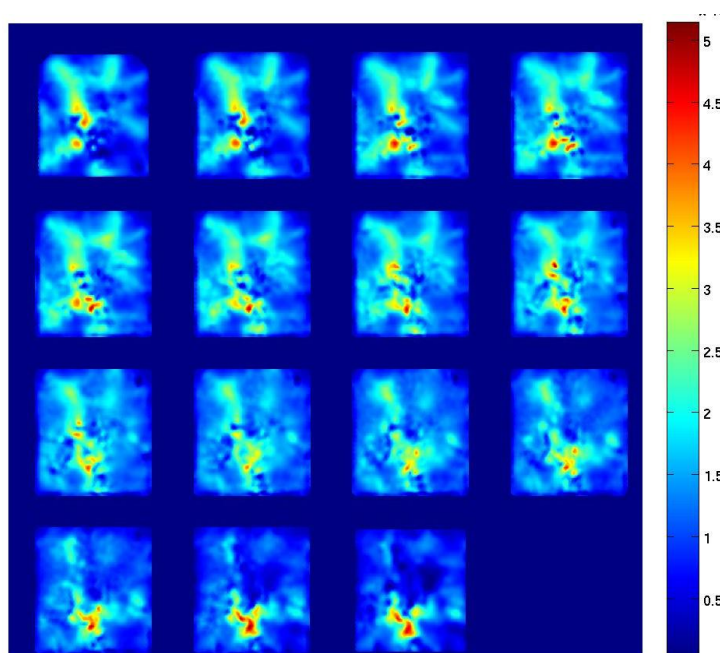
Figure 5.6: Shear Modulus reconstruction - X
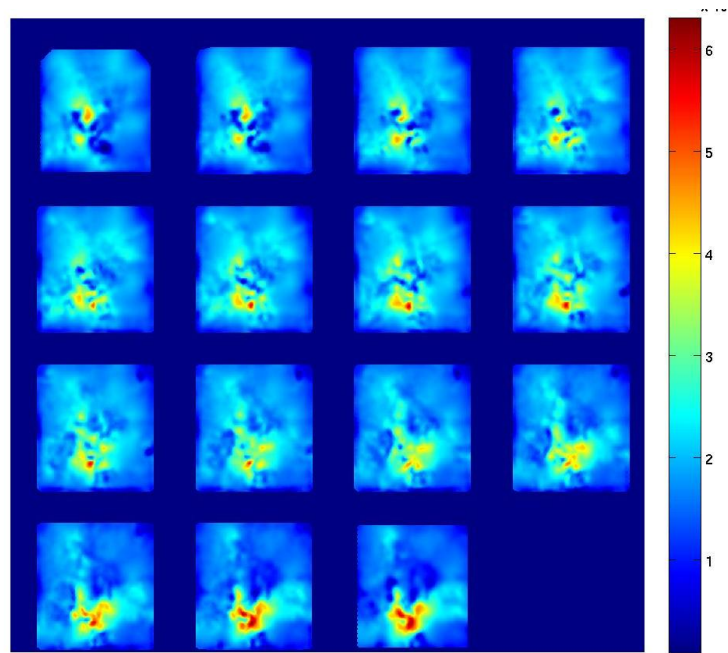
Figure 5.7: Shear Modulus reconstruction - Y
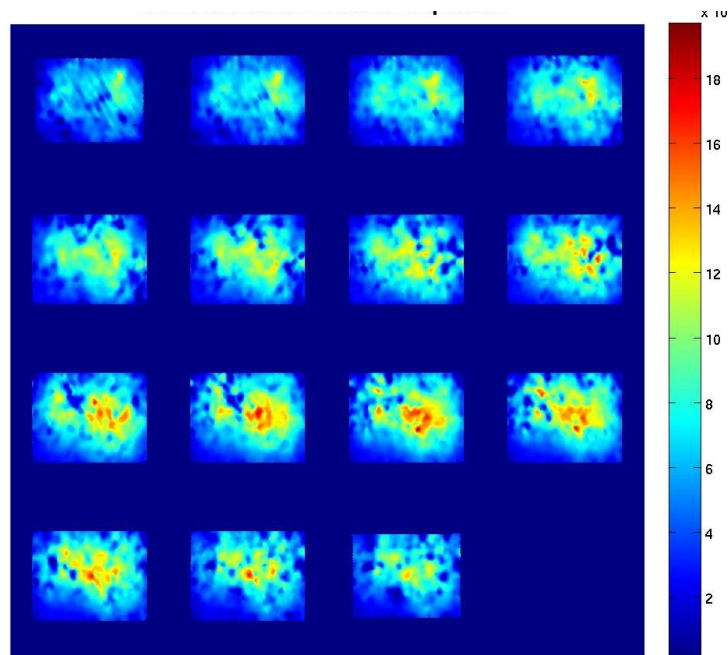
Figure 5.8: Shear Modulus reconstruction - Z

Fixation is a chemical procedure used to stabilize a tissue from degeneration. This method is widely used in histology, pathology etc. to terminate biochemical functions in tissue. The fixation process increases the mechanical stiffness and the stability of the tissue. Soft tissue can be preserved by different chemical agents known as fixatives such as acetone and formalin (formaldehyde) (Ryter, 1988 [181] and Friedrich et al, 2000 [182]).

In this case, formalin was used to create a stiff inclusion inside a muscle phantom. 2ml of formalin (A18-4, Fisher Scientific, Inc, USA) was injected inside the muscle phantom with a small syringe. From a central point of penetration, several injections were made at different angles to spread the formalin evenly throughout the phantom. This technique of injection was carried out to fabricate a three dimensional inclusion with sufficient thickness within the phantom.

After the formalin injection, the muscle phantom was cut for observation (Fig. 5.10). The colour conversion of the injected area can be interpreted to mean that material properties of this region have changed and a stiffer inclusion created.
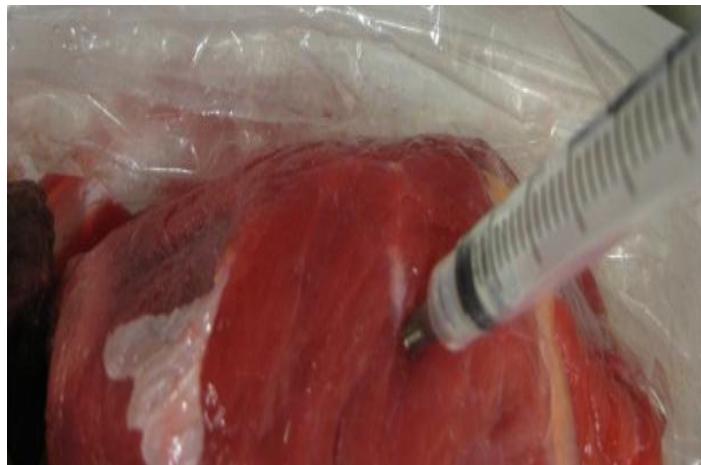
Figure 5.9: Syringe injecting Formalin into phantom

Figure 5.10: Dissected phantom to inspect chemical transformation

A pneumatic actuation system was used for exciting the phantom in the X direction with a frequency of 100 Hz. The free standing muscle phantom was scanned with a specific excitation frequency of 100 Hz in three dimensions by rotating the phantom in 3-D in three phases to collect sufficient motion data from this orthotropic phantom similar to the previous MRI data collection.

Boundary conditions applied to the muscle phantom allowed that only one face of the phantom which is located on the membrane of the pneumatic actuator is constrained. As a result, the phantom was free to move on its other five sides.

Figures 5.11 to 5.13 display the three directional reconstructions for chemically modified bovine phantom. The ortho-code recon managed to converge on a solution and the resulting calculation clearly depicts the presence of a stiff inclusion in the phantom.

Comparing the timing and performance of an direct analytical model to the finite difference algorithm was not possible, as the FD code was unable to converge on any solution, inversions where too computationally intensive. A several week reconstruction managed only a few initial iterations.
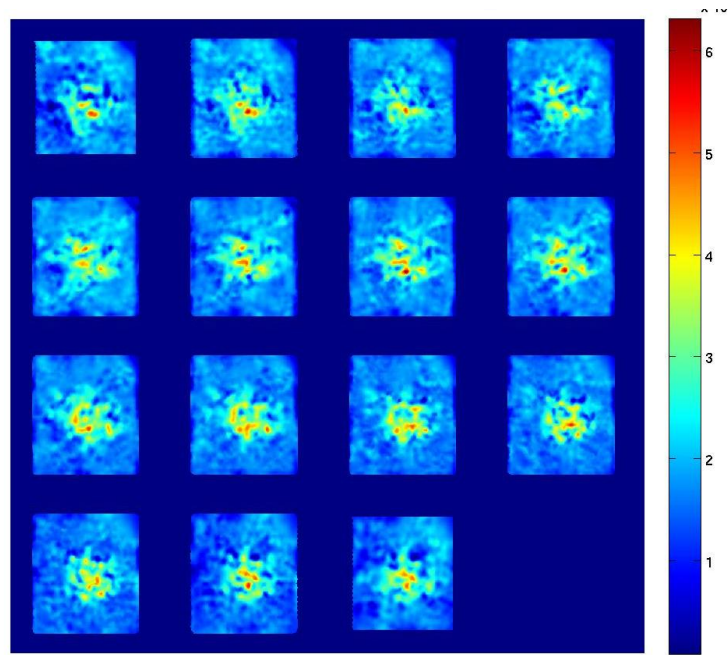
Figure 5.11: Shear Modulus reconstruction - X
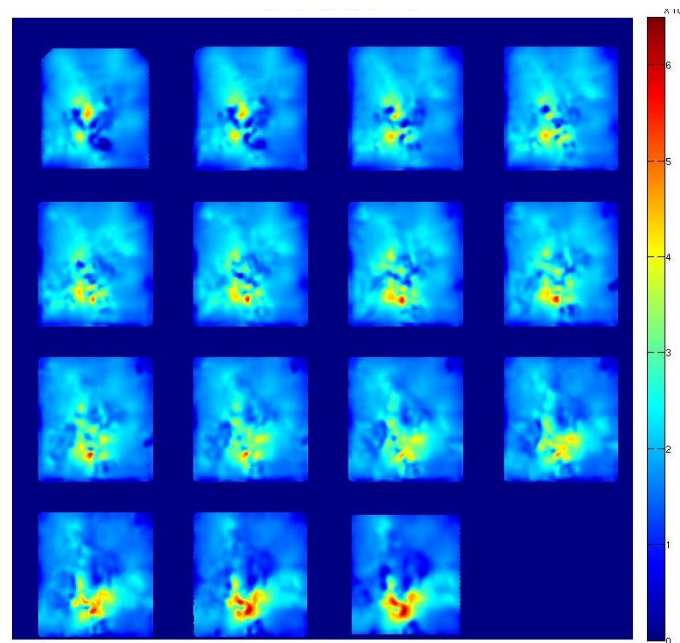
Figure 5.12: Shear Modulus reconstruction - Y
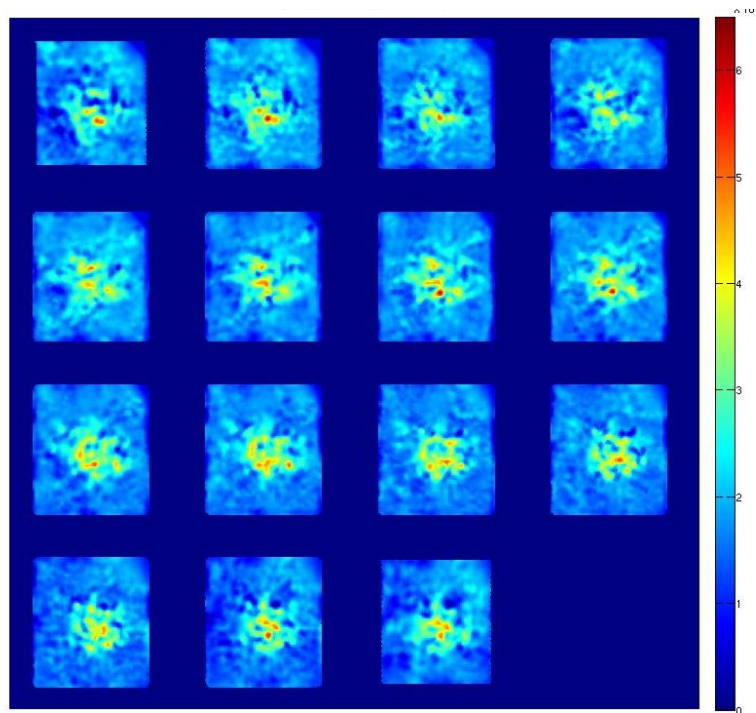
Figure 5.13: Shear Modulus reconstruction - Z

Chapter 6

Conclusions

Rayleigh Damped MRE reconstructions performed well. In comparison to conventional Viscoelastic reconstructions, Rayleigh damping could also identify stiff inclusions, through reconstructing the shear modulus and damping ratio. The Rayleigh composition added another parameter to characterize the material behaviour and hence added another degree of accuracy for identifying the inclusions. The Rayleigh Damped reconstructions showed promising results in simulations, gelatine phantoms, tofu (poro elastic) phantoms and in vivo reconstructions. Appropriate use of Total Variation improved the quality of the Rayleigh composition, which helped ascribe a degree of viscoelastic damping behaviour to specific regions of interest. Given the contrast observed in Rayleigh composition between healthy and cancerous regions, it's possible that the Rayleigh compositions will help to accurately identify and diagnose malignant tumours. A broader clinical trial is required, however the potential for Rayleigh damped reconstructions to form part of an MRE diagnostic tool, is evident.

Simulations to identify possible scattering effects within soft tissue revealed interesting attenuation behaviour. Scatterers present within a region of a mesh resulted in very minimal change in the damping response, a slight increase in stiffness, but noticeably a much higher change in viscoelastic behaviour, seen in the Rayleigh composition. Considering a model for frequency dispersion in breast tissue further supported the initial scattering results. Elastic dispersion relationships suggest a greater sensitivity from material property distributions, and a lower sensitivity from pore or scatterer density. This would was clearly visible in the simulation results where changes in shear modulus had a greater effect than varying the scatterer density. This has also been observed in poro elastic reconstructions where small variations in saturation, and hence bulk modulus, had significant effects on the reconstructed images. A better understanding of attenuation behaviour in specific tissue structures or regions could well contribute to a diagnostic model, especially as breast cancer significantly alter the tissue material properties.

A direct analytical formulation of the adjoint residual, vastly improved the reconstruction time for the orthotropic reconstruction algorithm. An average of 30% faster subzone and global iteration times, while maintaining an accurate residual. This reduction in run time would most likely increase further in more complex reconstructions with larger meshes, as the adjoint calculation only requires two complete forward solutions. With code run time reduced it may be viable to implement orthotropic material models, in inverse reconstructions improving their accuracy. A study with orthotropic phantoms and patient data would define the quality of an orthotropic reconstruction and its possible application to a diagnostic model.

The Rayleigh composition offers a new parameter to characterize regions within the breast, while the scattering and dispersion concepts identify specific attenuation behaviour in complex natural structures. The orthotropic algorithm, which may now be a viable reconstruction option, allows for a more accurate material model description. A clinical patient trial, where all three these results could be further analysed would most likely be very beneficial to future development.

References

1. American Cancer Society (2005). "Breast Cancer Facts & Figures 2005–2006" (PDF). http://www.cancer.org/downloads/ST/CAFF2005BrFacspdf2005.pdf.

2. Jemal A., Siegel R., Ward E., Hao Y., Xu J., Murray T. and Thun M.J. (2008). "Cancer Statistics, 2008". A Cancer Journal for Clinicians.

3. New Zealand Health Information Service (2006). "Cancer patient survival covering the period 1994 to 2003". NZ Ministry of Health.

4. Tabar L., Yen M.F., Vitak B., Chen H.H.T., Smith R.A. and Duffy S.W. (2003). "Mammography service screening and mortality in breast cancer patients: 20-year follow up before and after introduction of screening". The Lancet.

5. International Agency for Research on Cancer (2008). "World Cancer Report". http://globocan.iarc.fr/factsheets/populations/factsheet.asp?uno=900.

6. World Health Organization (2009). "WHO Disease and injury country estimates". http://www.who.int/healthinfo/global_burden_disease/estimates_country/en/index.html.

7. American Cancer Society (2007). "What Are the Key Statistics for Breast Cancer?". http://www.cancer.org/docroot/CRI/content/CRI_2_4_1X_What_are_the_key_statistics_for_breast_cancer_5.

8. Devilee P. and Tavassoli F. A., (2003). "Tumours of the Breast and Female Genital Organs". World Health Organization.

9. National Cancer Institute, (2011). "Stage Information for Breast Cancer". http://www.cancer.gov/cancertopics/pdq/treatment/breast/healthprofessional/page3

10. Tortora G. J. and Grabowski S. R., (2001). "Introduction to the Human Body: The Essentials of Anatomy and Physiology". John Wiley & Sons.

11. Gøtzsche P.C. and Nielsen M., (2009). "Screening for breast cancer with mammography". Cochrane Database System.

12. Cobbold R. S. C., (2006). "Foundations of Biomedical Ultrasound". Oxford University Press.

13. Morrow M., (2004). "Magnetic resonance imaging in breast cancer: one step forward, two steps back?". Journal of the American Medical Association.

14. Mendelson E. B., Chen J. and Karstaedt P., (2009). "Assessing tissue stiffness may boost breast imaging specificity". Diagnostic Imaging.

15. Oliphant T. E., Manduca A., Ehman R. L., and Greenleaf J. F., (2001). "Complex-valued stiffness reconstruction for magnetic resonance elastography by algebraic inversion of the differential equation". Magnetic Resonance in Medicine.

16. Sinkus R., Tanter M., Xydeas T., Catheline S., Bercoff J., and Fink M., (2005). "Viscoelastic shear properties of in vivo breast lesions measured by MR elastography". Magnetic Resonance Imaging.

17. Shewchuk J.R., (1994). "An introduction to the conjugate gradient method without the agonizing pain". unpublished paper.

18. Oberai A.A., Gokhale N.H., and Feij G.R., (2003). "Solution of inverse problems in elasticity imaging using the adjoint method". Inverse Problems.

19. Ling Liew H. and Pinsky P.M., (2005). "Recovery of shear modulus in elastography using an adjoint method with B-spline representation". Finite Elements in Analysis & Design.

20. Norton S.J., (1999). "Iterative inverse scattering algorithms: Methods of computing Fŕechet derivatives". The Journal of the Acoustical Society of America.

21. Vogel C.R., (2002). "Computational Methods for Inverse Problems". Society for Industrial Mathematics.

22. Van Houten E.E.W., Paulsen K.D., Miga M.I., Kennedy F.E., and Weaver J.B., (1999). "An overlapping subzone technique for MR-based elastic property reconstruction". Magnetic Resonance in Medicine.

23. Van Houten E. E. W., Weaver J. B., Miga M. I., Kennedy F. E., and Paulsen K. D., (2000). "Elasticity reconstruction from experimental MR displacement data: initial experience with an overlapping subzone finite element inversion process". Medical Physics.

24. Van Houten E. E. W., Miga M. I., Weaver J. B., Kennedy F. E., and Paulsen K. D., (2001). "Three dimensional subzone-based reconstruction algorithm for MR elastography". Magnetic Resonance in Medicine.

25. Sinkus R. , Siegmann K., Tanter M. , Xydeas T., Catheline S., Bercoff J., and Fink M., (2005). "Viscoelastic shear properties of in vivo breast lesions measured by MR Elastography". Magnetic Resonance Imaging.

26. Xydeas T., Siegmann K., Sinkus R., Krainick-Strobel U., Miller S., and Claussen C.D., (2005). "Magnetic resonance elastography of the breast: Correlation of signal intensity data with viscoelastic properties". Investigative Radiology.

27. Papazoglou S., Xu C., Hamhaber U., Siebert E., Bohner G., Klingebiel R., Braun J. and Sack I., (2009). "Scatter-based magnetic resonance elastography". Physics in Medicine and Biology.

28. Sinkus R., Siegmann K., Xydeas T., Tanter M., Claussen C., and Fink M., (2007). "MR elastography of breast lesions: understanding the solid/liquid duality can improve the specificity of contrast-enhanced MR mammography". Magnetic Resonance in Medicine.

29. Muki R. and Dong S.B., (2003). "A variational theorem for the scattering of steady elastic waves from inclusions". Mechanics Research Communications

30. Adelinet M., Fortin J., and Gueguen Y. (2010). "Dispersion of elastic moduli in a porous-cracked rock: Theoretical predictions for squirt-flow". Tectonophysics.

31. Shafiro B. and Kachanov M., (1996). "Materials with fluid-filled pores of various shapes: effective elastic properties and fluid pressure polarization". Solids Structures.

32. Zimmerman R.W., Somereton W.H. and King M.S., (1986). "Compressibility of Porous Rocks". Geophysical Research.

33. Taylor R.L. and Pister K.S., (1968). "On Variational Theorem for Incompressible and Nearly-Incompressible Orthotropic Elasticity". Solids Structures.

34. Sinkus R., Tanter M., Catheline S., Lorenzen J., Kuhl C., Sondermann E. and Fink M., (2005). "Imaging Anisotropic and Viscous Properties of Breast Tissue by Magnetic Resonance-Elastography". Magnetic Resonance in Medicine.

35. Perriñez P. R., Kennedy F. E., Van Houten E. E. W., Weaver J. B., and Paulsen K. D., (2010). "Member,Magnetic Resonance Poroelastography: An Algorithm for Estimating the Mechanical Properties of Fluid-Saturated Soft Tissues". IEEE.

36. Perriñez P. R., Kennedy F. E., Van Houten E. E. W., Weaver J. B., and Paulsen K. D., (2009). "Modeling of Soft Poroelastic Tissue in Time-Harmonic MR Elastography". IEEE.

37. Van Houten E. E. W., Miga M. I., Weaver J. B., Kennedy F. E., and Paulsen K. D., (2001). "Three-dimensional subzone-based reconstruction algorithm for MR elastography". Magnetic Resonance in Medicine.

38. Perreard I. M., Pattison A. J., Doyley M., McGarry M. D. J., Barani Z., Van Houten E. E. W., Weaver J. B. and Paulsen K. D., (2010). "Effects of frequency and direction dependent elastic materials on linearly elastic MRE image reconstructions". Physics in Medicine and Biology.

39. Sinkus R., Daire J., Van Beers B. E. and Vilgrain V., (2010). "Elasticity reconstruction: Beyond the assumption of local homogeneity". Comptes Rendus Mecanique.

40. Peters A., (2007) "Digital Image Elasto-Tomography: Mechanical property Reconstruction from Surface Measured Displacement Data". PhD thesis.

41. McGarry M. D. J., (2008). "Rayleigh Damped Magnetic Resonance Elastography". PhD Thesis.

42. Van Houten E.E.W., (2001). " Mechanical Property Reconstruction from MR Detected Harmonic Displacement Data". PhD Thesis.

43. Snoeren P.R. and Karssemeijer N., (2004). "Thickness correction of mammographic images by means of a global parameter model of the compressed breast". IEEE.

44. Moore S.K., (2001). "Better breast cancer detection". IEEE.

45. Sarvazyan A.P., Skovoroda A.R, Emelianov S.Y., Fowlkes J.B., Pipe J.G., Adler R.S, Boxton R.B., and Carson P.L., (1995). "Biophysical bases of elasticity imaging". Acoustical Imaging.

46. Sarvazyan A.P., (1998). "Mechanical imaging: A new technology for medical diagnostics". International Journal of Medical Informatics.

47. Krouskop T.A., Wheeler T.M., Kallel F., Garra B.S., and Hall T., (1998). "Elastic moduli of breast and prostate tissues under compression". Ultrasonic Imaging.

48. Samani A., Bishop J., Luginbuhl C., and Plewes D.B., (2003). "Measuring the elastic modulus of ex vivo small tissue samples". Physics in Medicine and Biology.

49. Samani A., Zubovits J., and Plewes D.B., (2007). "Elastic moduli of normal and pathological human breast tissues: An inversion technique based investigation of 169 samples". Physics in Medicine and Biology.

50. Wellman P.S., Howe R.D., Dalton E., and Kern K.A., (1999). "Breast tissue stiffness in compression is correlated to histological diagnosis". Technical report, Harvard BioRobotics Laboratory.

51. Ophir J., Cespedes I., Ponnekanti H., Yazdi Y., and Li X., (1991). "Elastography: A quantitative method for imaging the elasticity of biological tissues". Ultrasonic Imaging.

52. Warner E., Plewes D.B., Shumak R.S., Catzavelos G.C., Di Prospero L.S., Yaffe M.J., Goel V., Chart P.L., Ramsay E., Cole D.E.C., Taylor G.A., Cutrara M., Samuels T.H., Murphy J.P., Murphy J.M., and Narod S.A., (2001). "Comparison of breast magnetic resonance Imaging, mammography , and ultrasound for surveillance of women at high risk for hereditary breast cancer". Journal of Clinical Oncology.

53. Parker K. J., Taylor L. S., and Gracewski S., (2005). "A unified view of imaging the elastic properties of tissue". The Journal of the Acoustical Society of America.

54. Paulsen K.D., Meaney P.M., and Gilman L.C., (2005). "Alternative Breast Imaging: Four Model-Based Approaches". Springer.

55. Ophir J., Alam S.K., Garra B., Kallel F., Komofagou E., Krouskop T., and Varghese T., (1999). "Elastography: Ultrasonic estimation and imaging of the elastic properties of tissues". In Proceedings of the Institution of Mechanical Engineers.

56. Ophir J., Kallel F., Varghese T., Konofagou E., Alam S.K., Krouskop T., Garra B., and Righetti R., (2001). "Elastography". Comtes Rendus de l'Academiedes Sciences Series IV Physics.

57. Lerner R.M., Huang S.R., and Parker K.J. (1990)., " 'Sonoelasticity' images derived from ultrasound signals in mechanically vibrated tissues". Ultrasound in Medicine and Biology.

58. Lee F., Bronson J.P., Lerner R.M., Parker K.J., Huang S-R., and Roach J.B., (1990). "Sonoelastic imaging: Results in in-vitro tissue specimens". Radiology.

59. Barr R.G. (2006)., "Clinical applications of a real-time elastography technique in breast imaging". In Proceeding of the 5th International Conference on the Ultrasonic measurement and Imaging of Tissue Elasticity, Utah.

60. Frey H. (2003)., "Realtime elastography, a new ultrasound procedure for the reconstruction of tissue elasticity". Radiologe.

61. Bercoff J., Chaffai S., Tanter M., Sandrin L., Catheline S., Fink M., Gennisson J.L., and Meunier M. (2003)., "In vivo breast tumor detection using transient elastography". Ultrasound in Medicine and Biology.

62. Bercoff J., Tanter M., and Fink M. (2004)., "Supersonic shear imaging: A new technique for soft tissues elasticity mapping". IEEE Transactions on Ultrasonics, Ferroelectrics, and Frequency Control.

63. Lindop J.E., Treece G.M., Gee A.H., and Prager R.W. (2006)., "3D elastography using freehand ultrasound". Ultrasound in Medicine and Biology.

64. Park S., Aglyamov S.R., Scott W.G., and Emelianov S.Y., (2007). "Strain imaging using conventional and ultrafast ultrasound imaging: Numerical analysis". IEEE Transactions on Ultrasonics, Ferroelectrics, and Frequency Control.

65. Barbone P.E. and Bamber J.C., (2002). "Quantitative elasticity imaging: What you can do and cannot be inferred from strain images". Physics in Medicine and Biology.

66. Barbone P., Gokhale N., Richards M., Oberai A., and Doyley M., (2004). "Simultaneous elastic image registration and elastic modulus reconstruction". In Proceedings of the 2004 International Symposium on Biomedical Imaging: From Nano to Macro.

67. Barbone P.E. and Gokhale N. (2004)., "Elastic modulus imaging: On the uniqueness and nonuniqueness of the elastography inverse problem in two dimensions". Inverse Problems.

68. Doyley M.M., Srinivasan S., Pendergrass S.A., Wu Z., and Ophir J., (2005). "Comparative evaluation of strain-based and model-based modulus elastography". Ultrasound in Medicine and Biology.

69. Plewes D. B., Bishop J., Samani A., and Sciarretta J., (2000). "Visualization and quantification of breast cancer biomechanical properties with magnetic resonance elastography". Phys Med Biol.

70. Van Houten E.E.W., Miga M.I., Weaver J.B., Kennedy F.E., and Paulsen K.D., (2001). "Three-dimensional subzone-based reconstruction algorithm for MR elastography". Magnetic Resonance in Medicine.

71. Van Houten E.E.W., Doyley M.M., Kennedy F.E., Weaver J.B., and Paulsen K.D., (2003). "Initial in vivo experience with steady-state subzone-based MR elastography of the human breast". Journal of Magnetic Resonance Imaging.

72. Van Houten E.E.W., M.M. Doyley, Kennedy F.E., Paulsen K.D., and Weaver J.B., (2005)." A three parameter mechanical property reconstruction algorithm for MR-based elastic property imaging". IEEE Transactions on Medical Imaging.

73. Sinkus R., Lorenzen J., Schrader D., Lorenzen M., Dargatz M., and Holz D., (2000). "High-resolution tensor MR elastography for breast tumour detection". Physics in Medicine and Biology.

74. Manduca A., Oliphant T.E., Dresner M.A., Greenleaf J.F., and Ehman R.L. (2002). "Comparative evaluation of inversion algorithms for magnetic resonance elastography". In IEEE International Symposium on Biomedical Imaging.

75. Manduca A., Lake D.S., Kruse S.A., and Ehman R.L., (2003). "Spatio-temporal directional filtering for improved inversion of MR elastography images". Med Image Anal.

76. Sinkus R., Tanter M., Xydeas T., Catheline S., Bercoff J., and Fink M. (2005). "Viscoelastic shear properties of in vivo breast lesions measured by MR elastography". Magnetic Resonance in Medicine.

77. Barbone P.E. and Oberai A.A., (2007). "Elastic modulus imaging: Some exact solutions of the compressible elastography inverse problem". Physics in Medicine and Biology.

78. Aglyamov S.R., Skovoroda A.R., Xie H., Kim K., Rubin J.M., O'Donnell M., Wakefield T.W., Myers D., and Emelianov S.Y., (2007). "Model-based reconstructive elasticity imaging using ultrasound". International Journal of Biomedical Imaging.

79. Havre R.F., Elde E., Gilja O.H., Odegaard S., Eide G.E., Matre K., and Nesje L.B., (2008). "Freehand real-time elastography: Impact of scanning parameters on image quality and in-vitro intra- and intero-bserver validations". Ultrasound in Medicine and Biology.

80. Tohno E. and Ueno E., (2008). "Current improvements in breast ultrasound, with a special focus on elastography". Breast Cancer.

81. Zhu Q.L., Jiang Y.X., Liu J.B., Liu H., Sun Q., Dai Q., and Chen X., (2008). "Realtime ultrasound elastography: It's potential use in assessment of breast lesions". Ultrasound in Medicine and Biology.

82. McGarry M.D. and Van Houten E.E.W., (2008). "Use of a Rayleigh damping model in elastography". Medical and Biological Engineering and Computing.

83. Green M.A., Bilston L.E., and Sinkus R., (2008). "In vivo brain viscoelastic properties measured by magnetic resonance elastography". NMR in Biomedicine.

84. Wang H., Weaver J.B., Doyley M.M., Kennedy F.E., and Paulsen K.D., (2008). "Optimized motion estimation for MRE data with reduced motion encodes". Physics in Medicine and Biology.

85. Uffmann K. and Ladd M.E., (2008). "Actuation systems for MR elastography: design and applications". IEEE Engineering in Medicine and Biology Magazine.

86. Plewes D.B., Betty I., Urchuk S.N. and Soutar I., (1995). "Visualizing tissue compliance with MR imaging". Magn.Reson.Imaging.

87. Muthupillai R. and Ehman R. L., (1996). "Magnetic resonance elastography." Nat. Med.

88. Rothney M.P., Washington C.W., and Miga M.I., (2004). "Evaluation of a similarity-based elastography technique using four similarity metrics". In IEEE International Symposium on Biomedical Imaging.

89. Liu Y., Sun L.Z., and Wang G., (2005). "Tomography-based 3D anisotropic elastography using boundary measurements". IEEE Trans. Medical Imaging.

90. Van Houten E.E.W., Doyley M.M., Kennedy F.E., Paulsen K.D., and Weaver J.B., (2003). "A three-parameter mechanical property reconstruction & algorithm for MR based elastic property imaging". IEEE Transactions on Medical Imaging.

91. Van Houten E.E.W., Doyley M.M., Kennedy F.E., Weaver J.B., and Paulsen K.D., (2003). "Initial in vivo experience with steady-state subzone-based MR elastography of the human breast". Journal of Magnetic Resonance Imaging.

92. Weaver J.B., Van Houten E.E.W., Miga M.L., Kennedy F.E. and Paulsen K.D., (2001). "Magnetic resonance elastography using 3D gradient echo measurements of steady-state motion". Medical Physics.

93. Samani A., Plewes D., (2004). "A method to measure the hyperelastic parameters of ex vivo breast tissue samples". Phys. Med. Biol.

94. Perrinez P. R., (2005). "Determining the feasibility of reconstructing mechanical properties of living brain tissue using magnetic resonance elastography". Master of Science Thesis, Thayer School of Engineering, Dartmouth College, Hanover.

95. Hornak J.P., (1996). "The Basics of MRI". Department of Chemistry, Rochester Institute of Technology.

96. Morrow G., (2000). "Progress In MRI Magnets". Inter-magnetic General Corporation, Latham, New York, USA

97. Thomas S.R., Busse L.J., Schenck J.F., (1988). "Gradient Coil Technology in Magnetic Resonance Imaging". Saunders.

98. Kruse S. A., (2000). "characterization using magnetic resonance elastography: preliminary results". Phys. Med. Biol.

99. Muthupillai R., Lomas D. J., Rossman P. J., Greenleaf J. F., Manduca A., and Ehman R. L., (1995). "Magnetic resonance elastography by direct visualization of   propagating acoustic strain waves". Science.

100.   Engan H.E., Kim B.Y., Blake J.N., Shaw H.J., (1988). "Propagation and optical interaction of guided acoustic waves in two-mode optical fibers". Journal of Light wave Technology.

101.   Eringen C. A., Suhubi E. S., (1974). "Elastodynamics", Academic Press.

102.   Akalin Z., (1999). "Magnetic Resonance Elastography and Inverse problem solution in Elasticity". Proceeding of the first joint BMES/EMBS serving Humanity, Advancing technology.

103.   Mosher J.C., Leahy R.M., Lewis P.S., (1999). "EEG and MEG: Forward solutions for inverse methods". IEEE Transactions on Biomedical Engineering.

104.   Oliphant T.E., Manduca A., Ehman R.L., and Greenleaf J.F., (2001). "Complex-valued stiffness reconstruction for magnetic resonance elastography by algebraic inversion of the differential equation". Magnetic Resonance in Medicine.

105.   Weaver J.B., Van Houten E.E., Miga M. I., Kennedy F.E., and Paulsen K. D., (2001). "Magnetic resonance elastography using 3D gradient echo measurements of steady-state motion". Medical Physics.

106.   Glaser K.J., Felmlee J.P., Manduca A., and Ehman R.L., (2003). "Shear stiffness estimation using intra voxel phase dispersion in magnetic resonance elastography". Magnetic Resonance in Medicine.

107.   Wall D.J.N., Olssen P., and Van Houten E.E.W., (2006). "Some Results on the Conditioning of the Inverse Problem of Imaging in Magnetic Resonance Elastography" 5th International Conference on the Ultrasonic Measurement of Tissue Elasticity.

108.   Paulsen K.D., Meaney P.M., Gilman L.C., (2005). "Alternative Breast Imaging; Four Model-Based Approaches". Springer Science & Business.

109.   Bertaja M., Morigi S., Loli Piccolomini E., Sgallari F., Zama F., (2000). "Regularization of Large Discrete ill posed problems in image processing, Recent trends in Numerical analysis". Advances in the Theory of Computational Mathematics.

110.   Long-ji T., (1991). "Estimate of the condition number for some discrete ill-posed equation". Journal of Computational Mathematics.

111.   Chong E.K.P., Zak S.H., (2008). "An introduction to optimization". Wiley-Interscience.

112.   Absil P.A., Mahony R., Sepulchre R., (2008). "Optimization algorithms on matrix manifolds". Princeton University Press.

113.   Nocedal J., Wright S. J., (1999) "Numerical Optimization". Springer-Verlag.

114.   Liberti L., Maculan N., (2006). "Global optimization : from theory to implementation". Springer.

115.   Griva I., Nash S.G., Sofer A., (2009). "Linear and nonlinear optimization". Society for Industrial and Applied Mathematics.

116.   Buckley A.G., Goffin J.L., (1982). "Algorithms for constrained minimization of smooth nonlinear functions". Elsevier Science Pub.

117.   Bartholomew-Biggs M.C., (2005). "Nonlinear optimization with financial applications". Kluwer.

118.   Baldick R., (2006). "Applied optimization: formulation and algorithms for engineering systems". Cambridge University Press.

119.   Ortega J.M., Rheinboldt W.C., (2000). "Iterative Solution of Nonlinear Equations in Several Variables". Society for Industrial and Applied Mathematics.

120.   Norton S.J., (1999). "Iterative inverse scattering algorithms: Methods of computing Fŕechet derivatives". The Journal of the Acoustical Society of America.

121.   Jacoby S.L.S., Kowalik J.S., Pizzo J.T., (1972). "Iterative methods for nonlinear optimization problems". Prentice-Hall

122.   Kelley C.T., (1999). "Iterative methods for optimization". SIAM.

123.   Ipsen I.C.F., (2009). "Numerical matrix analysis: linear systems and least squares". Society for Industrial and Applied Mathematics.

124.   Epperson J. F., (2002). "An introduction to numerical methods and analysis". J. Wiley.

125.   Whittle P., (1983). "Prediction and regulation by linear least-square methods". Blackwell.

126.   Trombka J.I., Schmadebeck R.L., (1968). "A numerical least-square method for resolving complex pulse height spectra". National Aeronautics and Space Administration, Scientific and Technical Information Division.

127.   Marquadt D. W., (1953). "An algorithm for least-squares estimation of non-linear parameters". J. Soc. Indust. Appl. Math.

128.   Conn A.R., Gould, Nicholas I.M., Toint Ph.L., (2000). "Trust-region methods". Society for Industrial and Applied Mathematics.

129.   Bartholomew B., Michael C., (2008). "Nonlinear optimization with engineering applications". Springer.

130.   Ortega J.M., Rheinboldt W.C., (2000). "Iterative Solution of Nonlinear Equations in Several Variables". Classics in Applied Mathematics.

131.   Snyman J.A., (2005). "Practical mathematical optimization: an introduction to basic optimization theory and classical and new gradient-based algorithms". Springer.

132.   Lewis J.M., Lakshmivarahan S., Dhall S., (2006). "Dynamic data assimilation: a least squares approach". Cambridge University Press.

133.   Gilbert J.C. and Nocedal J., (1992). "Global convergence properties of conjugate gradient methods for optimization". Journal on Optimization.

134.   Wolfe P., (1969). "Convergence conditions for ascent methods". Review 11

135.   Fu M., Qiang Hu J., (1997). "Conditional Monte Carlo : gradient estimation and optimization applications". Kluwer Academic Publishers.

136.   Gill P.E., Murray W., (1979) "Conjugate-gradient methods for large scale nonlinear optimization". BUSAR.

137.   Shapira Y., (2008). "Matrix-based multi-grid : theory and applications". Springer Verlag.

138.   Adams L., Nazareth J.L., (1996). "Linear and nonlinear conjugate gradient-related methods". Society for Industrial and Applied Mathematics, Subject: Conjugate gradient methods.

139.   Kaltenbacher B., Neubauer A., Scherzer O., (2008). "Iterative regularization methods for nonlinear ill-posed problems". Walter de Gruyter

140.   Samarskii A.A., Vabishchevich P.N., (2007). "Numerical methods for solving inverse problems of mathematical physics". Walter de Gruyter.

141.   Aster R.C., Borchers B., Thurber C.H., (2005). "Parameter estimation and inverse problem". Elsevier Academic Press.

142.   Vogel C.R., (2002). "Computational Methods for Inverse Problems". Society for Industrial Mathematics.

143.   Aly H.A., (2005). "Image Up-Sampling Using Total-Variation Regularization with a New Observation Model". IEEE Transactions on Image Processing.

144.   Strong D., Chan T., (2003). "Edge-preserving and scale-dependent properties of total variation regularization". J. Inverse Problems.

145.   Osher S., Burger M., Goldfarb D., Xu J., Yin W., (2005). "An Iterative Regularization Method for Total Variation–Based Image Restoration". Multi-scale Model Simul.

146.   Ling Liew H. and Pinsky P.M., (2005). "Recovery of shear modulus in elastography using an adjoint method with B-spline representation". Finite Elements in Analysis & Design.

147.   Oberai A.A., Gokhale N.H., Doley M.M., Bamber J.C., (2004). "Evaluation of the adjoint equation based algorithm for elasticity imaging". Phys. Med. Biol

148.   Oberai A.A., Gokhale N.H., and Feij o G.R., (2003). "Solution of inverse problems in elasticity imaging using the adjoint method". Inverse Problems.

149.   Bland D.R., (1960). "The Theory of Linear Viscoelasticity". Pergamon Press, Oxford.

150.   Maniatty A.M., and Park E., (2005). "Finite Element Approach to Inverse Problem in Dynamic Elastography". Proceedings of the 5th International Conference on Inverse Problems in Engineering: Theory and Practice.

151.   Grandin H., (1991). "Fundamentals of the Finite Element Method". Waveland Press.

152. Cuvelier C., Segal A., and Van Steenhoven A.A., (1986). "Finite element methods and Navier-Stokes equation". D. Reidel Publishing Co.

153. Zienkiewicz O.C., Taylor R.L., (1994). "The Finite Element Method". McGraw Hill.

154. Nishinari K., Kohyama K., Zhang Y., Kitamura K., Sugimoto T., Saio K. and Kawamura Y., (1990). "Rheological Study on the Effect of the A5 Subunit on the Gelation Characteristics of Soybean Proteins". National Food Research Institute, National Agriculture Research Center.

155. Righetti R., Ophir J., Krouskop T.A., (2005). "A method for generating permeability elastograms and Poisson's ratio time-constant elastograms". Ultrasound Med.

156. Righetti R., Ophir J., Srinivasan S., Krouskop T.A., (2004). "The feasibility of using elastography for imaging the Poisson's ratio in porous media". Ultrasound Med.

157. Berry G.P., Bamber J.C., Armstrong C.G., Miller N.R., Barbone P.E., (2006). "Towards an acoustic modelbased poroelastic imaging method". Ultrasound Med.

158. Cheng AH-D., Badmus T., Beskos D.E., (1991). "Integral equation for dynamic poroelasticity in frequency domain with BEM solution". J Engrg Mech.

159. KROUSKOP T.A., DOUGHERTY D.R., VINSON F.S., (1987). "A pulsed Doppler ultrasonic system for making noninvasive measurements of the mechanical properties of soft tissue". Journal of Rehabilitation Research and Development.

160. Perrinez P., Kennedy F.E., Van Houten E.E., Weaver J.B., and Paulsen K. D., (2009). "Modeling of Soft Poroelastic Tissue in Time-Harmonic MR Elastography". IEEE.

161. Zhu Y. N., Hall T. J., and Jiang J. F., (2003). "A finite-element approach for Young's modulus reconstruction". IEEE Trans.

162. Kang H. B., Kim E., and Lee J. Y., (2003). "Identification of elastic inclusions and elastic moment tensors by boundary measurements". Inverse Prob., vol. 19.

163.   Liu H.T., Sun L.Z., Wang G., and Vannier M.W., (2003). "Analytic modelling of breast elastography". Med. Phys., vol. 30.

164.   Cox S.J., Gockenbach M., (1997). "Recovering planar Lame moduli from a single-traction experiment". Math. Mech. Solids.

165.   Fung Y. C., (1993). "Biomechanics: Mechanical Properties of Living Tissues". New York: Springer-Verlag.

166.   Sinkus R., Lorenzen J., Schrader D., Lorenzen M., Dargatz M., and Holz D., (2000). "High-resolution tensor MR elastography for breast tumor detection". Phys. Med. Biol

167.   Weaver J., Doyley M., Van Houten E., Hood M., Qin X. C., Kennedy F., Poplack S., and Paulsen K., (2002). "Evidence of the anisotropic nature of the mechanical properties of breast tissue". Med. Phys.

168.   Barber J.R., (1992). "Elasticity", Dordrecht ; Boston : Kluwer Academic Publishers

169.   François D., Pineau A., Zaoui A., (1998). "Mechanical behaviour of materials". Dordrecht; Boston: Kluwer Academic Publishers

170.   Ting T.C.T., (1996). "Anisotropic Elasticity: Theory and Applications". Oxford University Press; New York,

171.   Lekhnitskii S.G., (1981). "Theory of Elasticity of an Anisotropic Body". Moscow: MIR

172.   Ambartsumyan S.A., Kunin I.A., (1991). "Theory of anisotropic plates: strength, stability, and vibrations". New York : Hemisphere Pub.

173.   Lai W.M., Runin D., Krempl E., ()."Introduction to Continuum Mechanics", Program Press Inc.

174.   Haupt P., Kurth J. A., (2002). "Continuum mechanics and theory of materials", 2nd ed, Berlin: Springer-Verlag

175.   Love A. E., (1944). "A Treatise on the Theory of Elasticity". New York: Dover
         Publications

176.   Chen E. F., Saleeb A., (1982). "Constitutive Equations for Engineering
         Materials". New York: John Wiley &Sons, Inc.

177.   Desai C.S., Siriwardane H. J., (1984). "Constitutive Laws for Engineering Materials
         with Emphasis on Geologic Materials". New Jersey: Prentice-Hall

178.   Mascia N.T., Lahr F.A.R., (2006). "Remarks on orthotropic elastic models applied
         to wood". Mat. Res. vol.9

179.   Flewellen J.L., (2008). "Development of Clinically-Viable Applications of MR
         Elastography". MSc thesis in Physics, University of Canterbury

180.   Blemker S.S., Pinsky P.M., Delp S.L., (2005). "A 3D model of muscle reveals
         the cause of nonuniform strains in the biceps brachii". J. Biomechanics

181.   Ryter A., (1988). "Contribution of new cryomethods to a better knowledge
         of bacterial anatomy". Ann. Inst. Pasteur Microbiol.

182.   Friedrich C.L., Moyles D., Beveridge T.J., Hancock R.E.W., (2000). "Antibacterial
         Action of Structurally Diverse Cationic Peptides on Gram-Positive Bacteria",
         Antiomicrobial Agents and Chemotherapy

183.   Medical Illustrations by Patrick Lynch, generated for multimedia teaching
         projects by the Yale University School of Medicine, Center for Advanced
         Instructional Media, 1987-2000.

Appendices

A. Incompressible Elasticity Theory

The equations relating axial stress and strain for a compressible, linear elastic, isotropic material in three dimensions can be written as

$$\epsilon_x = \frac{1}{E}(\sigma_x - \nu(\sigma_y + \sigma_z))$$

$$\epsilon_y = \frac{1}{E}(\sigma_y - \nu(\sigma_x + \sigma_z))$$

$$\epsilon_z = \frac{1}{E}(\sigma_z - \nu(\sigma_x + \sigma_y))$$

[Eq. A.1]

where σx, σy and σz are the stresses in each of the coordinate directions, ϵ_x, ϵ_y and ϵ_z are the corresponding strains, E is the elastic modulus and ν is the Poisson's ratio. Rearranging Eq. A.1 to give stresses in terms of strains gives

$$\sigma_x = 2\mu\epsilon_x + \lambda(\epsilon_x + \epsilon_y + \epsilon_z)$$

$$\sigma_y = 2\mu\epsilon_y + \lambda(\epsilon_x + \epsilon_y + \epsilon_z)$$

$$\sigma_z = 2\mu\epsilon_z + \lambda(\epsilon_x + \epsilon_y + \epsilon_z)$$

with Lame's first parameter given by λ = vE(1+v)(1−2v), and Lame's second parameter, commonly known as the shear modulus, given by μ = E2(1+v). The definition of shear modulus gives the shear stresses, τ_{ij} as

$$\tau_{xy} = \mu\gamma_{xy}$$
$$\tau_{xz} = \mu\gamma_{xz}$$
$$\tau_{yz} = \mu\gamma_{yz}$$

[Eq. A.3]

where γ_{ij} are the corresponding shear strains. The volumetric strain, e, of an elastic solid is given by:

$$e = \frac{\Delta V}{V} = \epsilon_x + \epsilon_y + \epsilon_z$$

[Eq. A.4]

where ΔV is the change in total volume, V for a given strain state. The definitions of axial strains, $\varepsilon_x = \partial u/\partial x$, $\varepsilon_y = \partial u/\partial y$ and $\varepsilon_z = \partial u/\partial z$, mean the volumetric strain is also the divergence of the vector displacement field u, where $e = \nabla \cdot u$. As $v \rightarrow 0.5$, Eq. A.1 and Eq. A.4 show that $e \rightarrow 0$, therefore the material becomes incompressible.

Examining Eq. A.2, it is seen that the stresses are singular in this case, because as λ tends towards infinity, v tends towards 0.5. To deal with this singularity, the overall stress is broken down into two components, the dilatational stress, and the deviatoric stresses, so that

111

$$\sigma_x = \sigma'_x + \bar{\sigma}$$

$$\sigma_y = \sigma'_y + \bar{\sigma}$$

$$\sigma_z = \sigma'_z + \bar{\sigma}$$

[Eq. A.5]

where the dilatational stress is given by

$$\bar{\sigma} = \frac{1}{3}(\sigma_x + \sigma_y + \sigma_z) = \frac{1}{3}(2\mu + 3\lambda)e = Ke$$

[Eq. A.6]

And where the bulk modulus, K is given by

$$K = \frac{E}{3(1-2\nu)} = \frac{2\mu+3\lambda}{3}$$

[Eq. A.7]

The dilatational stress is often given as a scalar pressure,

$$\bar{\sigma} = Ke = -P$$

[Eq. A.8]

The deviatoric stresses are leftover once dilatational effects have been accounted for, so are given by

$$\sigma'_x = \sigma_x - \bar{\sigma}$$

$$\sigma'_y = \sigma_y - \bar{\sigma}$$

$$\sigma'_z = \sigma_z - \bar{\sigma}$$

[Eq. A.9]

and

$$\sigma_x + \sigma_y + \sigma_z = 3\bar{\sigma} + \sigma'_x + \sigma'_y + \sigma'_z = 3\frac{1}{3}(\sigma_x + \sigma_y + \sigma_z) + \sigma'_x + \sigma'_y + \sigma'_z$$

[Eq. A.10]

This implies

$$\sigma'_x + \sigma'_y + \sigma'_z = 0$$

[Eq. A.11]

The deviatoric stresses can be shown to produce no net volume change by considering the deviatoric strains,

$$\epsilon'_x = \frac{1}{E}(\sigma'_x - \nu(\sigma'_y + \sigma'_z))$$

$$\epsilon'_y = \frac{1}{E}(\sigma'_y - \nu(\sigma'_x + \sigma'_z))$$

$$\epsilon'_z = \frac{1}{E}(\sigma'_z - \nu(\sigma'_x + \sigma'_y))$$

113

The volumetric strain produced by the deviatoric stresses is given by

$$e' = \epsilon'_x + \epsilon'_y + \epsilon'_z = \frac{1 - 2\nu}{E}(\sigma'_x + \sigma'_y + \sigma'_z) = 0$$

The deviatoric stresses are therefore the components of the overall axial stress that produce changes in shape without any changes in volume. Using Eq. A.2, Eq. A.7 and Eq. A.9, the deviatoric stresses can be expressed as

$$\sigma'_x = 2\mu\epsilon_x + \lambda e - Ke$$
$$\sigma'_y = 2\mu\epsilon_y + \lambda e - Ke$$
$$\sigma'_z = 2\mu\epsilon_z + \lambda e - Ke$$

An incompressible material will have zero volumetric strain, e, therefore the deviatoric stresses in this case are given by

$$\sigma'_x = 2\mu\epsilon_x$$
$$\sigma'_y = 2\mu\epsilon_y$$
$$\sigma'_z = 2\mu\epsilon_z$$

The isotropic stress tensor, for an incompressible material is therefore given by

$$\vec{\vec{\sigma}} = \begin{pmatrix} \sigma_x & \tau_{xy} & \tau_{xz} \\ \tau_{yx} & \sigma_y & \tau_{yz} \\ \tau_{zx} & \tau_{zy} & \sigma_z \end{pmatrix}$$

[Eq. A.16]

where Eq. A.6, Eq. A.8 and Eq. A.15 give the axial stresses as

$$\sigma_x = 2\mu\epsilon_x - P$$
$$\sigma_y = 2\mu\epsilon_y - P$$
$$\sigma_z = 2\mu\epsilon_z - P$$

[Eq. A.17]

Eq. A.3 relating shear stresses and strains remains unchanged. Equilibrium conditions for the material occur when the internal stresses equal the sum of the inertial and external forces,

$$\nabla \cdot \vec{\vec{\sigma}} = \rho \frac{d^2 \mathbf{u}}{dt^2} + \mathbf{f}$$

[Eq. A.18]

where ρ is the density of the material and f represents the external forces. This divergence operation can be expanded in x, y, z coordinates as

$$\nabla \cdot \vec{\vec{\sigma}} = \nabla \cdot (\vec{\sigma_x}\hat{\mathbf{i}} + \vec{\sigma_y}\hat{\mathbf{j}} + \vec{\sigma_z}\hat{\mathbf{k}})$$

[Eq. A.19]

where

$$\vec{\sigma_x} = \sigma_x\hat{i} + \tau_{xy}\hat{j} + \tau_{xz}\hat{k}$$
$$\vec{\sigma_y} = \tau_{yx}\hat{i} + \sigma_y\hat{j} + \tau_{yz}\hat{k}$$
$$\vec{\sigma_y} = \tau_{zx}\hat{i} + \tau_{zy}\hat{j} + \sigma_z,\hat{k}$$

[Eq. A.20]

and i^, j^ and k^ are unit vectors in the x, y and z directions respectively. The definitions of axial and shear strains are given by

$$\epsilon_x = \frac{\partial u}{\partial x}$$
$$\epsilon_y = \frac{\partial v}{\partial y}$$
$$\epsilon_z = \frac{\partial w}{\partial z}$$

[Eq. A.21a]

$$\gamma_{xy} = \gamma_{yx} = \frac{\partial u}{\partial y} + \frac{\partial v}{\partial x}$$

$$\gamma_{xz} = \gamma_{zx} = \frac{\partial u}{\partial z} + \frac{\partial w}{\partial x}$$

$$\gamma_{yz} = \gamma_{zy} = \frac{\partial v}{\partial z} + \frac{\partial w}{\partial y}$$

[Eq. A.21b]

where u, v and w are the displacements in the x, y and z coordinate directions respectively. Combine Eq. A.17, Eq. A.3, Eq. A.19 and Eq.A.20 and Eq.A.21 gives

$$2\frac{\partial}{\partial x} \mu\frac{\partial u}{\partial x} + \frac{\partial}{\partial y} \mu(\frac{\partial u}{\partial y} + \frac{\partial v}{\partial x}) + \frac{\partial}{\partial z} \mu(\frac{\partial u}{\partial z} + \frac{\partial w}{\partial x}) - \frac{\partial P}{\partial x} - \rho\frac{\partial^2 u}{\partial t^2} = f_x$$

$$\frac{\partial}{\partial x} \mu(\frac{\partial v}{\partial x} + \frac{\partial u}{\partial y}) + 2\frac{\partial}{\partial y} \mu\frac{\partial v}{\partial y} + \frac{\partial}{\partial z} \mu(\frac{\partial v}{\partial z} + \frac{\partial w}{\partial y}) - \frac{\partial P}{\partial y} - \rho\frac{\partial^2 v}{\partial t^2} = f_y$$

$$\frac{\partial}{\partial x} \mu(\frac{\partial w}{\partial x} + \frac{\partial u}{\partial z}) + \frac{\partial}{\partial y} \mu(\frac{\partial w}{\partial y} + \frac{\partial v}{\partial z}) + 2\frac{\partial}{\partial z} \mu\frac{\partial w}{\partial z} - \frac{\partial P}{\partial z} - \rho\frac{\partial^2 w}{\partial t^2} = f_z$$

[Eq. A.22]

This can be written in the form of a partial differential equation (PDE) as,

$$\nabla \cdot \mu\nabla\tilde{\mathbf{u}} + \nabla(\mu\nabla \cdot \mathbf{u} - P) - \rho\frac{d^2\mathbf{u}}{dt^2} = \mathbf{f}$$

[Eq. A.23]

These equations, together with the continuity equation

117

$$K\frac{\partial u}{\partial x} + K\frac{\partial v}{\partial y} + K\frac{\partial w}{\partial z} = P$$

[Eq. A.24]

describe the behavior of a material with a Poisson's ratio of 0.499999 and higher. Standard compressible elasticity equations become highly sensitive for Poisson's ratio's of above about 0.495. Eq. A.24 means that the term $\nabla \cdot u$ in Eq. A.23 → zero as K → infinity. This term is left in the PDE to ensure the boundary integrals in the finite element weak form represent elastic stresses.

B. Finite Element Formulation

This section details the methods used to transform the incompressible elasticity equations into a finite element (FE) form. Figure B.1 shows the 27 node hexahedral elements used in the FE formulation, with the local (ξ, η, ζ) coordinate system.
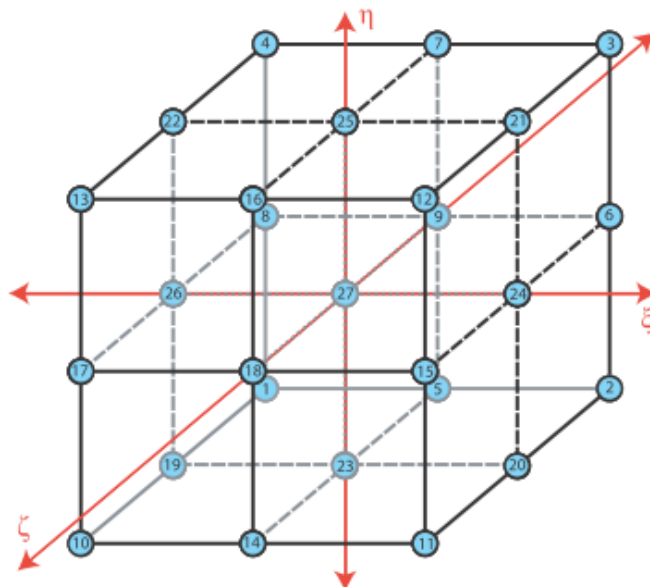
Figure B.1: 27 node Hexahedral element with node numbering scheme and local (ξ, η, ζ) coordinate system

Tri-quadratic displacement and tri-linear pressure support are used, as elements with displacement support one order above that of pressure give good convergence behavior for incompressible materials. The node numbering scheme is shown in the figure, and given by the nodal coordinates:

$$
\begin{array}{lll}
X_1 = (-1,-1,-1) & X_{10} = (-1,-1,\ 1) & X_{19} = (-1,-1,\ 0) \\
X_2 = (\ 1,-1,-1) & X_{11} = (\ 1,-1,\ 1) & X_{20} = (\ 1,-1,\ 0) \\
X_3 = (\ 1,\ 1,-1) & X_{12} = (\ 1,\ 1,\ 1) & X_{21} = (\ 1,\ 1,\ 0) \\
X_4 = (-1,\ 1,-1) & X_{13} = (-1,\ 1,\ 1) & X_{22} = (-1,\ 1,\ 0) \\
X_5 = (\ 0,-1,-1) & X_{14} = (\ 0,-1,\ 1) & X_{23} = (\ 0,-1,\ 0) \\
X_6 = (\ 1,\ 0,-1) & X_{15} = (\ 1,\ 0,\ 1) & X_{24} = (\ 1,\ 0,\ 0) \\
X_7 = (\ 0,\ 1,-1) & X_{16} = (\ 0,\ 1,\ 1) & X_{25} = (\ 0,\ 1,\ 0) \\
X_8 = (-1,\ 0,-1) & X_{17} = (-1,\ 0,\ 1) & X_{26} = (-1,\ 0,\ 0) \\
X_9 = (\ 0,\ 1,-1) & X_{18} = (\ 0,\ 1,\ 1) & X_{27} = (\ 0,\ 1,\ 0)
\end{array}
$$

[Eq. B.1]

Quadratic elements perform well for geometries with curved boundaries and displacement patterns, and hexahedral elements were chosen as the regular pattern of nodes is compatible with the voxel-based MRI motion data. Support of a function, g(ξ, η, ζ) on a set of basis functions is defined as

$$
g(\xi, \eta, \zeta) \approx \sum_{i=1}^{N} (g_i \phi_i(\xi, \eta, \zeta))
$$

[Eq. B.2]

where g_i is the function value at the N nodes of the element, and ϕ_i are the basis functions, given by

$$\phi_{1+9i}(\xi,\eta,\zeta) = \theta_1(\xi)\theta_1(\eta)\theta_{i+1}(\zeta)$$
$$\phi_{2+9i}(\xi,\eta,\zeta) = \theta_2(\xi)\theta_1(\eta)\theta_{i+1}(\zeta)$$
$$\phi_{3+9i}(\xi,\eta,\zeta) = \theta_2(\xi)\theta_2(\eta)\theta_{i+1}(\zeta)$$
$$\phi_{4+9i}(\xi,\eta,\zeta) = \theta_1(\xi)\theta_2(\eta)\theta_{i+1}(\zeta)$$
$$\phi_{5+9i}(\xi,\eta,\zeta) = \theta_3(\xi)\theta_1(\eta)\theta_{i+1}(\zeta)$$
$$\phi_{6+9i}(\xi,\eta,\zeta) = \theta_2(\xi)\theta_3(\eta)\theta_{i+1}(\zeta)$$
$$\phi_{7+9i}(\xi,\eta,\zeta) = \theta_3(\xi)\theta_2(\eta)\theta_{i+1}(\zeta)$$
$$\phi_{8+9i}(\xi,\eta,\zeta) = \theta_1(\xi)\theta_3(\eta)\theta_{i+1}(\zeta)$$
$$\phi_{9+9i}(\xi,\eta,\zeta) = \theta_3(\xi)\theta_3(\eta)\theta_{i+1}(\zeta)$$

[Eq. B.3]

where i = 0, 1, 2, and

$$\theta_1(s) = \frac{s}{2}(s-1)$$
$$\theta_2(s) = \frac{s}{2}(s+1)$$
$$\theta_3(s) = (1+s)(1-s)$$

[Eq. B.4]

Each basis function, ϕ_i, has a value of 1 at node i, and zero at all other nodes. They are constructed so that for any point $([\bar{\xi},\bar{\eta},\bar{\zeta}])$ within the element,

$$\sum_{i=1}^{27} \phi_i(\bar{\xi}, \bar{\eta}, \bar{\zeta}) = 1$$

the x, y and z coordinates, as well as the u, v and w displacements are supported on these basis functions, so this type of element is known as "Isoparametric", because both the displacements and coordinates are described by the same parametric variation. This ensures the element possesses rigid body modes, e.g. the element can displace as a whole with no internal stresses generated. If φ = [φ₁ φ₂ . . . φ₂₇], the displacements, u, v, w, and coordinates, x, y, z, are given by

$$\left\{ \begin{array}{c} \mathbf{u} \\ \mathbf{v} \\ \mathbf{w} \end{array} \right\} = \left[\begin{array}{ccc} \phi & 0 & 0 \\ 0 & \phi & 0 \\ 0 & 0 & \phi \end{array} \right] \left\{ \begin{array}{c} \mathbf{U}_i \\ \mathbf{V}_i \\ \mathbf{W}_i \end{array} \right\}$$

$$\left\{ \begin{array}{c} \mathbf{x} \\ \mathbf{y} \\ \mathbf{z} \end{array} \right\} = \left[\begin{array}{ccc} \phi & 0 & 0 \\ 0 & \phi & 0 \\ 0 & 0 & \phi \end{array} \right] \left\{ \begin{array}{c} \mathbf{X}_i \\ \mathbf{Y}_i \\ \mathbf{Z}_i \end{array} \right\}$$

where U_i, V_i and W_i are vectors containing the appropriate nodal displacement at all 27 nodes, and similarly X_i, Y_i, and Z_i contain the appropriate nodal coordinates. The tri-linear pressure function, P (x, y, z) is supported over the element by a constant P, ∂P/∂x, ∂P/∂y and ∂P/∂z. This basis function is denoted by ψ, so that the pressure distribution is given by

$$P(\xi, \eta, \zeta) = \sum_{i=1}^{4} [\mathbf{p}_i \psi_i(\xi, \eta, \zeta)]$$

where p_i is a vector which contains the constant pressure and its derivatives for a given element, and the basis functions ψ_i are given by

$$\psi_1 = 1$$
$$\psi_2 = \xi$$
$$\psi_3 = \eta$$
$$\psi_4 = \zeta$$

An arbitrarily shaped element in the (x, y, z) coordinate system is mapped onto the reference element shown in Fig. B.1 ((ξ, η, ζ) coordinate system) by the transformation

$$\mathbf{x} = F_e(\boldsymbol{\xi})$$

where x represents a coordinate in the x, y, z coordinate system, ξ represents a coordinate in the ξ, η, ζ coordinate system, and Fe is given by

$$F_e = \sum_{i=1}^{27} (x_i \phi_i(\boldsymbol{\xi}))$$

The derivatives of the basis functions between the two coordinate systems are related by

$$
\begin{bmatrix} \frac{\partial \phi_i}{\partial \xi} \\ \frac{\partial \phi_i}{\partial \eta} \\ \frac{\partial \phi_i}{\partial \zeta} \end{bmatrix} = \begin{bmatrix} \frac{\partial x}{\partial \xi} & \frac{\partial y}{\partial \xi} & \frac{\partial z}{\partial \xi} \\ \frac{\partial x}{\partial \eta} & \frac{\partial y}{\partial \eta} & \frac{\partial z}{\partial \eta} \\ \frac{\partial x}{\partial \zeta} & \frac{\partial y}{\partial \zeta} & \frac{\partial z}{\partial \zeta} \end{bmatrix} \begin{bmatrix} \frac{\partial \phi_i}{\partial x} \\ \frac{\partial \phi_i}{\partial y} \\ \frac{\partial \phi_i}{\partial z} \end{bmatrix} = \begin{bmatrix} \mathbf{J}_c \end{bmatrix} \begin{bmatrix} \frac{\partial \phi_i}{\partial x} \\ \frac{\partial \phi_i}{\partial y} \\ \frac{\partial \phi_i}{\partial z} \end{bmatrix}
$$

[Eq. B.11]

Using Eq. B.6b, the coordinate Jacobian, J_c, can be calculated by

$$
\begin{bmatrix} \mathbf{J}_c \end{bmatrix} = \begin{bmatrix} \frac{\partial \phi}{\partial \xi} \\ \frac{\partial \phi}{\partial \eta} \\ \frac{\partial \phi}{\partial \zeta} \end{bmatrix} \begin{bmatrix} \mathbf{X}_i & \mathbf{Y}_i & \mathbf{Z}_i \end{bmatrix}
$$

[Eq. B.12]

C. Regularization Techniques

The error function, Φ, places no restrictions on the material property values or their distribution. This means any distribution which decreases Φ will be acceptable as a solution, whether or not it is physically realistic. Some a-priori information about the true material property solution can be deduced by considering the structure of human tissue. Techniques which involve modifying Φ in an attempt to make the reconstruction algorithm prefer solutions which fit this a-priori information are known as regularization techniques. Three regularization methods are included in the reconstruction code, Tikhonov, Total variation minimization and spatial filtering. To increase the flexibility of the inversion algorithm, the relative level of each type of regularization is allowed to vary linearly as the iterations progress.

Tikhonov Regularization

A rough estimate for the material property values is provided as an initial guess to the material property distribution. Tikhonov regularization is a method of ensuring the material property solution does not vary wildly from this initial guess. The function for Φ is modified to Φ_{tk},

$$\Phi_{tk} = \frac{1}{2}(\mathbf{u}_c - \mathbf{u}_m)^H(\mathbf{u}_c - \mathbf{u}_m) + \alpha_{tk}(\boldsymbol{\theta} - \boldsymbol{\theta}_0)^H(\boldsymbol{\theta} - \boldsymbol{\theta}_0)$$

[Eq. C.1]

where θ is the current material property estimate, θ_0 is the initial material property guess, and α_{tk} is the weighting applied to Tikhonov regularization. This Regularization technique effectively penalizes solutions according to how far they deviate from the initial guess, therefore will preferentially select solutions which are closer to the initial guess. A modification to this method is where θ_0 is set to the previous material property estimate at each iteration, limiting the change in material properties for each iteration, but not the total deviation from the initial guess.

Total variation minimization

Human tissue contains areas of particular tissue types, with each area having approximately constant material properties. Total variation minimization (TV) provides a means to preferentially select material property distributions which consist of discrete regions of constant material properties over distributions with a greater degree of spatial variation. The function for Φ is modified to Φ_{tv},

$$\Phi_{tv} = \frac{1}{2}(\mathbf{u}_c - \mathbf{u}_m)^H(\mathbf{u}_c - \mathbf{u}_m) + \iiint\limits_{\Omega} \left(\alpha_{tv}\sqrt{\nabla\boldsymbol{\theta}^H\dot{\nabla}\boldsymbol{\theta}}\right)dV$$

where $\nabla\theta$ is the spatial variation of the material property, θ, and α_{tv} is the weighting applied to TV. The integral means that the level of total variation is the area under the $\sqrt{\nabla\theta H \nabla\theta}$ curve. The addition of total variation minimization will preferentially select material property distributions consisting of discrete regions of constant material properties over distributions with higher levels of spatial variation which will hopefully lead to cleaner, more physiologically correct image.

Spatial Filtering

Spatial filtering is a smoothing technique, based on the idea that there should not be large variations in material properties in regions of a particular tissue type. It does have the effect losing some of the definition of boundaries between tissue types, so is often used with a low weighting at later iterations. The technique involves simply replacing each material property value with a weighted average of the material property value and that of its closest neighbours, so that the spatially filtered value for a material is

$$\theta_k = (1 - W_{sf})\theta_k + \frac{w_{sf}}{N_{con}} \sum_{l=1}^{N_{con}} (\theta_l)$$

where w_{sf} is a weighting applied to spatial filtering, lt refers to the nodes in the vicinity of node k, and N_{con} is the number of these nodes.

D. Adjoint Residual Terms

$$\left(F_i\beta_{ij}F_j + F_i\beta_{ik}B_{kl}^{-1}\beta_{lj}F_j\right)H - F_i\beta_{ik}B_{kj}^{-1}\varepsilon_j = 0 \qquad i,j,k = 1,2,...,6$$

[Eq. 5.11]

Equation 5.11 with the expanded constitutive terms,

$$0 = \left\| \left(S_{11} - \frac{S_{32}S_{11} - S_{12}S_{31}}{S_{23}} + S_{21} + S_{31} + \frac{\left(S_{11} - \frac{S_{32}S_{11} - S_{12}S_{31}}{S_{23}} + S_{21} + S_{31} \right)^2 S_{23}}{S_{32}S_{11} - S_{12}S_{31}} \right) H \right.$$

$$- \frac{\left(S_{11} - \frac{S_{32}S_{11} - S_{12}S_{31}}{S_{23}} + S_{21} + S_{31} \right)\varepsilon_1 S_{23}}{S_{32}S_{11} - S_{12}S_{31}},$$

$$\left(S_{21} + S_{22} + \frac{S_{21}S_{32} - S_{22}S_{31}}{S_{13}} + S_{32} - \frac{\left(S_{21} + S_{22} + \frac{S_{21}S_{32} - S_{22}S_{31}}{S_{13}} + S_{32} \right)^2 S_{13}}{S_{21}S_{32} - S_{22}S_{31}} \right) H$$

$$+ \frac{\left(S_{21} + S_{22} + \frac{S_{21}S_{32} - S_{22}S_{31}}{S_{13}} + S_{32} \right)\varepsilon_2 S_{13}}{S_{21}S_{32} - S_{22}S_{31}},$$

$$\left(S_{31} + S_{32} + S_{33} - \frac{S_{21}S_{33} - S_{23}S_{31}}{S_{12}} + \frac{\left(S_{31} + S_{32} + S_{33} - \frac{S_{21}S_{33} - S_{23}S_{31}}{S_{12}} \right)^2 S_{12}}{S_{21}S_{33} - S_{23}S_{31}} \right) H$$

$$\left. - \frac{\left(S_{31} + S_{32} + S_{33} - \frac{S_{21}S_{33} - S_{23}S_{31}}{S_{12}} \right)\varepsilon_3 S_{12}}{S_{21}S_{33} - S_{23}S_{31}}, 0, 0, 0 \right\|$$

The Orthotropic Adjoint Stiffness matrix A =

$$\left[\left[\frac{\left(\frac{\partial}{\partial x}u(x,y,z)\right)S_{23}\left(\frac{\partial}{\partial x}\varphi_{ix}(x,y,z)\right)}{S_{32}S_{11}-S_{12}S_{31}}+\frac{\left(\frac{\partial}{\partial y}u(x,y,z)\right)\left(\frac{\partial}{\partial y}\varphi_{ix}(x,y,z)\right)}{S_{44}}+\frac{\left(\frac{\partial}{\partial z}u(x,y,z)\right)\left(\frac{\partial}{\partial z}\varphi_{ix}(x,y,z)\right)}{S_{66}},\right.\right.$$

$$\frac{\left(\frac{\partial}{\partial x}v(x,y,z)\right)\left(\frac{\partial}{\partial y}\varphi_{ix}(x,y,z)\right)}{S_{44}},\frac{\left(\frac{\partial}{\partial x}w(x,y,z)\right)\left(\frac{\partial}{\partial z}\varphi_{ix}(x,y,z)\right)}{S_{66}},$$

$$\left.-\frac{\left(S_{11}-\frac{S_{32}S_{11}-S_{12}S_{31}}{S_{23}}+S_{21}+S_{31}\right)HS_{23}\left(\frac{\partial}{\partial x}\varphi_{ix}(x,y,z)\right)}{S_{32}S_{11}-S_{12}S_{31}}\right],$$

$$\left[\frac{\left(\frac{\partial}{\partial y}u(x,y,z)\right)\left(\frac{\partial}{\partial x}\varphi_{iy}(x,y,z)\right)}{S_{44}},-\frac{\left(\frac{\partial}{\partial y}v(x,y,z)\right)S_{13}\left(\frac{\partial}{\partial y}\varphi_{iy}(x,y,z)\right)}{S_{21}S_{32}-S_{22}S_{31}}+\frac{\left(\frac{\partial}{\partial x}v(x,y,z)\right)\left(\frac{\partial}{\partial x}\varphi_{iy}(x,y,z)\right)}{S_{44}}+\right.$$

$$\frac{\left(\frac{\partial}{\partial z}v(x,y,z)\right)\left(\frac{\partial}{\partial z}\varphi_{iy}(x,y,z)\right)}{S_{55}},\frac{\left(\frac{\partial}{\partial y}w(x,y,z)\right)\left(\frac{\partial}{\partial z}\varphi_{iy}(x,y,z)\right)}{S_{55}},$$

$$\left.\frac{\left(S_{21}+S_{22}+\frac{S_{21}S_{32}-S_{22}S_{31}}{S_{13}}+S_{32}\right)HS_{13}\left(\frac{\partial}{\partial y}\varphi_{iy}(x,y,z)\right)}{S_{21}S_{32}-S_{22}S_{31}}\right],$$

$$\left[\frac{\left(\frac{\partial}{\partial z}u(x,y,z)\right)\left(\frac{\partial}{\partial x}\varphi_{iz}(x,y,z)\right)}{S_{66}},\frac{\left(\frac{\partial}{\partial z}v(x,y,z)\right)\left(\frac{\partial}{\partial y}\varphi_{iz}(x,y,z)\right)}{S_{55}},\frac{\left(\frac{\partial}{\partial z}w(x,y,z)\right)S_{12}\left(\frac{\partial}{\partial z}\varphi_{iz}(x,y,z)\right)}{S_{21}S_{33}-S_{23}S_{31}}+\right.$$

$$\frac{\left(\frac{\partial}{\partial y}w(x,y,z)\right)\left(\frac{\partial}{\partial y}\varphi_{iz}(x,y,z)\right)}{S_{55}}+\frac{\left(\frac{\partial}{\partial x}w(x,y,z)\right)\left(\frac{\partial}{\partial x}\varphi_{iz}(x,y,z)\right)}{S_{66}},$$

$$\left.\left.-\frac{\left(S_{31}+S_{32}+S_{33}-\frac{S_{21}S_{33}-S_{23}S_{31}}{S_{12}}\right)HS_{12}\left(\frac{\partial}{\partial z}\varphi_{iz}(x,y,z)\right)}{S_{21}S_{33}-S_{23}S_{31}}\right]\right]$$

In order to build the Jacobian matrix directly, it is necessary to determine the derivative terms for the stiffness matrix with respect to the compliance terms analytically. The 16 non-zero derivate terms have been expanded below,

$$\frac{d}{dS_{11}} A[1,1] = -\frac{\left(\frac{\partial}{\partial x} u(x,y,z)\right) S_{23} \left(\frac{\partial}{\partial x} \varphi_{ix}(x,y,z)\right) S_{32}}{\left(S_{32} S_{11} - S_{12} S_{31}\right)^2}$$

$$\frac{d}{dS_{11}} A[1,4] = -\frac{\left(1 - \frac{S_{32}}{S_{23}}\right) HS_{23} \left(\frac{\partial}{\partial x} \varphi_{ix}(x,y,z)\right)}{S_{32} S_{11} - S_{12} S_{31}} + \frac{\left(S_{11} - \frac{S_{32} S_{11} - S_{12} S_{31}}{S_{23}} + S_{21} + S_{31}\right) HS_{23} \left(\frac{\partial}{\partial x} \varphi_{ix}(x,y,z)\right) S_{32}}{\left(S_{32} S_{11} - S_{12} S_{31}\right)^2}$$

$$\frac{d}{dS_{22}} A[2,2] = -\frac{\left(\frac{\partial}{\partial y} v(x,y,z)\right) S_{13} \left(\frac{\partial}{\partial y} \varphi_{iy}(x,y,z)\right) S_{31}}{\left(S_{21} S_{32} - S_{22} S_{31}\right)^2}$$

$$\frac{d}{dS_{22}} A[2,4] = \frac{\left(1 - \frac{S_{31}}{S_{13}}\right) HS_{13} \left(\frac{\partial}{\partial y} \varphi_{iy}(x,y,z)\right)}{S_{21} S_{32} - S_{22} S_{31}} + \frac{\left(S_{21} + S_{22} + \frac{S_{21} S_{32} - S_{22} S_{31}}{S_{13}} + S_{32}\right) HS_{13} \left(\frac{\partial}{\partial y} \varphi_{iy}(x,y,z)\right) S_{31}}{\left(S_{21} S_{32} - S_{22} S_{31}\right)^2}$$

$$\frac{d}{dS_{33}} A[3,3] = -\frac{\left(\frac{\partial}{\partial z} w(x,y,z)\right) S_{12} \left(\frac{\partial}{\partial z} \varphi_{iz}(x,y,z)\right) S_{21}}{\left(S_{21} S_{33} - S_{23} S_{31}\right)^2}$$

$$\frac{\mathrm{d}}{\mathrm{d}S_{33}} A[3,4] = -\frac{\left(1 - \frac{S_{21}}{S_{12}}\right) H S_{12} \left(\frac{\partial}{\partial z} \varphi_{iz}(x,y,z)\right)}{S_{21} S_{33} - S_{23} S_{31}} +$$

$$\frac{\left(S_{31} + S_{32} + S_{33} - \frac{S_{21} S_{33} - S_{23} S_{31}}{S_{12}}\right) H S_{12} \left(\frac{\partial}{\partial z} \varphi_{iz}(x,y,z)\right) S_{21}}{\left(S_{21} S_{33} - S_{23} S_{31}\right)^2}$$

$$\frac{\mathrm{d}}{\mathrm{d}S_{12}} A[1,1] = \frac{\left(\frac{\partial}{\partial x} u(x,y,z)\right) S_{23} \left(\frac{\partial}{\partial x} \varphi_{ix}(x,y,z)\right) S_{31}}{\left(S_{32} S_{11} - S_{12} S_{31}\right)^2}$$

$$\frac{\mathrm{d}}{\mathrm{d}S_{12}} A[1,4] = -\frac{S_{31} H \left(\frac{\partial}{\partial x} \varphi_{ix}(x,y,z)\right)}{S_{32} S_{11} - S_{12} S_{31}} -$$

$$\frac{\left(S_{11} - \frac{S_{32} S_{11} - S_{12} S_{31}}{S_{23}} + S_{21} + S_{31}\right) H S_{23} \left(\frac{\partial}{\partial x} \varphi_{ix}(x,y,z)\right) S_{31}}{\left(S_{32} S_{11} - S_{12} S_{31}\right)^2}$$

$$\frac{\mathrm{d}}{\mathrm{d}S_{12}} A[3,3] = \frac{\left(\frac{\partial}{\partial z} w(x,y,z)\right) \left(\frac{\partial}{\partial z} \varphi_{iz}(x,y,z)\right)}{S_{21} S_{33} - S_{23} S_{31}}$$

$$\frac{\mathrm{d}}{\mathrm{d}S_{12}} A[3,4] = -\frac{H \left(\frac{\partial}{\partial z} \varphi_{iz}(x,y,z)\right)}{S_{12}} -$$

$$\frac{\left(S_{31} + S_{32} + S_{33} - \frac{S_{21} S_{33} - S_{23} S_{31}}{S_{12}}\right) H \left(\frac{\partial}{\partial z} \varphi_{iz}(x,y,z)\right)}{S_{21} S_{33} - S_{23} S_{31}}$$

$$\frac{\mathrm{d}}{\mathrm{d}S_{13}} A[2,2] = -\frac{\left(\frac{\partial}{\partial y} v(x,y,z)\right)\left(\frac{\partial}{\partial y} \varphi_{iy}(x,y,z)\right)}{S_{21}S_{32} - S_{22}S_{31}}$$

$$\frac{\mathrm{d}}{\mathrm{d}S_{13}} A[2,4] = -\frac{H\left(\frac{\partial}{\partial y} \varphi_{iy}(x,y,z)\right)}{S_{13}} +$$
$$\frac{\left(S_{21} + S_{22} + \frac{S_{21}S_{32} - S_{22}S_{31}}{S_{13}} + S_{32}\right)H\left(\frac{\partial}{\partial y} \varphi_{iy}(x,y,z)\right)}{S_{21}S_{32} - S_{22}S_{31}}$$

$$\frac{\mathrm{d}}{\mathrm{d}S_{23}} A[1,1] = \frac{\left(\frac{\partial}{\partial x} u(x,y,z)\right)\left(\frac{\partial}{\partial x} \varphi_{ix}(x,y,z)\right)}{S_{32}S_{11} - S_{12}S_{31}}$$

$$\frac{\mathrm{d}}{\mathrm{d}S_{23}} A[1,4] = -\frac{H\left(\frac{\partial}{\partial x} \varphi_{ix}(x,y,z)\right)}{S_{23}} -$$
$$\frac{\left(S_{11} - \frac{S_{32}S_{11} - S_{12}S_{31}}{S_{23}} + S_{21} + S_{31}\right)H\left(\frac{\partial}{\partial x} \varphi_{ix}(x,y,z)\right)}{S_{32}S_{11} - S_{12}S_{31}}$$

$$\frac{\mathrm{d}}{\mathrm{d}S_{23}} A[3,3] = \frac{\left(\frac{\partial}{\partial z} w(x,y,z)\right)S_{12}\left(\frac{\partial}{\partial z} \varphi_{iz}(x,y,z)\right)S_{31}}{\left(S_{21}S_{33} - S_{23}S_{31}\right)^2}$$

$$\frac{d}{dS_{23}} A[3,4] = -\frac{S_{31} H\left(\frac{\partial}{\partial z} \varphi_{iz}(x,y,z)\right)}{S_{21} S_{33} - S_{23} S_{31}} -$$

$$\frac{\left(S_{31} + S_{32} + S_{33} - \frac{S_{21} S_{33} - S_{23} S_{31}}{S_{12}}\right) H S_{12} \left(\frac{\partial}{\partial z} \varphi_{iz}(x,y,z)\right) S_{31}}{\left(S_{21} S_{33} - S_{23} S_{31}\right)^2}$$

E. FORTRAN Code Sample for Adjoint Residual

```
!ortho!
!ooooooooooooooooooooooooooooooooooooooooooooooooooooooooooooooooooo
oooooooooo
!ortho!
!ortho!     subroutine
orthoadjointgrad(adjntmesh,truedisp,adjntdisp,adjntmtrl,orthograd)
!ortho!
!ortho!     use reporterror
!ortho!     use optimizationparams
!ortho!     use hex27!, only
!ortho!     use gaussnewton
!ortho!     use FEmatrix
!ortho!     use FEmesh
!ortho!     use FEmaterial
!ortho!     use FEsolution
!ortho!     use FEproblem
!ortho!
!ortho!     implicit none
!ortho!
!ortho!     logical
dSind(6,6,9),dAddind(9,6,6),dApdind(3,6,6),dAppind(6,6)
!ortho!
!ortho!     integer
el,i,j,ii,jj,kk,ll,iii,jjj,kkk,lll,jjp,iip,mtrnod,iinod,jjnod
!ortho!     integer
ig,jg,kg,iia,iib,iic,jja,jjb,jjc,iix,iiy,iiz,jjx,jjy,jjz
!ortho!     integer np,adjntind
!ortho!
!ortho!     real*8 xi(numgp),eta(numgp),zeta(numgp),w(numgp)
!ortho!     real*8
phi(numgp,numgp,numgp,nodperelm),dphi(numgp,numgp,numgp,3,nodperelm)
!ortho!     real*8 psi(numgp,numgp,numgp,pressperpoint)
!ortho!     real*8
xyz(nodperelm,3),gaussg(numgp,numgp,numgp),diffphi(3,nodperelm),jacobd
et
```

```
!ortho!     real*8
dpx(numgp,numgp,numgp,nodperelm),dpy(numgp,numgp,numgp,nodperelm),dpz(
numgp,numgp,numgp,nodperelm)
!ortho!     real*8
dpxiig,dpxjjg,dpyiig,dpyjjg,dpziig,dpzjjg,Piig,Pjjg,Pkkg,wdetjg
!ortho!
!ortho!     real*8 omsqr,realscalar,imagscalar,dAdrho,symfac
!ortho!
!ortho!     complex*16 dAppg(pressperpoint,pressperpoint,9,nodperelm)
!ortho!     complex*16
dAddg(9,9,nodperelm),dApdg(pressperpoint,3,9,nodperelm)
!ortho!     complex*16 dAdd(9,6,6),dApd(3,6,6),dApp(6,6)
!ortho!
!ortho!     complex*16 longmod(3),shearmod(3),poissratio(6),density
!ortho!     complex*16
Sg(numgp,numgp,numgp,6,6),rhog(numgp,numgp,numgp)
!ortho!     complex*16
S11,S22,S33,S44,S55,S66,S12,S13,S21,S23,S31,S32,SB
!ortho!     complex*16
dS(numgp,numgp,numgp,6,6,9,nodperelm),dSg(6,6,9,nodperelm)
!ortho!
!ortho!     type(mesh), intent(in) :: adjntmesh
!ortho!     type(material), intent(in) :: adjntmtrl
!ortho!     type(displacement), intent(in) :: truedisp,adjntdisp
!ortho!     type(mtrlgrad), intent(inout) :: orthograd
!ortho!
!ortho!     if(.not.adjntmesh%initialized) print *,'!!! ERROR:
Assembling Orthotropic Adjoint from Uninialized Mesh'
!ortho!     if(.not.adjntmtrl%initialized) print *,'!!! ERROR:
Assembling Orthotropic Adjoint from Uninialized Material'
!ortho!     if(.not.adjntdisp%initialized) print *,'!!! ERROR:
Assembling Orthotropic Adjoint from Uninialized Displacement'
!ortho!
!ortho!     call gaussinit(xi,eta,zeta,w)
!ortho!     call localelement(phi,dphi,psi,xi,eta,zeta)
!ortho!     call orthoderivindex(dSind,dAddind,dApdind,dAppind)
!ortho!
!ortho!     omsqr=frqncy*frqncy
!ortho!
!ortho!    ! Begin Element Loop!
!ortho!    ! =================!
!ortho!     do 100 el = 1,adjntmesh%ne
!ortho!
!ortho!      np=3*adjntmesh%nn+pressperpoint*(el-1)
!ortho!
!ortho!     Sg(:,:,:,:,:)=dcmplx(0.d0,0.d0)
!ortho!     dS(:,:,:,:,:,:,:)=dcmplx(0.d0,0.d0)
!ortho!
!ortho!      do ii = 1,adjntmesh%npe
!ortho!        xyz(ii,1) = adjntmesh%node(adjntmesh%in(el,ii))%x
!ortho!        xyz(ii,2) = adjntmesh%node(adjntmesh%in(el,ii))%y
!ortho!        xyz(ii,3) = adjntmesh%node(adjntmesh%in(el,ii))%z
```

```
!ortho!     enddo
!ortho!
!ortho!     ! Perform coordinate transformation (dphi/deta->dphi/dx)
for the element:
!ortho!        do ii = 1,adjntmesh%ngp ! Loop! for xi_i
!ortho!           do jj = 1,adjntmesh%ngp ! Loop! for eta_i
!ortho!             do kk = 1,adjntmesh%ngp  ! Loop! for zeta_i
!ortho!
!ortho!               do i = 1,3
!ortho!                 do j = 1,adjntmesh%npe
!ortho!                   diffphi(i,j) = dphi(ii,jj,kk,i,j)
!ortho!                 enddo
!ortho!               enddo
!ortho!
!ortho!               call transcoord(jacobdet,diffphi,xyz)
!ortho!
!ortho!               gaussg(ii,jj,kk) = jacobdet*w(ii)*w(jj)*w(kk)
!ortho!
!ortho!               do i = 1,adjntmesh%npe
!ortho!                 dpx(ii,jj,kk,i) = diffphi(1,i)
!ortho!                 dpy(ii,jj,kk,i) = diffphi(2,i)
!ortho!                 dpz(ii,jj,kk,i) = diffphi(3,i)
!ortho!
!ortho!                 !property values
!ortho!                 mtrnod=adjntmesh%in(el,i)
!ortho!
!ortho!                   !longitudinal moduli (E1, E2, and E3):
!ortho!                 realscalar=adjntmtrl%prop(1)%scalar(1)
!ortho!                 imagscalar=adjntmtrl%prop(1)%scalar(2)
!ortho!                 do j=1,adjntmtrl%prop(1)%nvpp
!ortho!
longmod(j)=dcmplx(realscalar*dble(adjntmtrl%prop(1)%value(mtrnod,j)),i
magscalar*dimag(adjntmtrl%prop(1)%value(mtrnod,j)))
!ortho!                 enddo
!ortho!
!ortho!                   !shear moduli (mu12, mu23, and mu31):
!ortho!                 realscalar=adjntmtrl%prop(2)%scalar(1)
!ortho!                 imagscalar=adjntmtrl%prop(2)%scalar(2)
!ortho!                 do j=1,adjntmtrl%prop(2)%nvpp
!ortho!
shearmod(j)=dcmplx(realscalar*dble(adjntmtrl%prop(2)%value(mtrnod,j)),
imagscalar*dimag(adjntmtrl%prop(2)%value(mtrnod,j)))
!ortho!                 enddo
!ortho!
!ortho!                   !Poisson ratios (v12, v23, and v31):
!ortho!                 realscalar=adjntmtrl%prop(3)%scalar(1)
!ortho!                 imagscalar=adjntmtrl%prop(3)%scalar(2)
!ortho!                 do j=1,adjntmtrl%prop(3)%nvpp
!ortho!
poissratio(j)=dcmplx(realscalar*dble(adjntmtrl%prop(3)%value(mtrnod,j)
),imagscalar*dimag(adjntmtrl%prop(3)%value(mtrnod,j)))
!ortho!                 enddo
```

```fortran
!ortho!
!ortho!                        !Poisson ratios (v21, v32, and v13):
!ortho!
poissratio(4)=(longmod(2)/longmod(1))*poissratio(1) !v21
!ortho!
poissratio(5)=(longmod(3)/longmod(2))*poissratio(2) !v32
!ortho!
poissratio(6)=(longmod(1)/longmod(3))*poissratio(3) !v13
!ortho!
!ortho!                        !Compliance Matrix
!ortho!                        Sg(ii,jj,kk,1,1)=Sg(ii,jj,kk,1,1) +
phi(ii,jj,kk,i)*(1.d0/longmod(1))
!ortho!                        Sg(ii,jj,kk,2,2)=Sg(ii,jj,kk,2,2) +
phi(ii,jj,kk,i)*(1.d0/longmod(2))
!ortho!                        Sg(ii,jj,kk,3,3)=Sg(ii,jj,kk,3,3) +
phi(ii,jj,kk,i)*(1.d0/longmod(3))
!ortho!                        Sg(ii,jj,kk,4,4)=Sg(ii,jj,kk,4,4) +
phi(ii,jj,kk,i)*(1.d0/shearmod(1))
!ortho!                        Sg(ii,jj,kk,5,5)=Sg(ii,jj,kk,5,5) +
phi(ii,jj,kk,i)*(1.d0/shearmod(2))
!ortho!                        Sg(ii,jj,kk,6,6)=Sg(ii,jj,kk,6,6) +
phi(ii,jj,kk,i)*(1.d0/shearmod(3))
!ortho!                        Sg(ii,jj,kk,1,2)=Sg(ii,jj,kk,1,2) -
phi(ii,jj,kk,i)*(poissratio(4)/longmod(2))
!ortho!                        Sg(ii,jj,kk,2,3)=Sg(ii,jj,kk,2,3) -
phi(ii,jj,kk,i)*(poissratio(5)/longmod(3))
!ortho!                        Sg(ii,jj,kk,3,1)=Sg(ii,jj,kk,3,1) -
phi(ii,jj,kk,i)*(poissratio(6)/longmod(1))
!ortho!
!ortho!                        !Compliance Matrix Derivatives
!ortho!                        call
orthocompliancederivs(dS(ii,jj,kk,:,:,:,i),phi(ii,jj,kk,i),longmod,she
armod,poissratio)
!ortho!                enddo
!ortho!
!ortho!             enddo
!ortho!          enddo
!ortho!       enddo
!ortho!
!ortho!       !oooooooooooooooooooooooooooooooooooooooooooooooooooooooooooo
!ortho!        !o Nodal Looping Begins
ooo
!ortho!       !oooooooooooooooooooooooooooooooooooooooooooooooooooooooooooo
!ortho!
!ortho!       do 200 ii=1,adjntmesh%npe !Interpolaton Fucntion loop
!ortho!          iinod=adjntmesh%in(el,ii)
!ortho!          iia=3*ii-2
!ortho!          iib=3*ii-1
!ortho!          iic=3*ii
!ortho!          iix=3*adjntmesh%in(el,ii)-2
!ortho!          iiy=3*adjntmesh%in(el,ii)-1
!ortho!          iiz=3*adjntmesh%in(el,ii)
```

134

```
!ortho!
!ortho!          do 300 jj=ii,adjntmesh%npe !Weighting Function loop !
only build top half of symm matrix
!ortho!             jjnod=adjntmesh%in(el,jj)
!ortho!             jja=3*jj-2
!ortho!             jjb=3*jj-1
!ortho!             jjc=3*jj
!ortho!             jjx=3*adjntmesh%in(el,jj)-2
!ortho!             jjy=3*adjntmesh%in(el,jj)-1
!ortho!             jjz=3*adjntmesh%in(el,jj)
!ortho!
!ortho!             do 400 kk=1,adjntmesh%npe
!ortho!                mtrnod=adjntmesh%in(el,kk)
!ortho!
!ortho!                 dAddg(:,:,:)=dcmplx(0.d0,0.d0)
!ortho!                 dApdg(:,:,:,:)=dcmplx(0.d0,0.d0)
!ortho!                 dAppg(:,:,:,:)=dcmplx(0.d0,0.d0)
!ortho!                dAdrho=0.d0
!ortho!
!ortho!                 !ooooooooooooooooooooooooooooooooooooooooooooooo
!ortho!                 !o Gauss Point Looping Begins                 ooo
!ortho!                 !ooooooooooooooooooooooooooooooooooooooooooooooo
!ortho!
!ortho!                 do 500 ig = 1,adjntmesh%ngp  ! loop for xi_i
!ortho!                 do 500 jg = 1,adjntmesh%ngp  ! loop for eta_i
!ortho!                 do 500 kg = 1,adjntmesh%ngp  ! loop for zeta_i
!ortho!                   dpxiig=dpx(ig,jg,kg,ii)
!ortho!                   dpxjjg=dpx(ig,jg,kg,jj)
!ortho!                   dpyiig=dpy(ig,jg,kg,ii)
!ortho!                   dpyjjg=dpy(ig,jg,kg,jj)
!ortho!                   dpziig=dpz(ig,jg,kg,ii)
!ortho!                   dpzjjg=dpz(ig,jg,kg,jj)
!ortho!                   Piig=phi(ig,jg,kg,ii)
!ortho!                   Pjjg=phi(ig,jg,kg,jj)
!ortho!                   Pkkg=phi(ig,jg,kg,kk)
!ortho!                   wdetjg=gaussg(ig,jg,kg)
!ortho!
!ortho!                   S11=Sg(ig,jg,kg,1,1)
!ortho!                   S22=Sg(ig,jg,kg,2,2)
!ortho!                   S33=Sg(ig,jg,kg,3,3)
!ortho!                   S44=Sg(ig,jg,kg,4,4)
!ortho!                   S55=Sg(ig,jg,kg,5,5)
!ortho!                   S66=Sg(ig,jg,kg,6,6)
!ortho!                   S12=Sg(ig,jg,kg,1,2)
!ortho!                   S23=Sg(ig,jg,kg,2,3)
!ortho!                   S31=Sg(ig,jg,kg,3,1)
!ortho!
!ortho!                   dSg(:,:,:,:)=dS(ig,jg,kg,:,:,:,:)
!ortho!
!ortho!                   !Enforce symmetry of compliance matrix
!ortho!                   S21=S12
!ortho!                   S32=S23
```

135

```
!ortho!                   S13=S31
!ortho!
!ortho!                   call
orthostiffconstderivs(dAdd,dApd,dApp,S11,S22,S33,S44,S55,S66,S12,S13,S
21,S23,S31,S32,dpxiig,dpxjjg,dpyiig,dpyjjg,dpziig,dpzjjg)
!ortho!
!ortho!                   !Do required summations/integrations (STIFFNESS
MATRIX TERMS)
!ortho!
!ortho!                   do iii=1,adjntmtrl%prop(1)%nvpp !longitudinal
modulus terms (E1, E2, and E3):
!ortho!                   if(cmplxparamind(1,iii)) then
!ortho!
!ortho!                   do jjj=1,3
!ortho!                   do kkk=jjj,3 !S(1-3,1-3) terms
!ortho!                   if(dSind(jjj,kkk,iii)) then
!ortho!                   if(kkk.eq.jjj) then
!ortho!                   symfac=1.d0
!ortho!                   else
!ortho!                   symfac=2.d0
!ortho!                   endif
!ortho!
!ortho!                   if(dAddind(1,jjj,kkk)) dAddg(1,iii,kk) =
dAddg(1,iii,kk) + symfac*dSg(jjj,kkk,iii,kk)*dAdd(1,jjj,kkk)*wdetjg !
A(mx,nx): Eq. in x, Terms in u
!ortho!                   if(dAddind(4,jjj,kkk)) dAddg(4,iii,kk) =
dAddg(4,iii,kk) + symfac*dSg(jjj,kkk,iii,kk)*dAdd(4,jjj,kkk)*wdetjg !
A(mx,ny): Eq. in x, Terms in v
!ortho!                   if(dAddind(7,jjj,kkk)) dAddg(7,iii,kk) =
dAddg(7,iii,kk) + symfac*dSg(jjj,kkk,iii,kk)*dAdd(7,jjj,kkk)*wdetjg !
A(mx,nz): Eq. in x, Terms in w
!ortho!
!ortho!                   if(dAddind(2,jjj,kkk)) dAddg(2,iii,kk) =
dAddg(2,iii,kk) + symfac*dSg(jjj,kkk,iii,kk)*dAdd(2,jjj,kkk)*wdetjg !
A(my,nx): Eq. in y, Terms in u
!ortho!                   if(dAddind(5,jjj,kkk)) dAddg(5,iii,kk) =
dAddg(5,iii,kk) + symfac*dSg(jjj,kkk,iii,kk)*dAdd(5,jjj,kkk)*wdetjg !
A(my,ny): Eq. in y, Terms in v
!ortho!                   if(dAddind(8,jjj,kkk)) dAddg(8,iii,kk) =
dAddg(8,iii,kk) + symfac*dSg(jjj,kkk,iii,kk)*dAdd(8,jjj,kkk)*wdetjg !
A(my,nz): Eq. in y, Terms in w
!ortho!
!ortho!                   if(dAddind(3,jjj,kkk)) dAddg(3,iii,kk) =
dAddg(3,iii,kk) + symfac*dSg(jjj,kkk,iii,kk)*dAdd(3,jjj,kkk)*wdetjg !
A(mz,nx): Eq. in z, Terms in u
!ortho!                   if(dAddind(6,jjj,kkk)) dAddg(6,iii,kk) =
dAddg(6,iii,kk) + symfac*dSg(jjj,kkk,iii,kk)*dAdd(6,jjj,kkk)*wdetjg !
A(mz,ny): Eq. in z, Terms in v
!ortho!                   if(dAddind(9,jjj,kkk)) dAddg(9,iii,kk) =
dAddg(9,iii,kk) + symfac*dSg(jjj,kkk,iii,kk)*dAdd(9,jjj,kkk)*wdetjg !
A(mz,nz): Eq. in z, Terms in w
!ortho!
```

```
!ortho!                          ! Pressure terms
!ortho!                          if ((jj.eq.adjntmesh%npe)) then !fill in
pressure/disp terms (right side of matrix)
!ortho!                            do iip=1,pressperpoint
!ortho!                              if(dApdind(1,jjj,kkk))
dApdg(iip,1,iii,kk)=dApdg(iip,1,iii,kk)-
psi(ig,jg,kg,iip)*symfac*dSg(jjj,kkk,iii,kk)*dApd(1,jjj,kkk)*wdetjg !
A(mx,np): Eq. in x, Pressure Terms
!ortho!                              if(dApdind(2,jjj,kkk))
dApdg(iip,2,iii,kk)=dApdg(iip,2,iii,kk)-
psi(ig,jg,kg,iip)*symfac*dSg(jjj,kkk,iii,kk)*dApd(2,jjj,kkk)*wdetjg !
A(my,np): Eq. in y, Pressure Terms
!ortho!                              if(dApdind(3,jjj,kkk))
dApdg(iip,3,iii,kk)=dApdg(iip,3,iii,kk)-
psi(ig,jg,kg,iip)*symfac*dSg(jjj,kkk,iii,kk)*dApd(3,jjj,kkk)*wdetjg !
A(mz,np): Eq. in z, Pressure Terms
!ortho!                            enddo
!ortho!                          endif
!ortho!
!ortho!                          if
((ii.eq.adjntmesh%npe).and.(jj.eq.adjntmesh%npe)) then !fill in
pressure/pressure terms (bottom corner of matrix)
!ortho!                            do iip=1,pressperpoint
!ortho!                             do jjp=iip,pressperpoint
!ortho!                              if(dAppind(jjj,kkk))
dAppg(iip,jjp,iii,kk)=dAppg(iip,jjp,iii,kk)+psi(ig,jg,kg,iip)*psi(ig,j
g,kg,jjp)*symfac*dSg(jjj,kkk,iii,kk)*dApp(jjj,kkk)*wdetjg
!ortho!                             enddo
!ortho!                            enddo
!ortho!                          endif
!ortho!
!ortho!                          endif !end dSind condition
!ortho!                          enddo !end kkk loop
!ortho!
!ortho!                          lll=jjj+3 !S(4,4),S(5,5) & S(6,6) terms
!ortho!                          if(dSind(lll,lll,iii)) then
!ortho!
!ortho!                            if(dAddind(1,lll,lll)) dAddg(1,iii,kk) =
dAddg(1,iii,kk) + dSg(lll,lll,iii,kk)*dAdd(1,lll,lll)*wdetjg !
A(mx,nx): Eq. in x, Terms in u
!ortho!                            if(dAddind(4,lll,lll)) dAddg(4,iii,kk) =
dAddg(4,iii,kk) + dSg(lll,lll,iii,kk)*dAdd(4,lll,lll)*wdetjg !
A(mx,ny): Eq. in x, Terms in v
!ortho!                            if(dAddind(7,lll,lll)) dAddg(7,iii,kk) =
dAddg(7,iii,kk) + dSg(lll,lll,iii,kk)*dAdd(7,lll,lll)*wdetjg !
A(mx,nz): Eq. in x, Terms in w
!ortho!
!ortho!                            if(dAddind(2,lll,lll)) dAddg(2,iii,kk) =
dAddg(2,iii,kk) + dSg(lll,lll,iii,kk)*dAdd(2,lll,lll)*wdetjg !
A(my,nx): Eq. in y, Terms in u
```

```
!ortho!                         if(dAddind(5,lll,lll)) dAddg(5,iii,kk) =
dAddg(5,iii,kk) + dSg(lll,lll,iii,kk)*dAdd(5,lll,lll)*wdetjg !
A(my,ny): Eq. in y, Terms in v
!ortho!                         if(dAddind(8,lll,lll)) dAddg(8,iii,kk) =
dAddg(8,iii,kk) + dSg(lll,lll,iii,kk)*dAdd(8,lll,lll)*wdetjg !
A(my,nz): Eq. in y, Terms in w
!ortho!
!ortho!                         if(dAddind(3,lll,lll)) dAddg(3,iii,kk) =
dAddg(3,iii,kk) + dSg(lll,lll,iii,kk)*dAdd(3,lll,lll)*wdetjg !
A(mz,nx): Eq. in z, Terms in u
!ortho!                         if(dAddind(6,lll,lll)) dAddg(6,iii,kk) =
dAddg(6,iii,kk) + dSg(lll,lll,iii,kk)*dAdd(6,lll,lll)*wdetjg !
A(mz,ny): Eq. in z, Terms in v
!ortho!                         if(dAddind(9,lll,lll)) dAddg(9,iii,kk) =
dAddg(9,iii,kk) + dSg(lll,lll,iii,kk)*dAdd(9,lll,lll)*wdetjg !
A(mz,nz): Eq. in z, Terms in w
!ortho!
!ortho!                         ! Pressure terms
!ortho!                         if ((jj.eq.adjntmesh%npe)) then !fill in
pressure/disp terms (right side of matrix)
!ortho!                         do iip=1,pressperpoint
!ortho!                          if(dApdind(1,lll,lll))
dApdg(iip,1,iii,kk)=dApdg(iip,1,iii,kk)-
psi(ig,jg,kg,iip)*dSg(lll,lll,iii,kk)*dApd(1,lll,lll)*wdetjg !
A(mx,np): Eq. in x, Pressure Terms
!ortho!                          if(dApdind(2,lll,lll))
dApdg(iip,2,iii,kk)=dApdg(iip,2,iii,kk)-
psi(ig,jg,kg,iip)*dSg(lll,lll,iii,kk)*dApd(2,lll,lll)*wdetjg !
A(my,np): Eq. in y, Pressure Terms
!ortho!                          if(dApdind(3,lll,lll))
dApdg(iip,3,iii,kk)=dApdg(iip,3,iii,kk)-
psi(ig,jg,kg,iip)*dSg(lll,lll,iii,kk)*dApd(3,lll,lll)*wdetjg !
A(mz,np): Eq. in z, Pressure Terms
!ortho!                         enddo
!ortho!                         endif
!ortho!
!ortho!                         if
((ii.eq.adjntmesh%npe).and.(jj.eq.adjntmesh%npe)) then !fill in
pressure/pressure terms (bottom corner of matrix)
!ortho!                         do iip=1,pressperpoint
!ortho!                          do jjp=iip,pressperpoint
!ortho!                           if(dAppind(lll,lll))
dAppg(iip,jjp,iii,kk)=dAppg(iip,jjp,iii,kk)+psi(ig,jg,kg,iip)*psi(ig,j
g,kg,jjp)*dSg(lll,lll,iii,kk)*dApp(lll,lll)*wdetjg
!ortho!                          enddo
!ortho!                         enddo
!ortho!                         endif
!ortho!
!ortho!                         endif !end dSind(lll,lll,iii) condition
!ortho!                         enddo !end jjj loop
!ortho!                         endif
!ortho!                         enddo !end iii loop
```

138

```
!ortho!
!ortho!                     do iii=1,adjntmtrl%prop(2)%nvpp !shear modulus
terms (mu12, mu23, and mu31):
!ortho!                     if(cmplxparamind(2,iii)) then
!ortho!
!ortho!                     do jjj=1,3
!ortho!                     do kkk=jjj,3 !S(1-3,1-3) terms
!ortho!                     if(dSind(jjj,kkk,iii+3)) then
!ortho!                     if(kkk.eq.jjj) then
!ortho!                     symfac=1.d0
!ortho!                     else
!ortho!                     symfac=2.d0
!ortho!                     endif
!ortho!
!ortho!                     if(dAddind(1,jjj,kkk)) dAddg(1,iii+3,kk) =
dAddg(1,iii+3,kk) +
symfac*dSg(jjj,kkk,iii+3,kk)*dAdd(1,jjj,kkk)*wdetjg ! A(mx,nx): Eq. in
x, Terms in u
!ortho!                     if(dAddind(4,jjj,kkk)) dAddg(4,iii+3,kk) =
dAddg(4,iii+3,kk) +
symfac*dSg(jjj,kkk,iii+3,kk)*dAdd(4,jjj,kkk)*wdetjg ! A(mx,ny): Eq. in
x, Terms in v
!ortho!                     if(dAddind(7,jjj,kkk)) dAddg(7,iii+3,kk) =
dAddg(7,iii+3,kk) +
symfac*dSg(jjj,kkk,iii+3,kk)*dAdd(7,jjj,kkk)*wdetjg ! A(mx,nz): Eq. in
x, Terms in w
!ortho!
!ortho!                     if(dAddind(2,jjj,kkk)) dAddg(2,iii+3,kk) =
dAddg(2,iii+3,kk) +
symfac*dSg(jjj,kkk,iii+3,kk)*dAdd(2,jjj,kkk)*wdetjg ! A(my,nx): Eq. in
y, Terms in u
!ortho!                     if(dAddind(5,jjj,kkk)) dAddg(5,iii+3,kk) =
dAddg(5,iii+3,kk) +
symfac*dSg(jjj,kkk,iii+3,kk)*dAdd(5,jjj,kkk)*wdetjg ! A(my,ny): Eq. in
y, Terms in v
!ortho!                     if(dAddind(8,jjj,kkk)) dAddg(8,iii+3,kk) =
dAddg(8,iii+3,kk) +
symfac*dSg(jjj,kkk,iii+3,kk)*dAdd(8,jjj,kkk)*wdetjg ! A(my,nz): Eq. in
y, Terms in w
!ortho!
!ortho!                     if(dAddind(3,jjj,kkk)) dAddg(3,iii+3,kk) =
dAddg(3,iii+3,kk) +
symfac*dSg(jjj,kkk,iii+3,kk)*dAdd(3,jjj,kkk)*wdetjg ! A(mz,nx): Eq. in
z, Terms in u
!ortho!                     if(dAddind(6,jjj,kkk)) dAddg(6,iii+3,kk) =
dAddg(6,iii+3,kk) +
symfac*dSg(jjj,kkk,iii+3,kk)*dAdd(6,jjj,kkk)*wdetjg ! A(mz,ny): Eq. in
z, Terms in v
!ortho!                     if(dAddind(9,jjj,kkk)) dAddg(9,iii+3,kk) =
dAddg(9,iii+3,kk) +
symfac*dSg(jjj,kkk,iii+3,kk)*dAdd(9,jjj,kkk)*wdetjg ! A(mz,nz): Eq. in
z, Terms in w
```

```
!ortho!
!ortho!                     ! Pressure terms
!ortho!                     if ((jj.eq.adjntmesh%npe)) then !fill in
pressure/disp terms (right side of matrix)
!ortho!                       do iip=1,pressperpoint
!ortho!                         if(dApdind(1,jjj,kkk))
dApdg(iip,1,iii+3,kk)=dApdg(iip,1,iii+3,kk)-
psi(ig,jg,kg,iip)*symfac*dSg(jjj,kkk,iii+3,kk)*dApd(1,jjj,kkk)*wdetjg
! A(mx,np): Eq. in x, Pressure Terms
!ortho!                         if(dApdind(2,jjj,kkk))
dApdg(iip,2,iii+3,kk)=dApdg(iip,2,iii+3,kk)-
psi(ig,jg,kg,iip)*symfac*dSg(jjj,kkk,iii+3,kk)*dApd(2,jjj,kkk)*wdetjg
! A(my,np): Eq. in y, Pressure Terms
!ortho!                         if(dApdind(3,jjj,kkk))
dApdg(iip,3,iii+3,kk)=dApdg(iip,3,iii+3,kk)-
psi(ig,jg,kg,iip)*symfac*dSg(jjj,kkk,iii+3,kk)*dApd(3,jjj,kkk)*wdetjg
! A(mz,np): Eq. in z, Pressure Terms
!ortho!                       enddo
!ortho!                     endif
!ortho!
!ortho!                     if
((ii.eq.adjntmesh%npe).and.(jj.eq.adjntmesh%npe)) then !fill in
pressure/pressure terms (bottom corner of matrix)
!ortho!                       do iip=1,pressperpoint
!ortho!                         do jjp=iip,pressperpoint
!ortho!                           if(dAppind(jjj,kkk))
dAppg(iip,jjp,iii+3,kk)=dAppg(iip,jjp,iii+3,kk)+psi(ig,jg,kg,iip)*psi(
ig,jg,kg,jjp)*symfac*dSg(jjj,kkk,iii+3,kk)*dApp(jjj,kkk)*wdetjg
!ortho!                         enddo
!ortho!                       enddo
!ortho!                     endif
!ortho!
!ortho!                   endif !end dSind condition
!ortho!                 enddo !end kkk loop
!ortho!
!ortho!                 lll=jjj+3 !S(4,4),S(5,5) & S(6,6) terms
!ortho!                 if(dSind(lll,lll,iii+3)) then
!ortho!
!ortho!                   if(dAddind(1,lll,lll)) dAddg(1,iii+3,kk) =
dAddg(1,iii+3,kk) + dSg(lll,lll,iii+3,kk)*dAdd(1,lll,lll)*wdetjg !
A(mx,nx): Eq. in x, Terms in u
!ortho!                   if(dAddind(4,lll,lll)) dAddg(4,iii+3,kk) =
dAddg(4,iii+3,kk) + dSg(lll,lll,iii+3,kk)*dAdd(4,lll,lll)*wdetjg !
A(mx,ny): Eq. in x, Terms in v
!ortho!                   if(dAddind(7,lll,lll)) dAddg(7,iii+3,kk) =
dAddg(7,iii+3,kk) + dSg(lll,lll,iii+3,kk)*dAdd(7,lll,lll)*wdetjg !
A(mx,nz): Eq. in x, Terms in w
!ortho!
!ortho!                   if(dAddind(2,lll,lll)) dAddg(2,iii+3,kk) =
dAddg(2,iii+3,kk) + dSg(lll,lll,iii+3,kk)*dAdd(2,lll,lll)*wdetjg !
A(my,nx): Eq. in y, Terms in u
```

```
!ortho!                      if(dAddind(5,lll,lll)) dAddg(5,iii+3,kk) =
dAddg(5,iii+3,kk) + dSg(lll,lll,iii+3,kk)*dAdd(5,lll,lll)*wdetjg !
A(my,ny): Eq. in y, Terms in v
!ortho!                      if(dAddind(8,lll,lll)) dAddg(8,iii+3,kk) =
dAddg(8,iii+3,kk) + dSg(lll,lll,iii+3,kk)*dAdd(8,lll,lll)*wdetjg !
A(my,nz): Eq. in y, Terms in w
!ortho!
!ortho!                      if(dAddind(3,lll,lll)) dAddg(3,iii+3,kk) =
dAddg(3,iii+3,kk) + dSg(lll,lll,iii+3,kk)*dAdd(3,lll,lll)*wdetjg !
A(mz,nx): Eq. in z, Terms in u
!ortho!                      if(dAddind(6,lll,lll)) dAddg(6,iii+3,kk) =
dAddg(6,iii+3,kk) + dSg(lll,lll,iii+3,kk)*dAdd(6,lll,lll)*wdetjg !
A(mz,ny): Eq. in z, Terms in v
!ortho!                      if(dAddind(9,lll,lll)) dAddg(9,iii+3,kk) =
dAddg(9,iii+3,kk) + dSg(lll,lll,iii+3,kk)*dAdd(9,lll,lll)*wdetjg !
A(mz,nz): Eq. in z, Terms in w
!ortho!
!ortho!                      ! Pressure terms
!ortho!                      if ((jj.eq.adjntmesh%npe)) then !fill in
pressure/disp terms (right side of matrix)
!ortho!                         do iip=1,pressperpoint
!ortho!                          if(dApdind(1,lll,lll))
dApdg(iip,1,iii+3,kk)=dApdg(iip,1,iii+3,kk)-
psi(ig,jg,kg,iip)*dSg(lll,lll,iii+3,kk)*dApd(1,lll,lll)*wdetjg !
A(mx,np): Eq. in x, Pressure Terms
!ortho!                          if(dApdind(2,lll,lll))
dApdg(iip,2,iii+3,kk)=dApdg(iip,2,iii+3,kk)-
psi(ig,jg,kg,iip)*dSg(lll,lll,iii+3,kk)*dApd(2,lll,lll)*wdetjg !
A(my,np): Eq. in y, Pressure Terms
!ortho!                          if(dApdind(3,lll,lll))
dApdg(iip,3,iii+3,kk)=dApdg(iip,3,iii+3,kk)-
psi(ig,jg,kg,iip)*dSg(lll,lll,iii+3,kk)*dApd(3,lll,lll)*wdetjg !
A(mz,np): Eq. in z, Pressure Terms
!ortho!                         enddo
!ortho!                      endif
!ortho!
!ortho!                      if
((ii.eq.adjntmesh%npe).and.(jj.eq.adjntmesh%npe)) then !fill in
pressure/pressure terms (bottom corner of matrix)
!ortho!                         do iip=1,pressperpoint
!ortho!                          do jjp=iip,pressperpoint
!ortho!                           if(dAppind(lll,lll))
dAppg(iip,jjp,iii+3,kk)=dAppg(iip,jjp,iii+3,kk)+psi(ig,jg,kg,iip)*psi(
ig,jg,kg,jjp)*dSg(lll,lll,iii+3,kk)*dApp(lll,lll)*wdetjg
!ortho!                          enddo
!ortho!                         enddo
!ortho!                      endif
!ortho!
!ortho!                      endif !end dSind(lll,lll,iii+3) condition
!ortho!                      enddo !end jjj loop
!ortho!                      endif
!ortho!                      enddo !end iii loop
```

141

```
!ortho!
!ortho!                     do iii=1,adjntmtrl%prop(3)%nvpp !Poisson's
ratio terms (v12, v23, and v31):
!ortho!                     if(cmplxparamind(3,iii)) then
!ortho!
!ortho!                     do jjj=1,3
!ortho!                     do kkk=jjj,3 !S(1-3,1-3) terms
!ortho!                     if(dSind(jjj,kkk,iii+6)) then
!ortho!                     if(kkk.eq.jjj) then
!ortho!                     symfac=1.d0
!ortho!                     else
!ortho!                     symfac=2.d0
!ortho!                     endif
!ortho!
!ortho!                     if(dAddind(1,jjj,kkk)) dAddg(1,iii+6,kk) =
dAddg(1,iii+6,kk) +
symfac*dSg(jjj,kkk,iii+6,kk)*dAdd(1,jjj,kkk)*wdetjg ! A(mx,nx): Eq. in
x, Terms in u
!ortho!                     if(dAddind(4,jjj,kkk)) dAddg(4,iii+6,kk) =
dAddg(4,iii+6,kk) +
symfac*dSg(jjj,kkk,iii+6,kk)*dAdd(4,jjj,kkk)*wdetjg ! A(mx,ny): Eq. in
x, Terms in v
!ortho!                     if(dAddind(7,jjj,kkk)) dAddg(7,iii+6,kk) =
dAddg(7,iii+6,kk) +
symfac*dSg(jjj,kkk,iii+6,kk)*dAdd(7,jjj,kkk)*wdetjg ! A(mx,nz): Eq. in
x, Terms in w
!ortho!
!ortho!                     if(dAddind(2,jjj,kkk)) dAddg(2,iii+6,kk) =
dAddg(2,iii+6,kk) +
symfac*dSg(jjj,kkk,iii+6,kk)*dAdd(2,jjj,kkk)*wdetjg ! A(my,nx): Eq. in
y, Terms in u
!ortho!                     if(dAddind(5,jjj,kkk)) dAddg(5,iii+6,kk) =
dAddg(5,iii+6,kk) +
symfac*dSg(jjj,kkk,iii+6,kk)*dAdd(5,jjj,kkk)*wdetjg ! A(my,ny): Eq. in
y, Terms in v
!ortho!                     if(dAddind(8,jjj,kkk)) dAddg(8,iii+6,kk) =
dAddg(8,iii+6,kk) +
symfac*dSg(jjj,kkk,iii+6,kk)*dAdd(8,jjj,kkk)*wdetjg ! A(my,nz): Eq. in
y, Terms in w
!ortho!
!ortho!                     if(dAddind(3,jjj,kkk)) dAddg(3,iii+6,kk) =
dAddg(3,iii+6,kk) +
symfac*dSg(jjj,kkk,iii+6,kk)*dAdd(3,jjj,kkk)*wdetjg ! A(mz,nx): Eq. in
z, Terms in u
!ortho!                     if(dAddind(6,jjj,kkk)) dAddg(6,iii+6,kk) =
dAddg(6,iii+6,kk) +
symfac*dSg(jjj,kkk,iii+6,kk)*dAdd(6,jjj,kkk)*wdetjg ! A(mz,ny): Eq. in
z, Terms in v
!ortho!                     if(dAddind(9,jjj,kkk)) dAddg(9,iii+6,kk) =
dAddg(9,iii+6,kk) +
symfac*dSg(jjj,kkk,iii+6,kk)*dAdd(9,jjj,kkk)*wdetjg ! A(mz,nz): Eq. in
z, Terms in w
```

```
!ortho!
!ortho!                         ! Pressure terms
!ortho!                         if ((jj.eq.adjntmesh%npe)) then !fill in
pressure/disp terms (right side of matrix)
!ortho!                           do iip=1,pressperpoint
!ortho!                             if(dApdind(1,jjj,kkk))
dApdg(iip,1,iii+6,kk)=dApdg(iip,1,iii+6,kk)-
psi(ig,jg,kg,iip)*symfac*dSg(jjj,kkk,iii+6,kk)*dApd(1,jjj,kkk)*wdetjg
! A(mx,np): Eq. in x, Pressure Terms
!ortho!                             if(dApdind(2,jjj,kkk))
dApdg(iip,2,iii+6,kk)=dApdg(iip,2,iii+6,kk)-
psi(ig,jg,kg,iip)*symfac*dSg(jjj,kkk,iii+6,kk)*dApd(2,jjj,kkk)*wdetjg
! A(my,np): Eq. in y, Pressure Terms
!ortho!                             if(dApdind(3,jjj,kkk))
dApdg(iip,3,iii+6,kk)=dApdg(iip,3,iii+6,kk)-
psi(ig,jg,kg,iip)*symfac*dSg(jjj,kkk,iii+6,kk)*dApd(3,jjj,kkk)*wdetjg
! A(mz,np): Eq. in z, Pressure Terms
!ortho!                           enddo
!ortho!                         endif
!ortho!
!ortho!                         if
((ii.eq.adjntmesh%npe).and.(jj.eq.adjntmesh%npe)) then !fill in
pressure/pressure terms (bottom corner of matrix)
!ortho!                           do iip=1,pressperpoint
!ortho!                             do jjp=iip,pressperpoint
!ortho!                               if(dAppind(jjj,kkk))
dAppg(iip,jjp,iii+6,kk)=dAppg(iip,jjp,iii+6,kk)+psi(ig,jg,kg,iip)*psi(
ig,jg,kg,jjp)*symfac*dSg(jjj,kkk,iii+6,kk)*dApp(jjj,kkk)*wdetjg
!ortho!                             enddo
!ortho!                           enddo
!ortho!                         endif
!ortho!
!ortho!                       endif !end dSind condition
!ortho!                     enddo !end kkk loop
!ortho!
!ortho!                     lll=jjj+3 !S(4,4),S(5,5) & S(6,6) terms
!ortho!                     if(dSind(lll,lll,iii+6)) then
!ortho!
!ortho!                       if(dAddind(1,lll,lll)) dAddg(1,iii+6,kk) =
dAddg(1,iii+6,kk) + dSg(lll,lll,iii+6,kk)*dAdd(1,lll,lll)*wdetjg !
A(mx,nx): Eq. in x, Terms in u
!ortho!                       if(dAddind(4,lll,lll)) dAddg(4,iii+6,kk) =
dAddg(4,iii+6,kk) + dSg(lll,lll,iii+6,kk)*dAdd(4,lll,lll)*wdetjg !
A(mx,ny): Eq. in x, Terms in v
!ortho!                       if(dAddind(7,lll,lll)) dAddg(7,iii+6,kk) =
dAddg(7,iii+6,kk) + dSg(lll,lll,iii+6,kk)*dAdd(7,lll,lll)*wdetjg !
A(mx,nz): Eq. in x, Terms in w
!ortho!
!ortho!                       if(dAddind(2,lll,lll)) dAddg(2,iii+6,kk) =
dAddg(2,iii+6,kk) + dSg(lll,lll,iii+6,kk)*dAdd(2,lll,lll)*wdetjg !
A(my,nx): Eq. in y, Terms in u
```

```
!ortho!                    if(dAddind(5,lll,lll)) dAddg(5,iii+6,kk) =
dAddg(5,iii+6,kk) + dSg(lll,lll,iii+6,kk)*dAdd(5,lll,lll)*wdetjg !
A(my,ny): Eq. in y, Terms in v
!ortho!                    if(dAddind(8,lll,lll)) dAddg(8,iii+6,kk) =
dAddg(8,iii+6,kk) + dSg(lll,lll,iii+6,kk)*dAdd(8,lll,lll)*wdetjg !
A(my,nz): Eq. in y, Terms in w
!ortho!
!ortho!                    if(dAddind(3,lll,lll)) dAddg(3,iii+6,kk) =
dAddg(3,iii+6,kk) + dSg(lll,lll,iii+6,kk)*dAdd(3,lll,lll)*wdetjg !
A(mz,nx): Eq. in z, Terms in u
!ortho!                    if(dAddind(6,lll,lll)) dAddg(6,iii+6,kk) =
dAddg(6,iii+6,kk) + dSg(lll,lll,iii+6,kk)*dAdd(6,lll,lll)*wdetjg !
A(mz,ny): Eq. in z, Terms in v
!ortho!                    if(dAddind(9,lll,lll)) dAddg(9,iii+6,kk) =
dAddg(9,iii+6,kk) + dSg(lll,lll,iii+6,kk)*dAdd(9,lll,lll)*wdetjg !
A(mz,nz): Eq. in z, Terms in w
!ortho!
!ortho!                    ! Pressure terms
!ortho!                    if ((jj.eq.adjntmesh%npe)) then !fill in
pressure/disp terms (right side of matrix)
!ortho!                      do iip=1,pressperpoint
!ortho!                        if(dApdind(1,lll,lll))
dApdg(iip,1,iii+6,kk)=dApdg(iip,1,iii+6,kk)-
psi(ig,jg,kg,iip)*dSg(lll,lll,iii+6,kk)*dApd(1,lll,lll)*wdetjg !
A(mx,np): Eq. in x, Pressure Terms
!ortho!                        if(dApdind(2,lll,lll))
dApdg(iip,2,iii+6,kk)=dApdg(iip,2,iii+6,kk)-
psi(ig,jg,kg,iip)*dSg(lll,lll,iii+6,kk)*dApd(2,lll,lll)*wdetjg !
A(my,np): Eq. in y, Pressure Terms
!ortho!                        if(dApdind(3,lll,lll))
dApdg(iip,3,iii+6,kk)=dApdg(iip,3,iii+6,kk)-
psi(ig,jg,kg,iip)*dSg(lll,lll,iii+6,kk)*dApd(3,lll,lll)*wdetjg !
A(mz,np): Eq. in z, Pressure Terms
!ortho!                      enddo
!ortho!                    endif
!ortho!
!ortho!                    if
((ii.eq.adjntmesh%npe).and.(jj.eq.adjntmesh%npe)) then !fill in
pressure/pressure terms (bottom corner of matrix)
!ortho!                      do iip=1,pressperpoint
!ortho!                       do jjp=iip,pressperpoint
!ortho!                        if(dAppind(lll,lll))
dAppg(iip,jjp,iii+6,kk)=dAppg(iip,jjp,iii+6,kk)+psi(ig,jg,kg,iip)*psi(
ig,jg,kg,jjp)*dSg(lll,lll,iii+6,kk)*dApp(lll,lll)*wdetjg
!ortho!                       enddo
!ortho!                      enddo
!ortho!                    endif
!ortho!
!ortho!                    endif !end dSind(lll,lll,iii+6) condition
!ortho!                    enddo !end jjj loop
!ortho!                    endif
!ortho!                    enddo !end iii loop
```

```
!ortho!
!ortho!                        ! Density terms  (MASS MATRIX TERMS)
!ortho!                        dAdrho = dAdrho - omsqr*Piig*Pjjg*wdetjg*Pkkg
     !same derivative term for all directions
!ortho!
!ortho! 500                    continue
!ortho!
!ortho!                    !ooooooooooooooooooooooooooooooooooooooooooooooo
!ortho!                    !o Gauss Point Looping Ends                 ooo
!ortho!                    !ooooooooooooooooooooooooooooooooooooooooooooooo
!ortho!
!ortho!             !Insert dA*sol into jacrhs
!ortho!
!ortho!                    do ll=1,truedisp%numdispsets  !loop over all
displacement data
!ortho!
!ortho!                    !longitudinal modulus terms (E1, E2, and E3):
!ortho!                    do iii=1,adjntmtrl%prop(1)%nvpp
!ortho!                    if(cmplxparamind(1,iii)) then
!ortho!
     adjntind=orthograd%cmplxprop2param(1,iii)+(mtrnod-1)
!ortho!
!ortho!                        orthograd%cvalue(adjntind) =
orthograd%cvalue(adjntind) -
(dAddg(1,iii,kk)*adjntdisp%disp(iinod,ll)%u*truedisp%disp(jjnod,ll)%u)
!ortho!                        orthograd%cvalue(adjntind) =
orthograd%cvalue(adjntind) -
(dAddg(4,iii,kk)*adjntdisp%disp(iinod,ll)%u*truedisp%disp(jjnod,ll)%v)
!ortho!                        orthograd%cvalue(adjntind) =
orthograd%cvalue(adjntind) -
(dAddg(7,iii,kk)*adjntdisp%disp(iinod,ll)%u*truedisp%disp(jjnod,ll)%w)
!ortho!
!ortho!                        orthograd%cvalue(adjntind) =
orthograd%cvalue(adjntind) -
(dAddg(2,iii,kk)*adjntdisp%disp(iinod,ll)%v*truedisp%disp(jjnod,ll)%u)
!ortho!                        orthograd%cvalue(adjntind) =
orthograd%cvalue(adjntind) -
(dAddg(5,iii,kk)*adjntdisp%disp(iinod,ll)%v*truedisp%disp(jjnod,ll)%v)
!ortho!                        orthograd%cvalue(adjntind) =
orthograd%cvalue(adjntind) -
(dAddg(8,iii,kk)*adjntdisp%disp(iinod,ll)%v*truedisp%disp(jjnod,ll)%w)
!ortho!
!ortho!                        orthograd%cvalue(adjntind) =
orthograd%cvalue(adjntind) -
(dAddg(3,iii,kk)*adjntdisp%disp(iinod,ll)%w*truedisp%disp(jjnod,ll)%u)
!ortho!                        orthograd%cvalue(adjntind) =
orthograd%cvalue(adjntind) -
(dAddg(6,iii,kk)*adjntdisp%disp(iinod,ll)%w*truedisp%disp(jjnod,ll)%v)
!ortho!                        orthograd%cvalue(adjntind) =
orthograd%cvalue(adjntind) -
(dAddg(9,iii,kk)*adjntdisp%disp(iinod,ll)%w*truedisp%disp(jjnod,ll)%w)
!ortho!
```

```
!ortho!                    if ((jj.eq.adjntmesh%npe)) then !fill in
pressure/disp terms (right side of matrix)
!ortho!                       do iip=1,pressperpoint
!ortho!                         orthograd%cvalue(adjntind) =
orthograd%cvalue(adjntind) -
dApdg(iip,1,iii,kk)*adjntdisp%disp(iinod,ll)%u*truedisp%press(el,ll)%v
alue(iip) ! A(mx,np): Eq. in x, Pressure Terms
!ortho!                         orthograd%cvalue(adjntind) =
orthograd%cvalue(adjntind) -
dApdg(iip,2,iii,kk)*adjntdisp%disp(iinod,ll)%v*truedisp%press(el,ll)%v
alue(iip) ! A(my,np): Eq. in y, Pressure Terms
!ortho!                         orthograd%cvalue(adjntind) =
orthograd%cvalue(adjntind) -
dApdg(iip,3,iii,kk)*adjntdisp%disp(iinod,ll)%w*truedisp%press(el,ll)%v
alue(iip) ! A(mz,np): Eq. in z, Pressure Terms
!ortho!                       enddo
!ortho!                     endif
!ortho!
!ortho!                     if(ii.ne.jj) then !Add symmetic lower corner of
dA*sol contribution !!! NOTE: Switched Order for Addressing dAsmodg!!!
!ortho!                       orthograd%cvalue(adjntind) =
orthograd%cvalue(adjntind) -
(dAddg(1,iii,kk)*adjntdisp%disp(jjnod,ll)%u*truedisp%disp(iinod,ll)%u)
!ortho!                       orthograd%cvalue(adjntind) =
orthograd%cvalue(adjntind) -
(dAddg(2,iii,kk)*adjntdisp%disp(jjnod,ll)%u*truedisp%disp(iinod,ll)%v)
!ortho!                       orthograd%cvalue(adjntind) =
orthograd%cvalue(adjntind) -
(dAddg(3,iii,kk)*adjntdisp%disp(jjnod,ll)%u*truedisp%disp(iinod,ll)%w)
!ortho!
!ortho!                       orthograd%cvalue(adjntind) =
orthograd%cvalue(adjntind) -
(dAddg(4,iii,kk)*adjntdisp%disp(jjnod,ll)%v*truedisp%disp(iinod,ll)%u)
!ortho!                       orthograd%cvalue(adjntind) =
orthograd%cvalue(adjntind) -
(dAddg(5,iii,kk)*adjntdisp%disp(jjnod,ll)%v*truedisp%disp(iinod,ll)%v)
!ortho!                       orthograd%cvalue(adjntind) =
orthograd%cvalue(adjntind) -
(dAddg(6,iii,kk)*adjntdisp%disp(jjnod,ll)%v*truedisp%disp(iinod,ll)%w)
!ortho!
!ortho!                       orthograd%cvalue(adjntind) =
orthograd%cvalue(adjntind) -
(dAddg(7,iii,kk)*adjntdisp%disp(jjnod,ll)%w*truedisp%disp(iinod,ll)%u)
!ortho!                       orthograd%cvalue(adjntind) =
orthograd%cvalue(adjntind) -
(dAddg(8,iii,kk)*adjntdisp%disp(jjnod,ll)%w*truedisp%disp(iinod,ll)%v)
!ortho!                       orthograd%cvalue(adjntind) =
orthograd%cvalue(adjntind) -
(dAddg(9,iii,kk)*adjntdisp%disp(jjnod,ll)%w*truedisp%disp(iinod,ll)%w)
!ortho!
!ortho!                     if ((jj.eq.adjntmesh%npe)) then !fill in
pressure/disp terms (right side of matrix)
```

```
!ortho!                      do jjp=1,pressperpoint
!ortho!                        orthograd%cvalue(adjntind) =
orthograd%cvalue(adjntind) -
dApdg(jjp,1,iii,kk)*adjntdisp%press(el,ll)%value(jjp)*truedisp%disp(ii
nod,ll)%u ! A(mp,nx): Pressure Eq. Terms
!ortho!                        orthograd%cvalue(adjntind) =
orthograd%cvalue(adjntind) -
dApdg(jjp,2,iii,kk)*adjntdisp%press(el,ll)%value(jjp)*truedisp%disp(ii
nod,ll)%v ! A(mp,ny): Pressure Eq. Terms
!ortho!                        orthograd%cvalue(adjntind) =
orthograd%cvalue(adjntind) -
dApdg(jjp,3,iii,kk)*adjntdisp%press(el,ll)%value(jjp)*truedisp%disp(ii
nod,ll)%w ! A(mp,nz): Pressure Eq. Terms
!ortho!                      enddo
!ortho!                    endif
!ortho!
!ortho!                  endif
!ortho!
!ortho!                  if
((ii.eq.adjntmesh%npe).and.(jj.eq.adjntmesh%npe)) then !fill in
pressure/pressure terms (both upper and lower corners)
!ortho!                    do iip=1,pressperpoint
!ortho!                      do jjp=1,pressperpoint
!ortho!                        orthograd%cvalue(adjntind) =
orthograd%cvalue(adjntind) -
dAppg(iip,jjp,iii,kk)*adjntdisp%press(el,ll)%value(iip)*truedisp%press
(el,ll)%value(jjp)
!ortho!                      enddo
!ortho!                    enddo
!ortho!                  endif
!ortho!
!ortho!                endif
!ortho!              enddo
!ortho!
!ortho!              !shear modulus terms (mu12, mu23, and mu31):
!ortho!              do iii=1,adjntmtrl%prop(2)%nvpp
!ortho!                if(cmplxparamind(2,iii)) then
!ortho!
     adjntind=orthograd%cmplxprop2param(2,iii)+(mtrnod-1)
!ortho!
!ortho!                  orthograd%cvalue(adjntind) =
orthograd%cvalue(adjntind) -
(dAddg(1,iii+3,kk)*adjntdisp%disp(iinod,ll)%u*truedisp%disp(jjnod,ll)%
u)
!ortho!                  orthograd%cvalue(adjntind) =
orthograd%cvalue(adjntind) -
(dAddg(4,iii+3,kk)*adjntdisp%disp(iinod,ll)%u*truedisp%disp(jjnod,ll)%
v)
!ortho!                  orthograd%cvalue(adjntind) =
orthograd%cvalue(adjntind) -
(dAddg(7,iii+3,kk)*adjntdisp%disp(iinod,ll)%u*truedisp%disp(jjnod,ll)%
w)
```

```
!ortho!
!ortho!                orthograd%cvalue(adjntind) =
orthograd%cvalue(adjntind) -
(dAddg(2,iii+3,kk)*adjntdisp%disp(iinod,ll)%v*truedisp%disp(jjnod,ll)%
u)
!ortho!                orthograd%cvalue(adjntind) =
orthograd%cvalue(adjntind) -
(dAddg(5,iii+3,kk)*adjntdisp%disp(iinod,ll)%v*truedisp%disp(jjnod,ll)%
v)
!ortho!                orthograd%cvalue(adjntind) =
orthograd%cvalue(adjntind) -
(dAddg(8,iii+3,kk)*adjntdisp%disp(iinod,ll)%v*truedisp%disp(jjnod,ll)%
w)
!ortho!
!ortho!                orthograd%cvalue(adjntind) =
orthograd%cvalue(adjntind) -
(dAddg(3,iii+3,kk)*adjntdisp%disp(iinod,ll)%w*truedisp%disp(jjnod,ll)%
u)
!ortho!                orthograd%cvalue(adjntind) =
orthograd%cvalue(adjntind) -
(dAddg(6,iii+3,kk)*adjntdisp%disp(iinod,ll)%w*truedisp%disp(jjnod,ll)%
v)
!ortho!                orthograd%cvalue(adjntind) =
orthograd%cvalue(adjntind) -
(dAddg(9,iii+3,kk)*adjntdisp%disp(iinod,ll)%w*truedisp%disp(jjnod,ll)%
w)
!ortho!
!ortho!                if ((jj.eq.adjntmesh%npe)) then !fill in
pressure/disp terms (right side of matrix)
!ortho!                   do iip=1,pressperpoint
!ortho!                    orthograd%cvalue(adjntind) =
orthograd%cvalue(adjntind) -
dApdg(iip,1,iii+3,kk)*adjntdisp%disp(iinod,ll)%u*truedisp%press(el,ll)
%value(iip) ! A(mx,np): Eq. in x, Pressure Terms
!ortho!                    orthograd%cvalue(adjntind) =
orthograd%cvalue(adjntind) -
dApdg(iip,2,iii+3,kk)*adjntdisp%disp(iinod,ll)%v*truedisp%press(el,ll)
%value(iip) ! A(my,np): Eq. in y, Pressure Terms
!ortho!                    orthograd%cvalue(adjntind) =
orthograd%cvalue(adjntind) -
dApdg(iip,3,iii+3,kk)*adjntdisp%disp(iinod,ll)%w*truedisp%press(el,ll)
%value(iip) ! A(mz,np): Eq. in z, Pressure Terms
!ortho!                   enddo
!ortho!                endif
!ortho!
!ortho!                if(ii.ne.jj) then !Add symmetic lower corner of
dA*sol contribution !!! NOTE: Switched Order for Addressing dAsmodg!!!
!ortho!                orthograd%cvalue(adjntind) =
orthograd%cvalue(adjntind) -
(dAddg(1,iii+3,kk)*adjntdisp%disp(jjnod,ll)%u*truedisp%disp(iinod,ll)%
u)
```

148

```
!ortho!                    orthograd%cvalue(adjntind) =
orthograd%cvalue(adjntind) -
(dAddg(2,iii+3,kk)*adjntdisp%disp(jjnod,ll)%u*truedisp%disp(iinod,ll)%
v)
!ortho!                    orthograd%cvalue(adjntind) =
orthograd%cvalue(adjntind) -
(dAddg(3,iii+3,kk)*adjntdisp%disp(jjnod,ll)%u*truedisp%disp(iinod,ll)%
w)
!ortho!
!ortho!                    orthograd%cvalue(adjntind) =
orthograd%cvalue(adjntind) -
(dAddg(4,iii+3,kk)*adjntdisp%disp(jjnod,ll)%v*truedisp%disp(iinod,ll)%
u)
!ortho!                    orthograd%cvalue(adjntind) =
orthograd%cvalue(adjntind) -
(dAddg(5,iii+3,kk)*adjntdisp%disp(jjnod,ll)%v*truedisp%disp(iinod,ll)%
v)
!ortho!                    orthograd%cvalue(adjntind) =
orthograd%cvalue(adjntind) -
(dAddg(6,iii+3,kk)*adjntdisp%disp(jjnod,ll)%v*truedisp%disp(iinod,ll)%
w)
!ortho!
!ortho!                    orthograd%cvalue(adjntind) =
orthograd%cvalue(adjntind) -
(dAddg(7,iii+3,kk)*adjntdisp%disp(jjnod,ll)%w*truedisp%disp(iinod,ll)%
u)
!ortho!                    orthograd%cvalue(adjntind) =
orthograd%cvalue(adjntind) -
(dAddg(8,iii+3,kk)*adjntdisp%disp(jjnod,ll)%w*truedisp%disp(iinod,ll)%
v)
!ortho!                    orthograd%cvalue(adjntind) =
orthograd%cvalue(adjntind) -
(dAddg(9,iii+3,kk)*adjntdisp%disp(jjnod,ll)%w*truedisp%disp(iinod,ll)%
w)
!ortho!
!ortho!                    if ((jj.eq.adjntmesh%npe)) then !fill in
pressure/disp terms (right side of matrix)
!ortho!                       do jjp=1,pressperpoint
!ortho!                         orthograd%cvalue(adjntind) =
orthograd%cvalue(adjntind) -
dApdg(jjp,1,iii+3,kk)*adjntdisp%press(el,ll)%value(jjp)*truedisp%disp(
iinod,ll)%u ! A(mp,nx): Pressure Eq. Terms
!ortho!                         orthograd%cvalue(adjntind) =
orthograd%cvalue(adjntind) -
dApdg(jjp,2,iii+3,kk)*adjntdisp%press(el,ll)%value(jjp)*truedisp%disp(
iinod,ll)%v ! A(mp,ny): Pressure Eq. Terms
!ortho!                         orthograd%cvalue(adjntind) =
orthograd%cvalue(adjntind) -
dApdg(jjp,3,iii+3,kk)*adjntdisp%press(el,ll)%value(jjp)*truedisp%disp(
iinod,ll)%w ! A(mp,nz): Pressure Eq. Terms
!ortho!                       enddo
!ortho!                    endif
```

```
!ortho!
!ortho!                  endif
!ortho!
!ortho!                  if
((ii.eq.adjntmesh%npe).and.(jj.eq.adjntmesh%npe)) then !fill in
pressure/pressure terms (both upper and lower corners)
!ortho!                      do iip=1,pressperpoint
!ortho!                       do jjp=1,pressperpoint
!ortho!                        orthograd%cvalue(adjntind) =
orthograd%cvalue(adjntind) -
dAppg(iip,jjp,iii+3,kk)*adjntdisp%press(el,ll)%value(iip)*truedisp%pre
ss(el,ll)%value(jjp)
!ortho!                       enddo
!ortho!                      enddo
!ortho!                  endif
!ortho!
!ortho!                  endif
!ortho!                  enddo
!ortho!
!ortho!              !Poisson's ratio terms (v12, v23, and v31):
!ortho!              do iii=1,adjntmtrl%prop(3)%nvpp
!ortho!              if(cmplxparamind(3,iii)) then
!ortho!
     adjntind=orthograd%cmplxprop2param(3,iii)+(mtrnod-1)
!ortho!
!ortho!                  orthograd%cvalue(adjntind) =
orthograd%cvalue(adjntind) -
(dAddg(1,iii+6,kk)*adjntdisp%disp(iinod,ll)%u*truedisp%disp(jjnod,ll)%
u)
!ortho!                  orthograd%cvalue(adjntind) =
orthograd%cvalue(adjntind) -
(dAddg(4,iii+6,kk)*adjntdisp%disp(iinod,ll)%u*truedisp%disp(jjnod,ll)%
v)
!ortho!                  orthograd%cvalue(adjntind) =
orthograd%cvalue(adjntind) -
(dAddg(7,iii+6,kk)*adjntdisp%disp(iinod,ll)%u*truedisp%disp(jjnod,ll)%
w)
!ortho!
!ortho!              orthograd%cvalue(adjntind) =
orthograd%cvalue(adjntind) -
(dAddg(2,iii+6,kk)*adjntdisp%disp(iinod,ll)%v*truedisp%disp(jjnod,ll)%
u)
!ortho!                  orthograd%cvalue(adjntind) =
orthograd%cvalue(adjntind) -
(dAddg(5,iii+6,kk)*adjntdisp%disp(iinod,ll)%v*truedisp%disp(jjnod,ll)%
v)
!ortho!                  orthograd%cvalue(adjntind) =
orthograd%cvalue(adjntind) -
(dAddg(8,iii+6,kk)*adjntdisp%disp(iinod,ll)%v*truedisp%disp(jjnod,ll)%
w)
!ortho!
```

```
!ortho!               orthograd%cvalue(adjntind) =
orthograd%cvalue(adjntind) -
(dAddg(3,iii+6,kk)*adjntdisp%disp(iinod,ll)%w*truedisp%disp(jjnod,ll)%
u)
!ortho!               orthograd%cvalue(adjntind) =
orthograd%cvalue(adjntind) -
(dAddg(6,iii+6,kk)*adjntdisp%disp(iinod,ll)%w*truedisp%disp(jjnod,ll)%
v)
!ortho!               orthograd%cvalue(adjntind) =
orthograd%cvalue(adjntind) -
(dAddg(9,iii+6,kk)*adjntdisp%disp(iinod,ll)%w*truedisp%disp(jjnod,ll)%
w)
!ortho!
!ortho!               if ((jj.eq.adjntmesh%npe)) then !fill in
pressure/disp terms (right side of matrix)
!ortho!                 do iip=1,pressperpoint
!ortho!                   orthograd%cvalue(adjntind) =
orthograd%cvalue(adjntind) -
dApdg(iip,1,iii+6,kk)*adjntdisp%disp(iinod,ll)%u*truedisp%press(el,ll)
%value(iip) ! A(mx,np): Eq. in x, Pressure Terms
!ortho!                   orthograd%cvalue(adjntind) =
orthograd%cvalue(adjntind) -
dApdg(iip,2,iii+6,kk)*adjntdisp%disp(iinod,ll)%v*truedisp%press(el,ll)
%value(iip) ! A(my,np): Eq. in y, Pressure Terms
!ortho!                   orthograd%cvalue(adjntind) =
orthograd%cvalue(adjntind) -
dApdg(iip,3,iii+6,kk)*adjntdisp%disp(iinod,ll)%w*truedisp%press(el,ll)
%value(iip) ! A(mz,np): Eq. in z, Pressure Terms
!ortho!                 enddo
!ortho!               endif
!ortho!
!ortho!               if(ii.ne.jj) then !Add symmetic lower corner of
dA*sol contribution !!! NOTE: Switched Order for Addressing dAsmodg!!!
!ortho!                 orthograd%cvalue(adjntind) =
orthograd%cvalue(adjntind) -
(dAddg(1,iii+6,kk)*adjntdisp%disp(jjnod,ll)%u*truedisp%disp(iinod,ll)%
u)
!ortho!                 orthograd%cvalue(adjntind) =
orthograd%cvalue(adjntind) -
(dAddg(2,iii+6,kk)*adjntdisp%disp(jjnod,ll)%u*truedisp%disp(iinod,ll)%
v)
!ortho!                 orthograd%cvalue(adjntind) =
orthograd%cvalue(adjntind) -
(dAddg(3,iii+6,kk)*adjntdisp%disp(jjnod,ll)%u*truedisp%disp(iinod,ll)%
w)
!ortho!
!ortho!                 orthograd%cvalue(adjntind) =
orthograd%cvalue(adjntind) -
(dAddg(4,iii+6,kk)*adjntdisp%disp(jjnod,ll)%v*truedisp%disp(iinod,ll)%
u)
!ortho!                 orthograd%cvalue(adjntind) =
orthograd%cvalue(adjntind) -
```

```
(dAddg(5,iii+6,kk)*adjntdisp%disp(jjnod,ll)%v*truedisp%disp(iinod,ll)%
v)
!ortho!                orthograd%cvalue(adjntind) =
orthograd%cvalue(adjntind) -
(dAddg(6,iii+6,kk)*adjntdisp%disp(jjnod,ll)%v*truedisp%disp(iinod,ll)%
w)
!ortho!
!ortho!                orthograd%cvalue(adjntind) =
orthograd%cvalue(adjntind) -
(dAddg(7,iii+6,kk)*adjntdisp%disp(jjnod,ll)%w*truedisp%disp(iinod,ll)%
u)
!ortho!                orthograd%cvalue(adjntind) =
orthograd%cvalue(adjntind) -
(dAddg(8,iii+6,kk)*adjntdisp%disp(jjnod,ll)%w*truedisp%disp(iinod,ll)%
v)
!ortho!                orthograd%cvalue(adjntind) =
orthograd%cvalue(adjntind) -
(dAddg(9,iii+6,kk)*adjntdisp%disp(jjnod,ll)%w*truedisp%disp(iinod,ll)%
w)
!ortho!
!ortho!                if ((jj.eq.adjntmesh%npe)) then !fill in
pressure/disp terms (right side of matrix)
!ortho!                  do jjp=1,pressperpoint
!ortho!                   orthograd%cvalue(adjntind) =
orthograd%cvalue(adjntind) -
dApdg(jjp,1,iii+6,kk)*adjntdisp%press(el,ll)%value(jjp)*truedisp%disp(
iinod,ll)%u ! A(mp,nx): Pressure Eq. Terms
!ortho!                   orthograd%cvalue(adjntind) =
orthograd%cvalue(adjntind) -
dApdg(jjp,2,iii+6,kk)*adjntdisp%press(el,ll)%value(jjp)*truedisp%disp(
iinod,ll)%v ! A(mp,ny): Pressure Eq. Terms
!ortho!                   orthograd%cvalue(adjntind) =
orthograd%cvalue(adjntind) -
dApdg(jjp,3,iii+6,kk)*adjntdisp%press(el,ll)%value(jjp)*truedisp%disp(
iinod,ll)%w ! A(mp,nz): Pressure Eq. Terms
!ortho!                  enddo
!ortho!                endif
!ortho!
!ortho!                endif
!ortho!
!ortho!                if
((ii.eq.adjntmesh%npe).and.(jj.eq.adjntmesh%npe)) then !fill in
pressure/pressure terms (both upper and lower corners)
!ortho!                  do iip=1,pressperpoint
!ortho!                   do jjp=1,pressperpoint
!ortho!                    orthograd%cvalue(adjntind) =
orthograd%cvalue(adjntind) -
dAppg(iip,jjp,iii+6,kk)*adjntdisp%press(el,ll)%value(iip)*truedisp%pre
ss(el,ll)%value(jjp)
!ortho!                   enddo
!ortho!                  enddo
!ortho!                endif
```

```
!ortho!
!ortho!                 endif
!ortho!                 enddo
!ortho!
!ortho!                 !density terms
!ortho!                 if(cmplxparamind(4,1)) then
!ortho!                 adjntind=orthograd%cmplxprop2param(4,1)+(mtrnod-
1)
!ortho!
!ortho!                 orthograd%cvalue(adjntind) =
orthograd%cvalue(adjntind) -
dAdrho*adjntdisp%disp(iinod,ll)%u*truedisp%disp(jjnod,ll)%u
!ortho!                 orthograd%cvalue(adjntind) =
orthograd%cvalue(adjntind) -
dAdrho*adjntdisp%disp(iinod,ll)%v*truedisp%disp(jjnod,ll)%v
!ortho!                 orthograd%cvalue(adjntind) =
orthograd%cvalue(adjntind) -
dAdrho*adjntdisp%disp(iinod,ll)%w*truedisp%disp(jjnod,ll)%w
!ortho!
!ortho!                 if(ii.ne.jj) then !Add symmetic lower corner of
dA*sol contribution !!! NOTE: Switched Order for Addressing dAsmodg!!!
!ortho!                 orthograd%cvalue(adjntind) =
orthograd%cvalue(adjntind) -
dAdrho*adjntdisp%disp(jjnod,ll)%u*truedisp%disp(iinod,ll)%u
!ortho!                 orthograd%cvalue(adjntind) =
orthograd%cvalue(adjntind) -
dAdrho*adjntdisp%disp(jjnod,ll)%v*truedisp%disp(iinod,ll)%v
!ortho!                 orthograd%cvalue(adjntind) =
orthograd%cvalue(adjntind) -
dAdrho*adjntdisp%disp(jjnod,ll)%w*truedisp%disp(iinod,ll)%w
!ortho!                 endif
!ortho!                 endif
!ortho!
!ortho!                 enddo
!ortho!
!ortho! 400                 continue ! End of Material Property Loop!
!ortho!
!ortho! 300                 continue ! End of weighting function loop
!ortho!
!ortho! 200          continue ! End of interpolating Function loop
!ortho!
!ortho! 100  continue !End of Element loop
!ortho!
!ortho!    if(verb) then
!ortho!    print *,'!!! Adjoint Orthotropic Gradient Terms Calculated'
!ortho!    do ii=1,adjntmtrl%numprop
!ortho!    do jj=1,adjntmtrl%prop(ii)%nvpp
!ortho!    do kk=1,5
!ortho!    adjntind=orthograd%cmplxprop2param(ii,jj)+(kk-1)
!ortho!    print *,'!!! FD Ortho Grad: <prop> <value> <point>:
',ii,jj,kk,orthograd%cvalue(adjntind)
!ortho!    enddo
```

153

```
!ortho!     enddo
!ortho!     enddo
!ortho!     endif
!ortho!
!ortho!
!oooooooooooooooooooooooooooooooooooooooooooooooooooooooooooooo
oooo
!ortho!
!ortho!     end subroutine orthoadjointgrad
!ortho!
!ortho!
!oooooooooooooooooooooooooooooooooooooooooooooooooooooooooooooo
ooooooooooo
```

F. BlueFern pSeries Technical Overview

The following bullet points highlight the University of Canterbury's IBM eServer Cluster 1600 High Performance Computing (HPC) cluster's technical specifications:

- The machine is comprised of 10 IBM System p5 p575 nodes
- Each p5-p575 node contains 8 dual-core IBM POWER5+ CPUs running at 1.9 GHz
- Each of the POWER5+ processor/memory modules contains a dual-core processor chip with both cores active, eight memory DIMM slots and a 36 Megabyte Level 3 (L3) cache chip
- The private 36 Megabyte L3 cache is located out of the path of main memory and operates at half the chip frequency
- Sustained memory bandwidth is 105.5 Gigabytes/sec
- Each processor chip contains shared 1.9 Megabytes Level 2 (L2) cache, a memory controller and L3 cache directory
- Each processor is able to read from the L2 and L3 caches of the other chips but can only store to its own L2 andL3 caches
- Node RAM is expandable to a maximum of 256 Gigabytes DDR2 memory per node
- L2 and L3 cache is expandable to 300 Megabytes per node
- 9 of the p5-p575 nodes have 32 Gigabytes of RAM
- The BestGRID node has 64 Gigabytes of RAM
- The eight p5-575 nodes are partitioned into a number of Logical Partitions (LPARs) which take care of various functions including production computation, login, storage management and job scheduling etc.

- Various interconnect networks exist in the machine, connecting the nodes together, including Gigabit Ethernet and dual-channel InfiniBand
- Each LPAR is a logical Operating System Instance (OSI) and as such has its own network identity, allocated RAM, allocated hard-drives and is in essence a "stand alone" shared memory parallel (SMP) computer
- Some LPARs in the machine run AIX 5.3 OSIs and other run Suse Linux Enterprise Server 9 (SLES9) OSIs. Hence the machine is a heterogeneous system
- All cluster-wide file-systems utilize IBM's high bandwidth parallel file-system technology called GPFS and are hosted by DS4100 and DS4200 RAID 5 arrays
- The machine uses IBM's batch scheduling technology, called LoadLeveler, to keep the machine loaded with user-jobs and give user's a fair share of the machine